NSTYTUT FIZYKI JĄDROWEJ
NSTITUTE OF NUCLEAR PHYSICS
ИНСТИТУТ ЯДЕРНОЙ ФИЗИКИ

KRAKÓW

PL9600333 - 345

RAPORT No 1588

INP--1588

KRAKÓW - BERLIN WORKSHOP ON NUCLEAR PHYSICS (SLIDE REPORT)

ZAKOPANE, DECEMBER 1991

ORGANIZED BY J. STYCZEŃ AND K. H. MAIER

KRAKÓW 1992

VOL. 27 № 10

INP--1588

First Berlin-Krakow Workshop on Nuclear Physics

Zakopane, December 1991

organized by J. Styczeń and K.H. Maier

SLIDE REPORT

WYDANO NAKŁADEM
INSTYTUTU FIZYKI JĄDROWEJ
IM. HENRYKA NIEWODNICZAŃSKIEGO
KRAKÓW, UL. RADZIKOWSKIEGO 152

Kopię kserograficzną, druk i oprawę wykonano w IFJ Kraków

Wydanie I *Zam. 52/92* *Nakład 65 egz.*

Participants:

Hahn Meitner Institute Berlin:
H. Grawe, J. Heese, H. Kluge, K.H. Maier, M. Schramm, R. Schubart, K. Spohr.

IKP der KFA Jülich: P. Kleinheinz.

Niewodniczanski Institute of Nuclear Physics, Kraków:
P. Bednarczyk, R. Broda, J. Grębosz, W. Królas, M. Lach, A. Maj, W. Męczyński, J. Styczeń, J. Wrzesiński.

J. Heese, W. Męczyński

THE DETECTOR FOR EVAPORATION RESIDUES

PHYSICAL MOTIVATION

spectroscopy of $^{186,188}Pb$ N=82 to 126 shell

difficulties:

- small production cross section
- fission competition (>50%)
- Coulomb excitation
- transfer reactions etc.

- Doppler shifts ($v/c \sim 0.01-0.05$)

solution:

a detector for evaporation residues in coincidence with γ-quanta (detected with OSIRIS)

sum energy and multiplicity (OSIRIS BGO-ball)

PRINCIPLE OF OPERATION

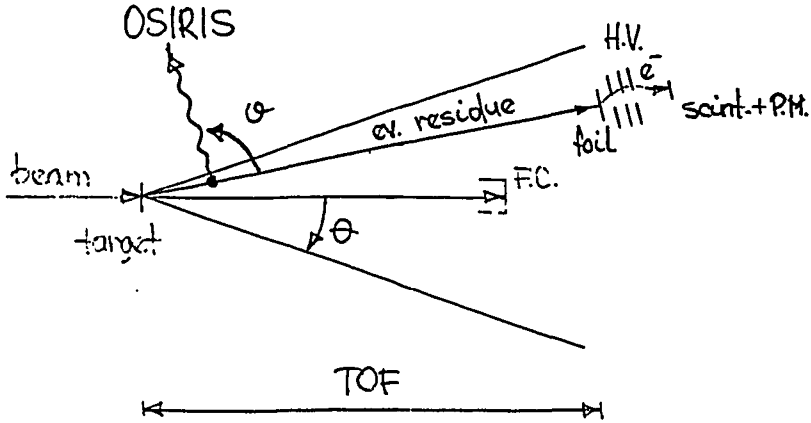

foil: ~ 1mg/cm^2
$\bar{n}$ ~ dE/dx ~ 10–50e$^-$
el. lens: ~20 keV
scint.+PM: plastic; fast ~ 10 MHz (scatt. beam!)
eff.: ~ 100%
signal: $\bar{n} \times$ 20 keV

how to identifie ev. residues?

- signal
- TOF → (examples)

how to correct Doppler shifts?

- granularity of the detector (ϑ)
- recoil velocity (TOF)

θ:

- ev. residues $\theta = 200\,\mathrm{mrad} \cong 12^\circ$
- VICKSI - beam $< 10\,\mathrm{mrad} \times \mathrm{C.E.} \cong 2^\circ$

TOF – example:

$^{183}W(^{20}Ne,5n)^{198}Po$

$E = 115$ MeV
$d = 70$ cm

	v (cm/ns)	TOF (ns)
beam	3.3	21
ev. residue	0.3	210
fission product	1.4	58
ev. residue from ^{12}C, ^{16}O react.	2.0	35

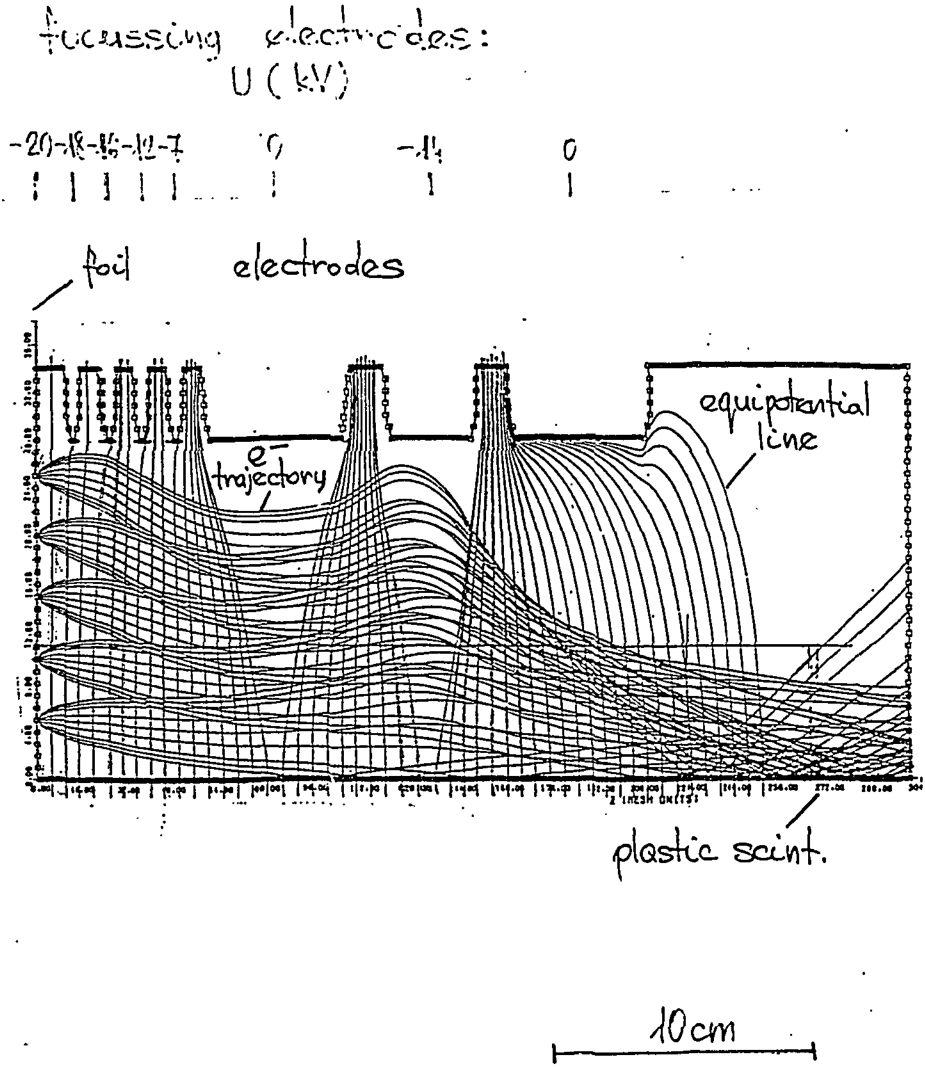
focussing electrodes:
U (kV)
-20 -18 -16 -12 -7
0
-14
0
foil
electrodes
e⁻
trajectory
equipotential
line
plastic scint.
10cm

OSIRIS & recoil detector:

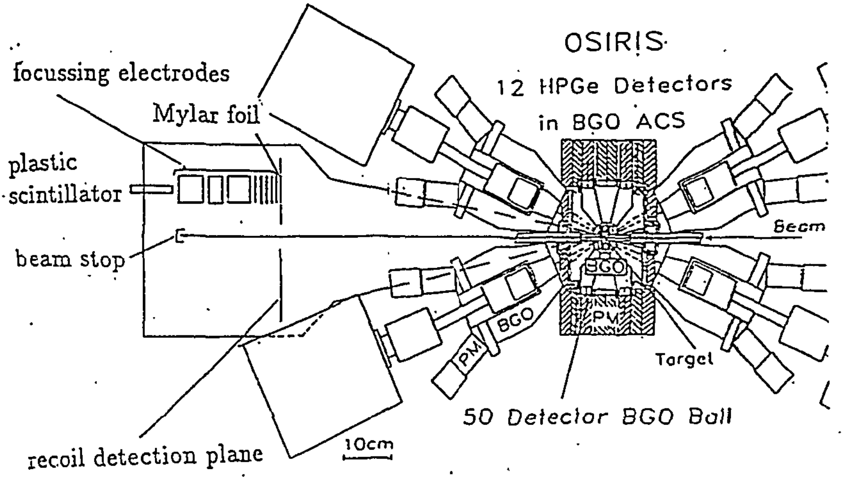

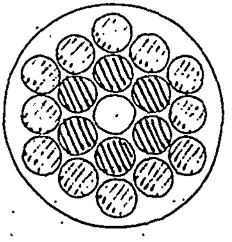

OSIRIS BGO- ball

50 elements = 4π sterad
1 element = 0.24 sterad ?

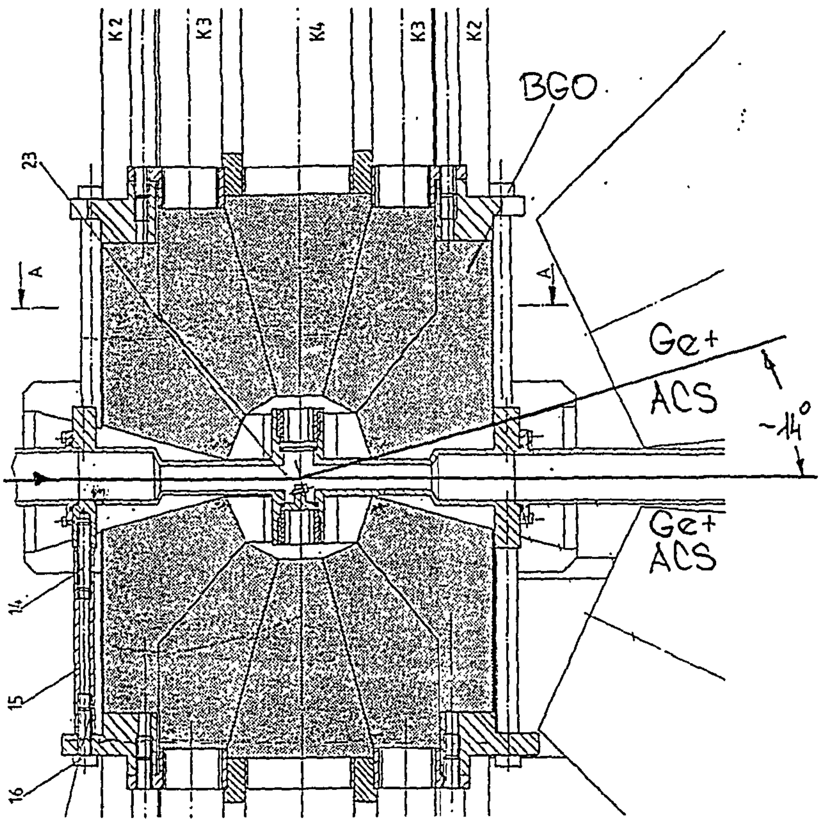

Recoil detector

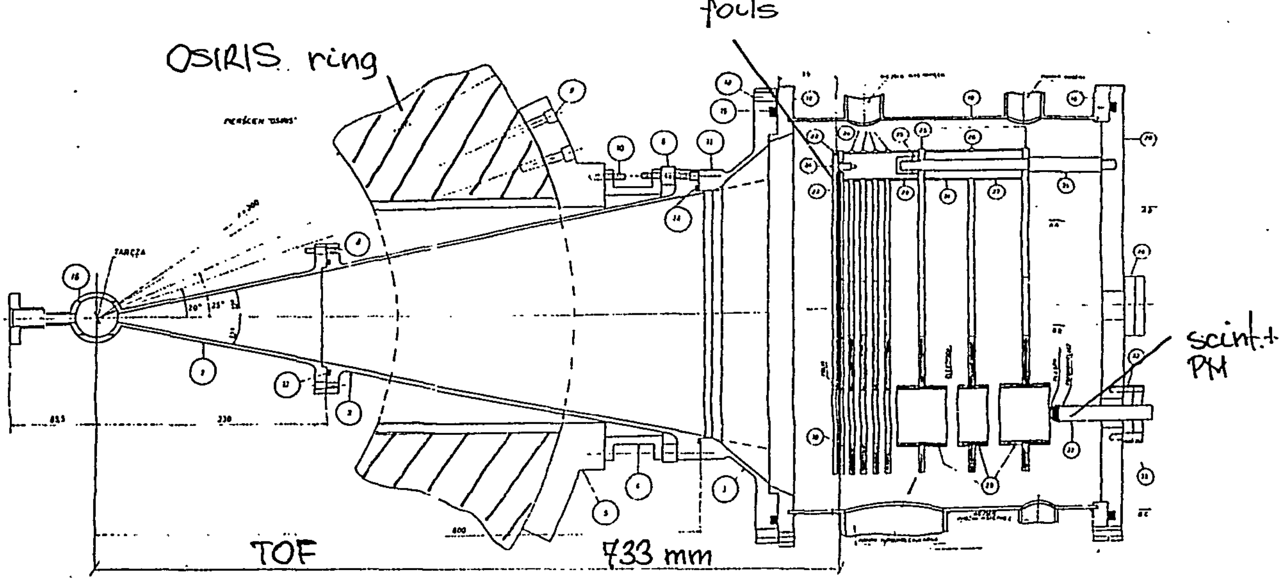

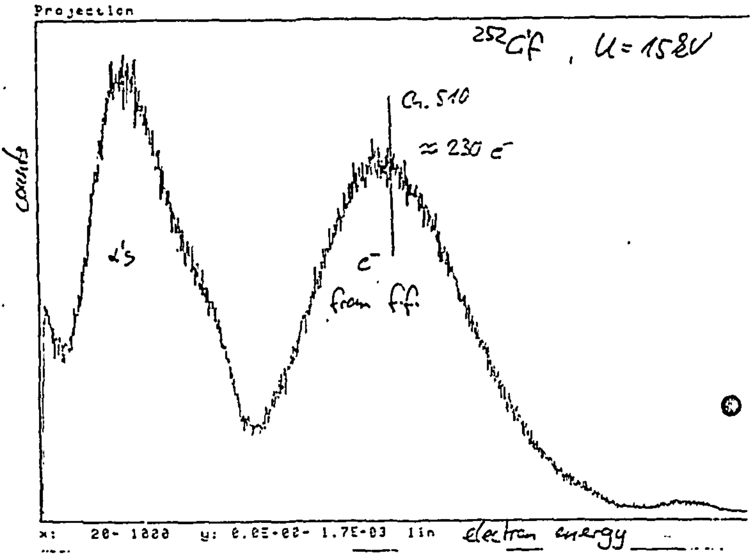

Projection
252Cf , U=15kV
ch. 510
≈ 230 e⁻
counts
α's
e⁻
from f.f.
x: 20- 1000 y: 0.0E+00- 1.7E+03 lin
electron energy

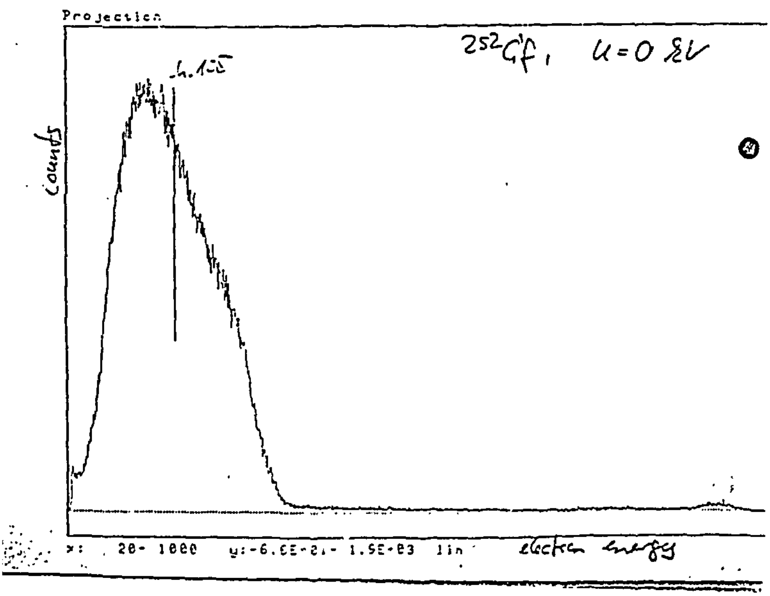

Projection
252Cf, U=0 kV
counts
x: 20- 1000
lin
electron energy

electron yield (or energy calibration):

measured e⁻-yields for fission fragments:

source	foil / thickness	$\bar{n}$	Reference
^{235}U	Ni, Al, Cu, Ag, Au ~600 μg/cm²	70 ± 10%	Stein + Leachman Rev. Sci. Instr. 27 (1956), 1049
	Be	+30%	
	MgO	+270%	
?	VYNS 8 μg/cm²	115 (15)	Fraser + Milton Nucl. Instr. 3 (1958), 275
^{252}Cf	C, 10 μg/cm²	180	Dietz et al. NIM 97 (1971), 581
^{252}Cf	C, 6 μg/cm²	170-190	Clerc et al. NIM 113 (1973), 325

estimated value for our setup (using the light output ratio $\frac{S(A)}{S(e^-)}$ for NE 102 A :
(von Schmeling, Z. Phys. 160 (1960) 520).

$\bar{n} \simeq 230$ for Mylar/Al

$\bar{n} \simeq 340$ for MgO/Al/MgO

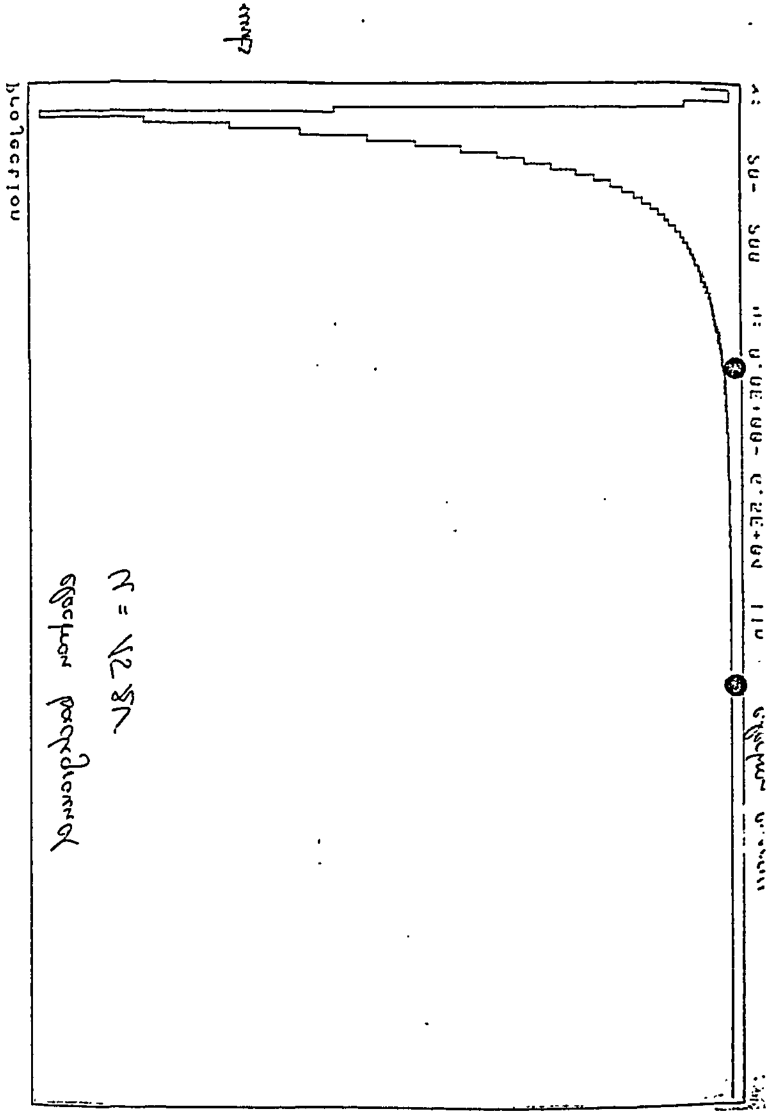

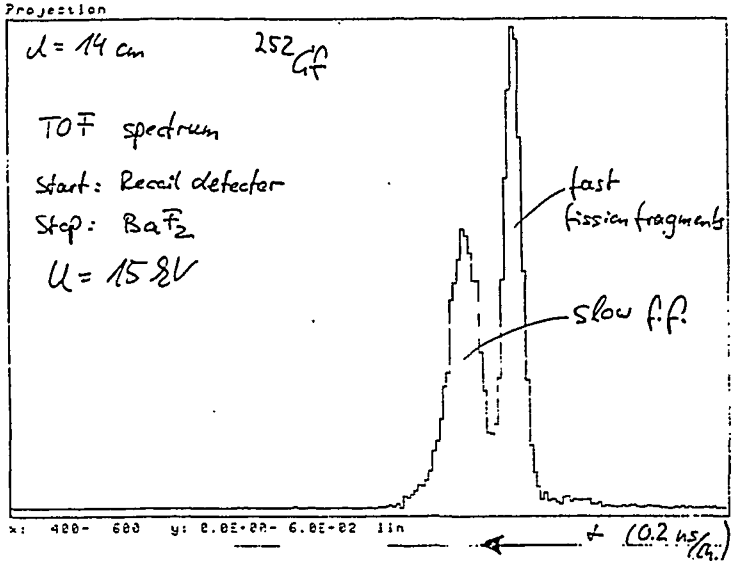
Projection
d = 14 cm
^{252}Cf
TOF spectrum
Start: Recoil detector
Stop: BaF_2
U = 15 kV
fast fission fragments
slow f.f.
x: 400- 600 y: 0.0E+00- 6.0E+02 lin
t (0.2 ns/ch.)

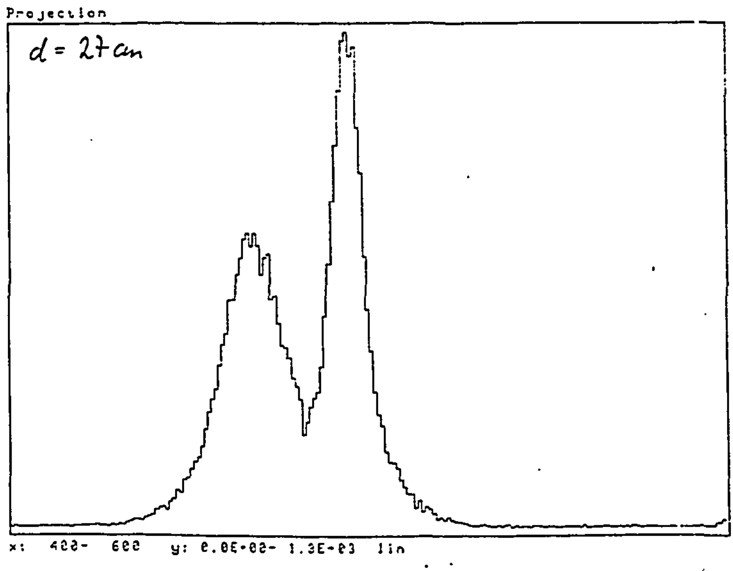
Projection
d = 27 cm
x: 400- 600 y: 0.0E+00- 1.3E+03 lin

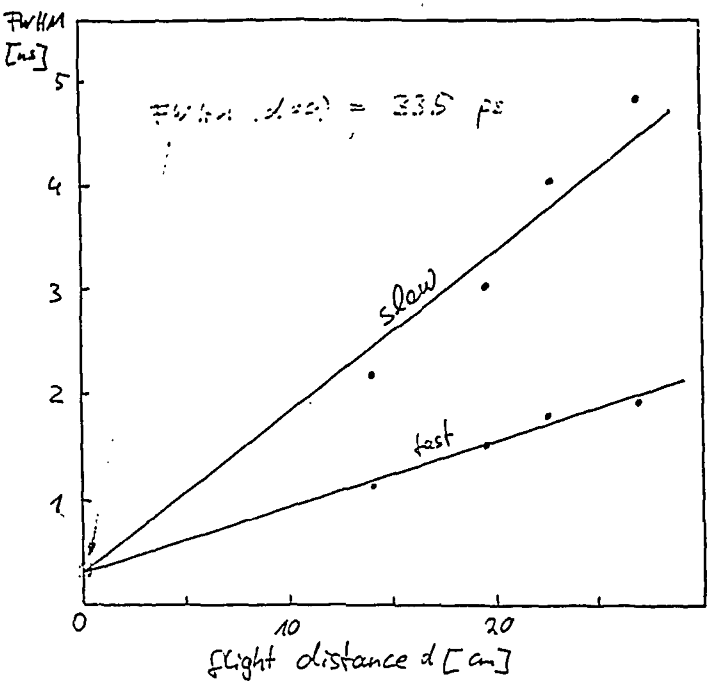
FWHM [ns]
5
4
3
2
1
0
10
20
slow
fast
flight distance d [cm]

some numbers:

- angles of inner ring: 2.7° – 7.2°
- angles of outer ring: 6.4° – 12.1°

estimated scattering of beam in the inner ring (TRIM):

170 MeV $^{40}Ar \rightarrow {}^{152}Sm$

(A) : 0.5 mg/cm^2 target : 2.0 %

(B) : 1.0 mg/cm^2 target : 4.6 %

assume beam current I = 1pnA , 10 MHz

$\left.\begin{array}{l} A: \ 2 \\ B: \ 5 \end{array}\right\}$ hits per det-element and beam pulse

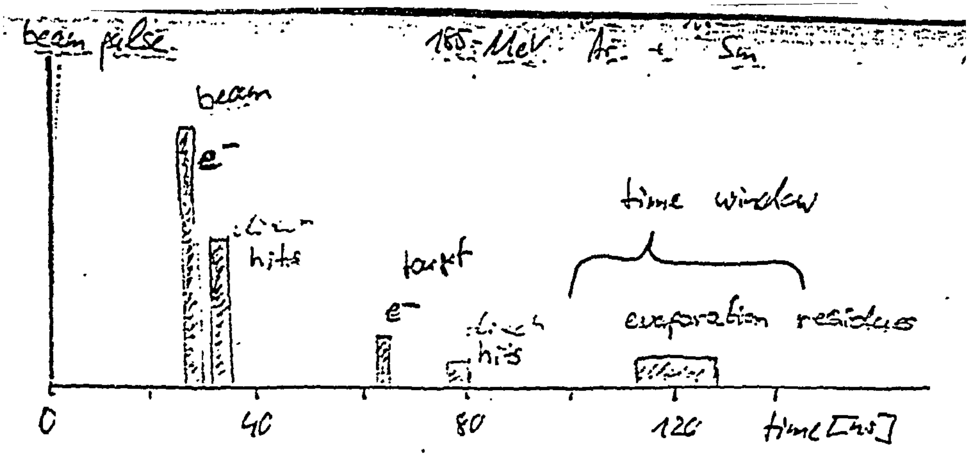
beam pulse
165 MeV Ar + Sn
beam
e⁻
hits
target
e⁻
hits
time window
evaporation residues
0
40
80
120
time [ns]

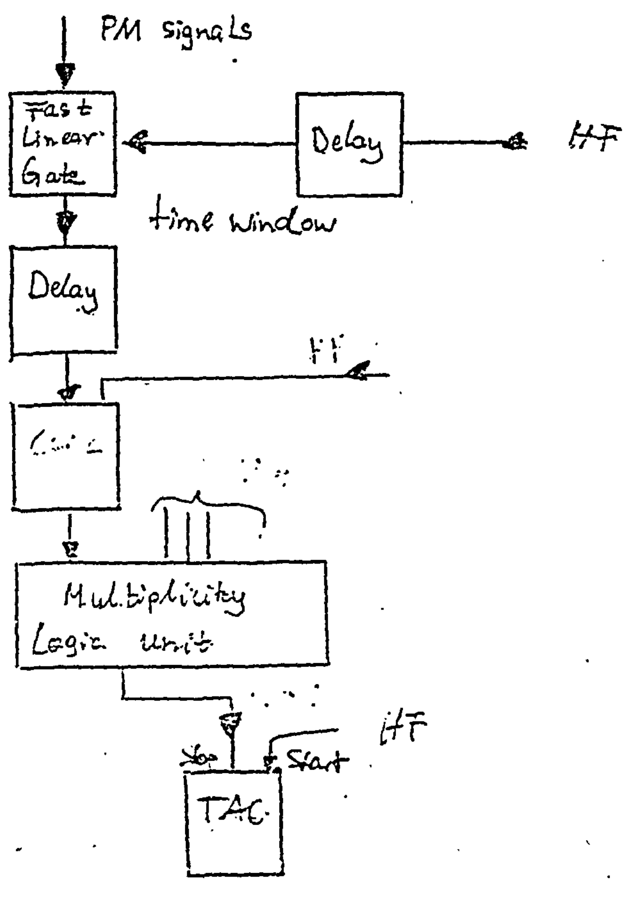
PM signals
Fast Linear Gate
Delay
HF
time window
Delay
HF
Multiplicity Logic unit
Stop
Start
HF
TAC

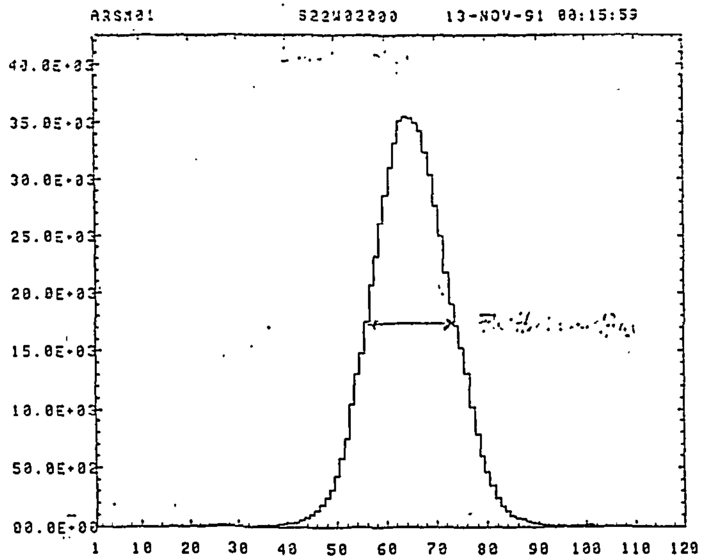

ARSM01
S22U02200
13-NOV-91 00:15:59
40.0E+03
35.0E+03
30.0E+03
25.0E+03
20.0E+03
15.0E+03
10.0E+03
50.0E+02
00.0E+00
1 10 20 30 40 50 60 70 80 90 100 110 120

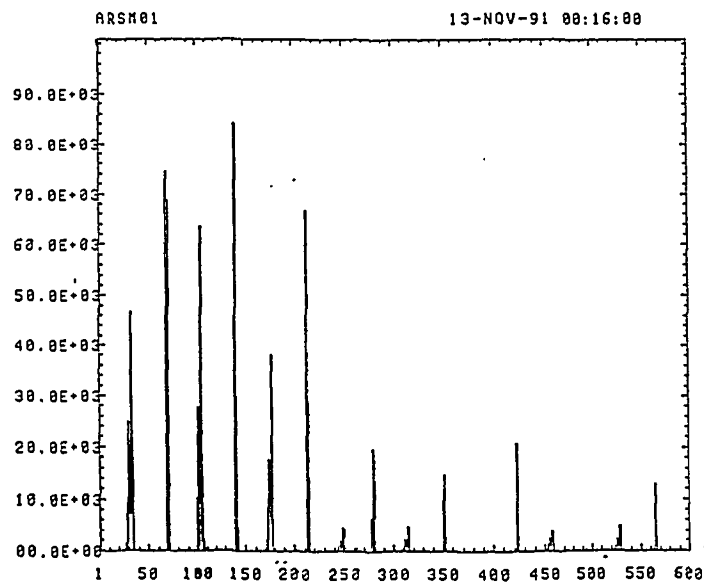

ARSM01
13-NOV-91 00:16:00
90.0E+03
80.0E+03
70.0E+03
60.0E+03
50.0E+03
40.0E+03
30.0E+03
20.0E+03
10.0E+03
00.0E+00
1 50 100 150 200 250 300 350 400 450 500 550 600

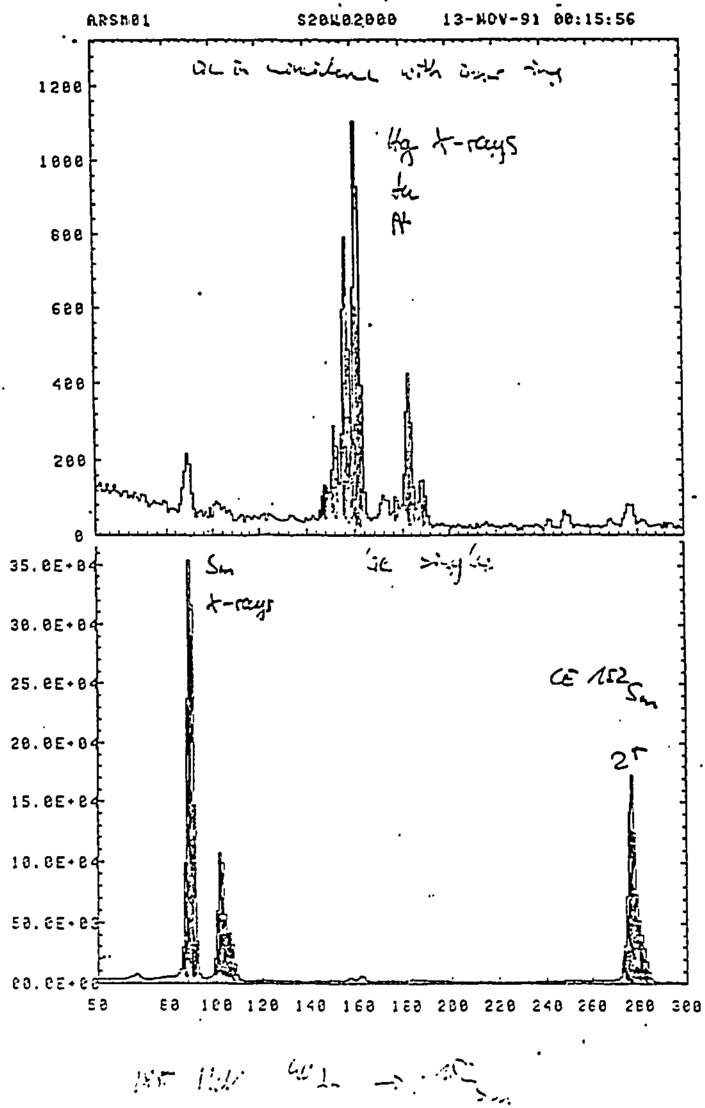
ARSM01 S20W02000 13-NOV-91 00:15:56
1200
1000
800
600
400
200
0
Hg X-rays
35.0E+04
30.0E+04
25.0E+04
20.0E+04
15.0E+04
10.0E+04
50.0E+03
00.0E+00
Sm
X-rays
CE 152Sm
2+
50
80
100
120
140
160
180
200
220
240
260
280
300

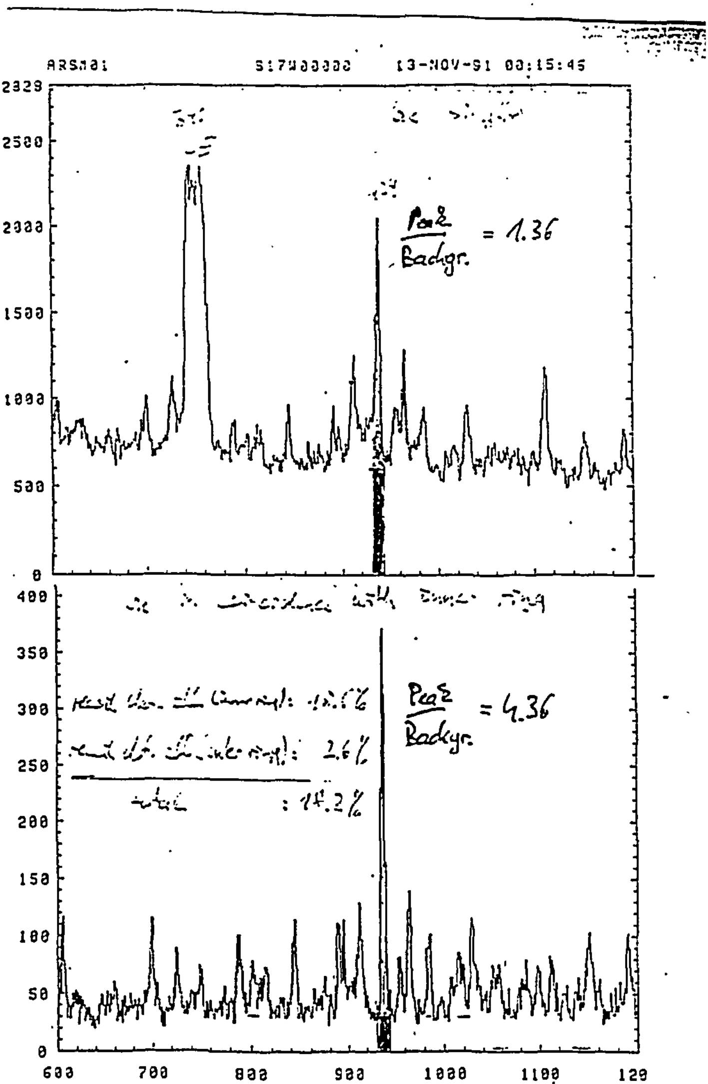

145 MeV ^{40}Ar + ^{152}Sm   52% fission

target thickness: [illegible] μg/cm²

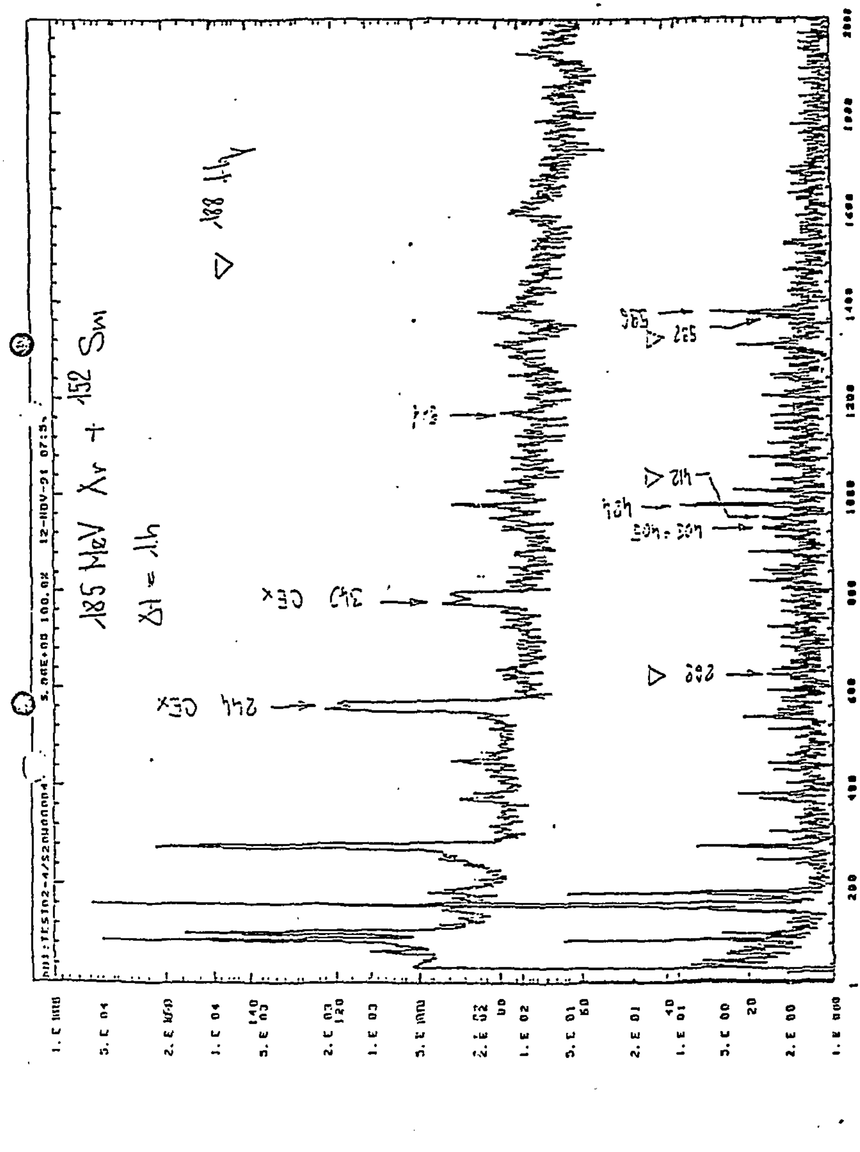
185 MeV Xe + 152 Sm
Δt = 1μ
244 CEX
342 CEX
188 Hg
ADZON

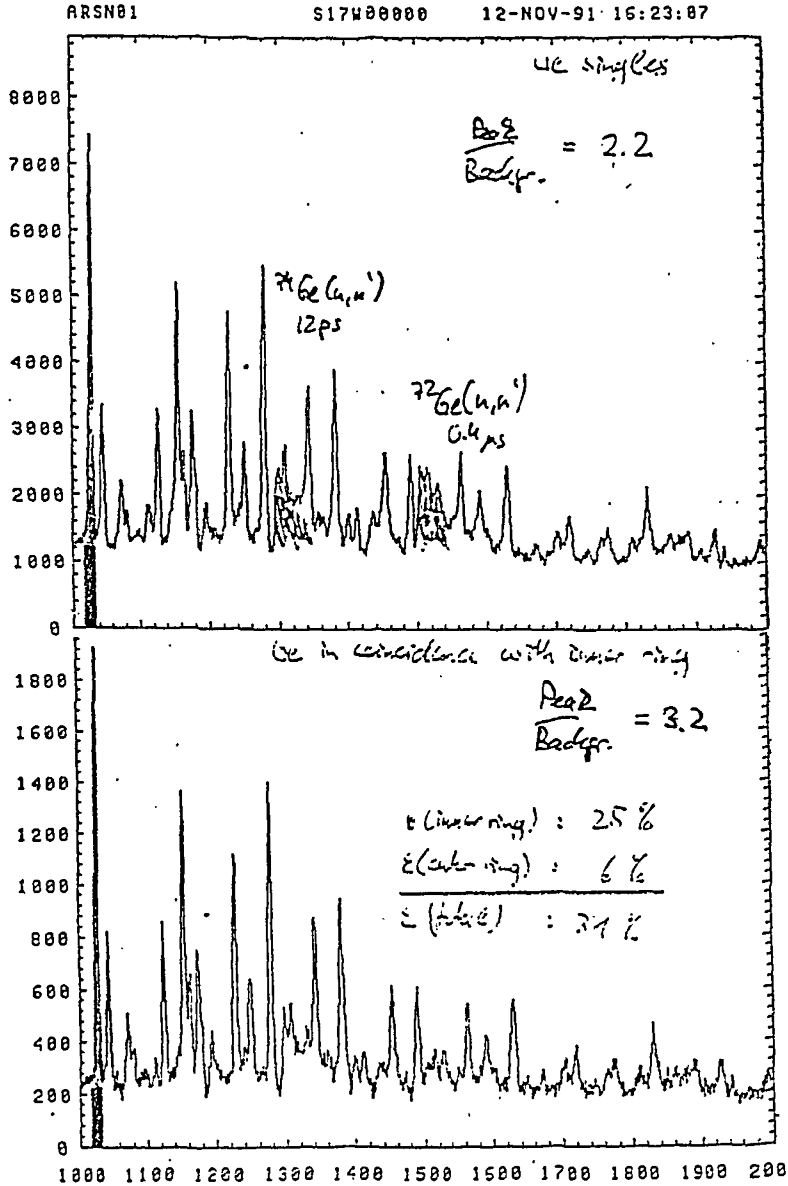

6 % fission

14 mg/cm²

TRIM simulations:

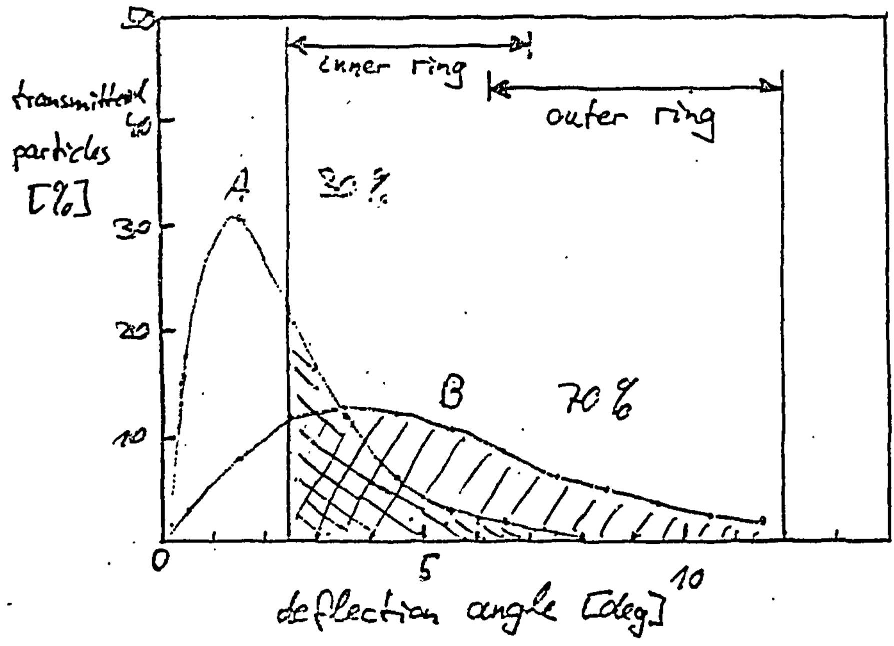

A: ^{160}Er in 0.3 $\frac{mg}{cm^2}$ ^{124}Sn 425 MeV

B: ^{188}Hg in 0.6 $\frac{mg}{cm^2}$ ^{152}Sm 356 MeV

$\frac{1}{2}$ target half-thickness !

current problems and future

problems

mechanics:
- rigid coupling of beamline, target chamber and detector

electronics:
- DC shifts
- limiting countrate

detector
- e^- yield for evaporation residues too small
- efficiency

future

- reduce HV
- use thinner scintillators
- optimise target thickness
- optimise foils
- e^- focussing

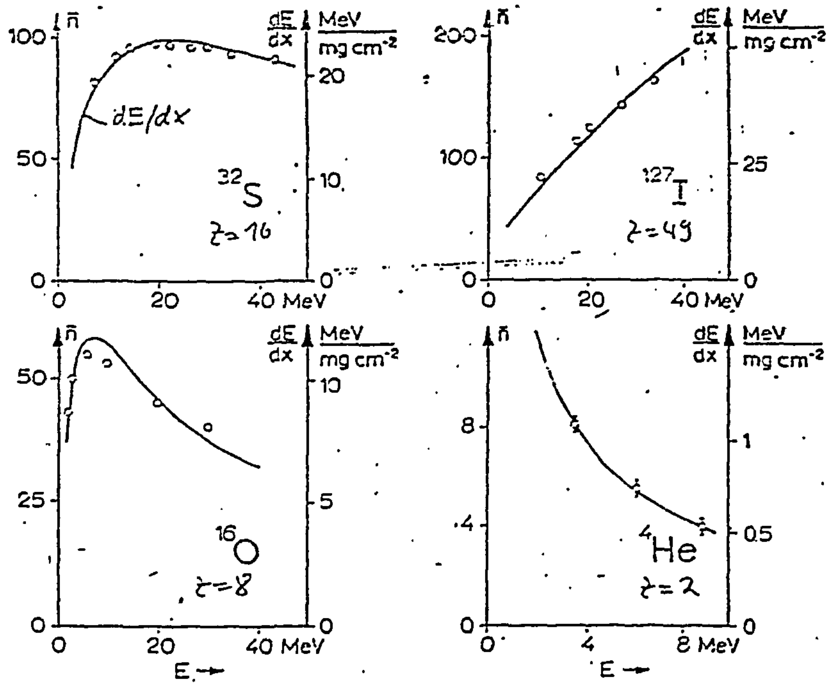

Fig. 7. Average number $\bar{n}$ of secondary electrons (left scales) emitted from one foil as a function of ion energy. Solid lines: Differential energy loss according to Northcliffe and Schilling[12]) (right scales). The normalization is different for different ions: $dE/dx = 1$ MeV/mg cm^{-2} corresponds to the following average numbers of secondary electrons: 7.4 (^{4}He), 5.0 (^{16}O), 4.2 (^{32}S), 3.8 (^{127}I).

Clerc et al.,

NIM 113 (1973), 325

24.

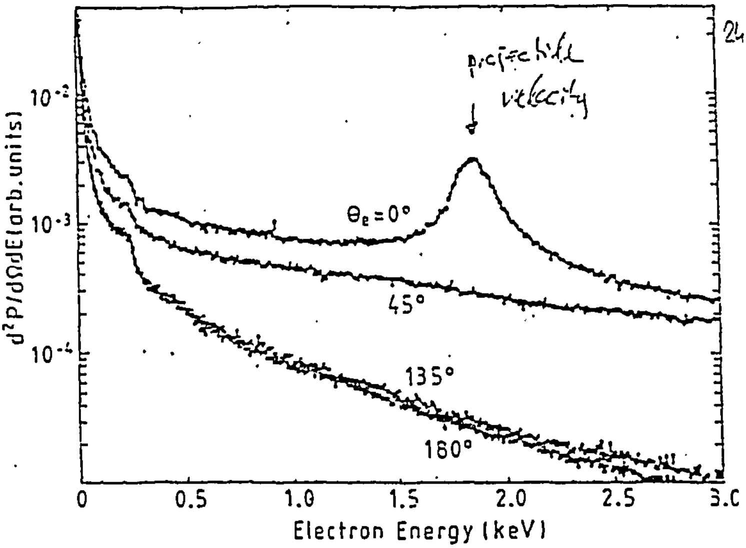

FIG. 1. Measured electron-energy spectra for different ejection angles in 70-MeV Ne^{10+} collisions with a 20 $\mu g/cm^2$ C foil (normal incidence).

Schwartz et al.
Phys. Rev. A 4?
(19??) 62?2

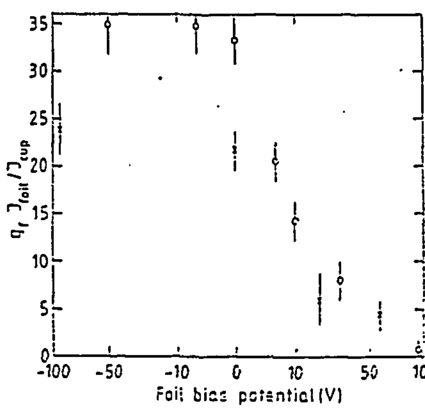

FIG. 2. Number of ejected electrons per incident ion as a function of the foil bias potential. Circles: 100-MeV Ne^{10+} − 20 $\mu g/cm^2$ C foil; crosses: 170-MeV Ne^{7+} − 100 $\mu g/cm^2$ C foil.

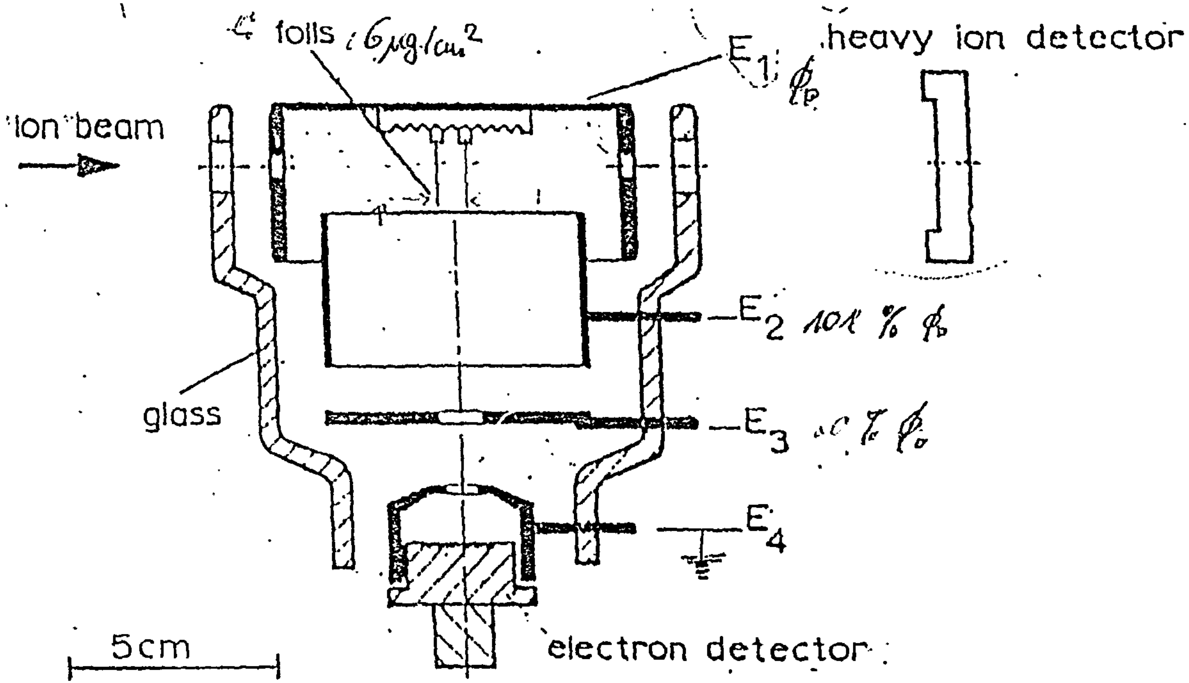

4 foils ; 6 µg/cm²
heavy ion detector
E1
ion beam
E2
E3
glass
E4
5cm
electron detector

e^- energies at projectile velocity:

- beam (185 MeV ^{40}Ar) : 25 keV

  Range in C : 1200 Å

- evaporation residues (38 MeV ^{187}Hg):

  100 eV

  Range in C: ~ 5 Å

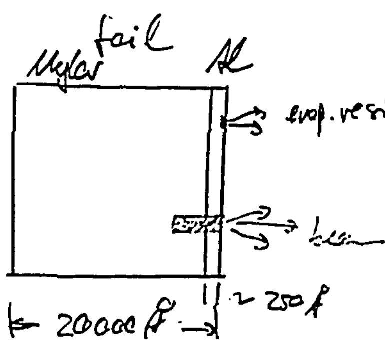

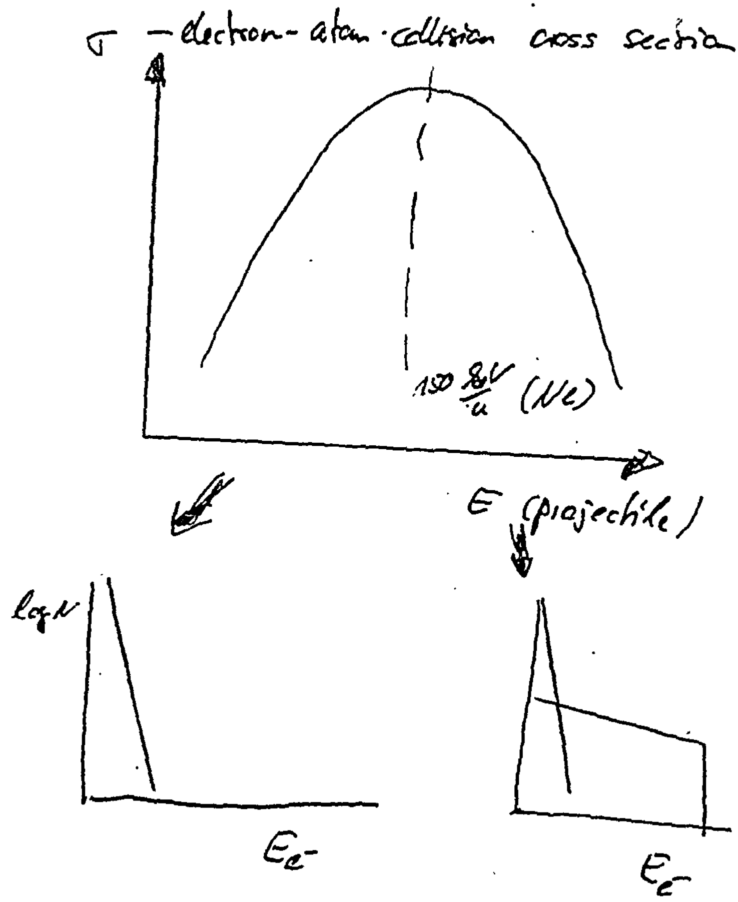

δ electron spectra

SPECTROSCOPY OF $^{199}_{84}Po_{115}$

D.B. FOSSAN, H. GRAWE, J. HEESE, H. KLUGE, K.H. MAIER,
M. SCHRAMM, R. SCHUBART, M. WARING, M.L.

HMI – BERLIN
IFJ – KRAKOW

- experiments
- results
- interpretation ?

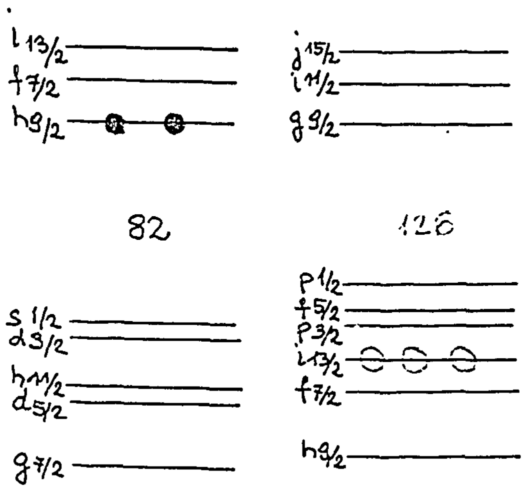

$^{183}W(^{20}Ne, 4n)^{199}Po$

I. EXPERIMENT;

target: ^{183}W; 2.3 mg/cm^2 on 50 mg/cm^2 Pb
beam: $^{20}Ne^{5+}$; 115 MeV, pulsing
detection: 6 OSIRIS detectors + neutron detector

II. EXPERIMENT;

target: ^{183}W; 18 mg/cm^2 on 50 mg/cm^2 Pb
beam: $^{20}Ne^{5+}$; 115 MeV, without pulsing
detection: 12 OSIRIS detectors

What was known before?

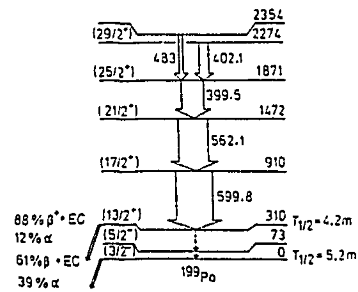

T. Weckström ... - Z. Phys. A321 (85) 231

Is there any chance to learn more?

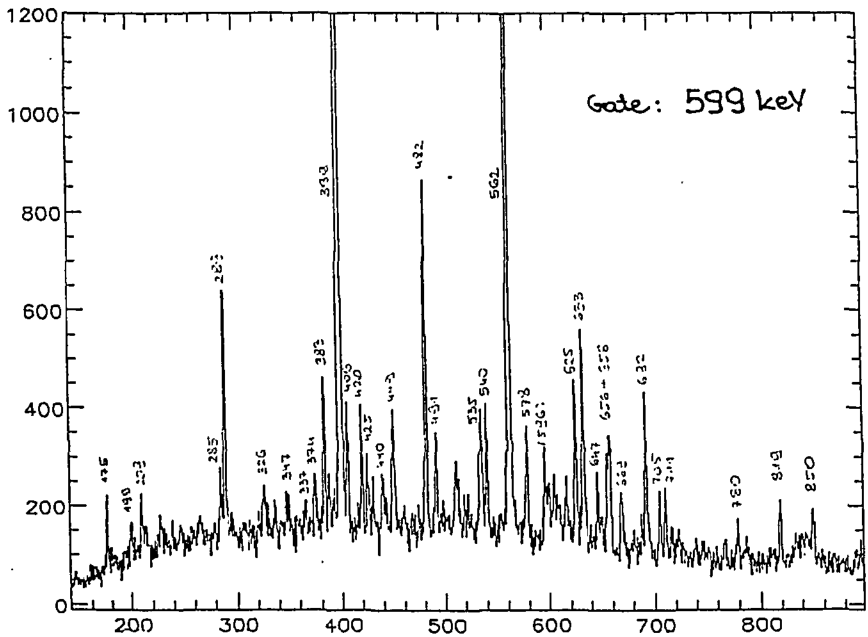

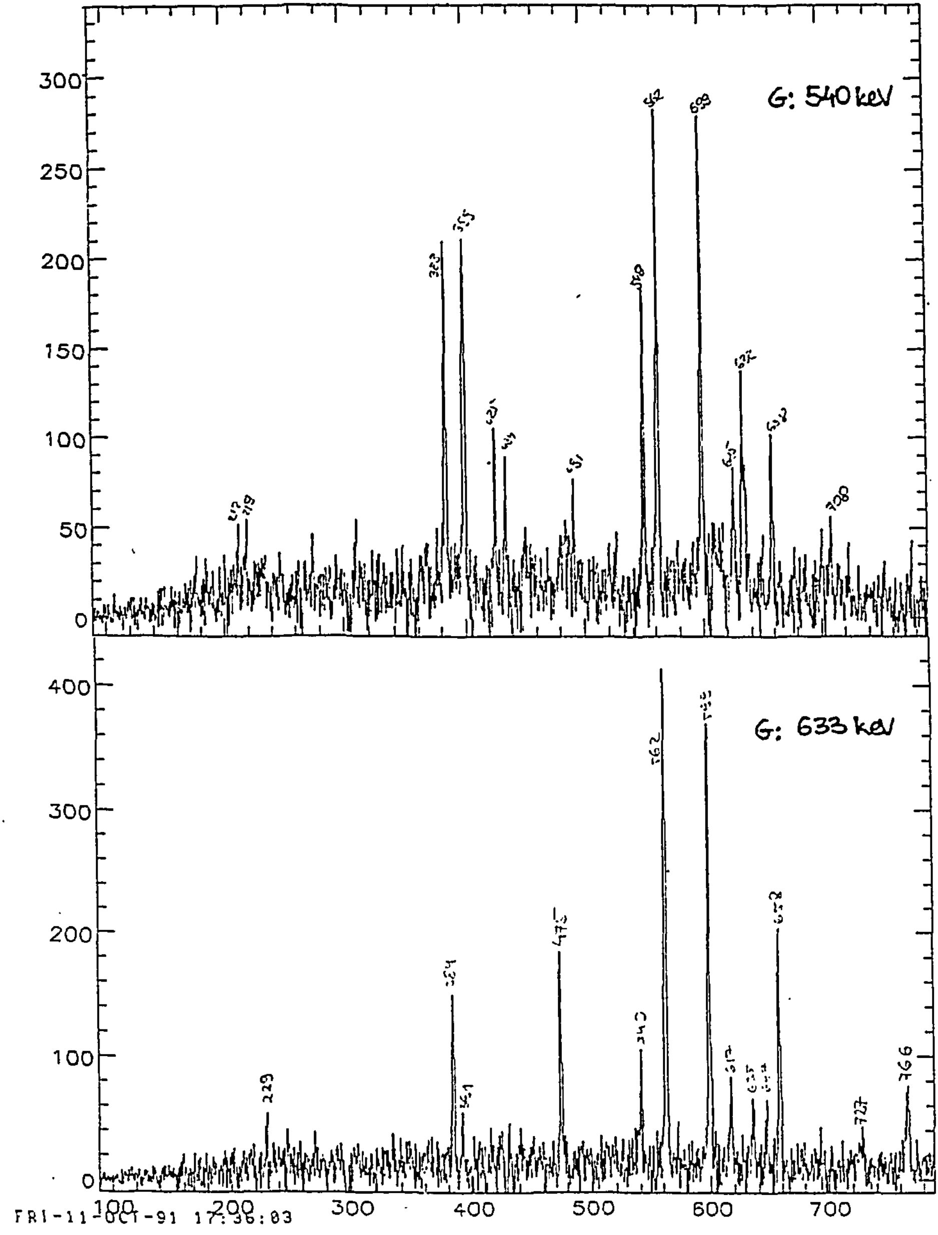

G: 540 keV
G: 633 keV
FRI-11-OCT-91 17:36:03

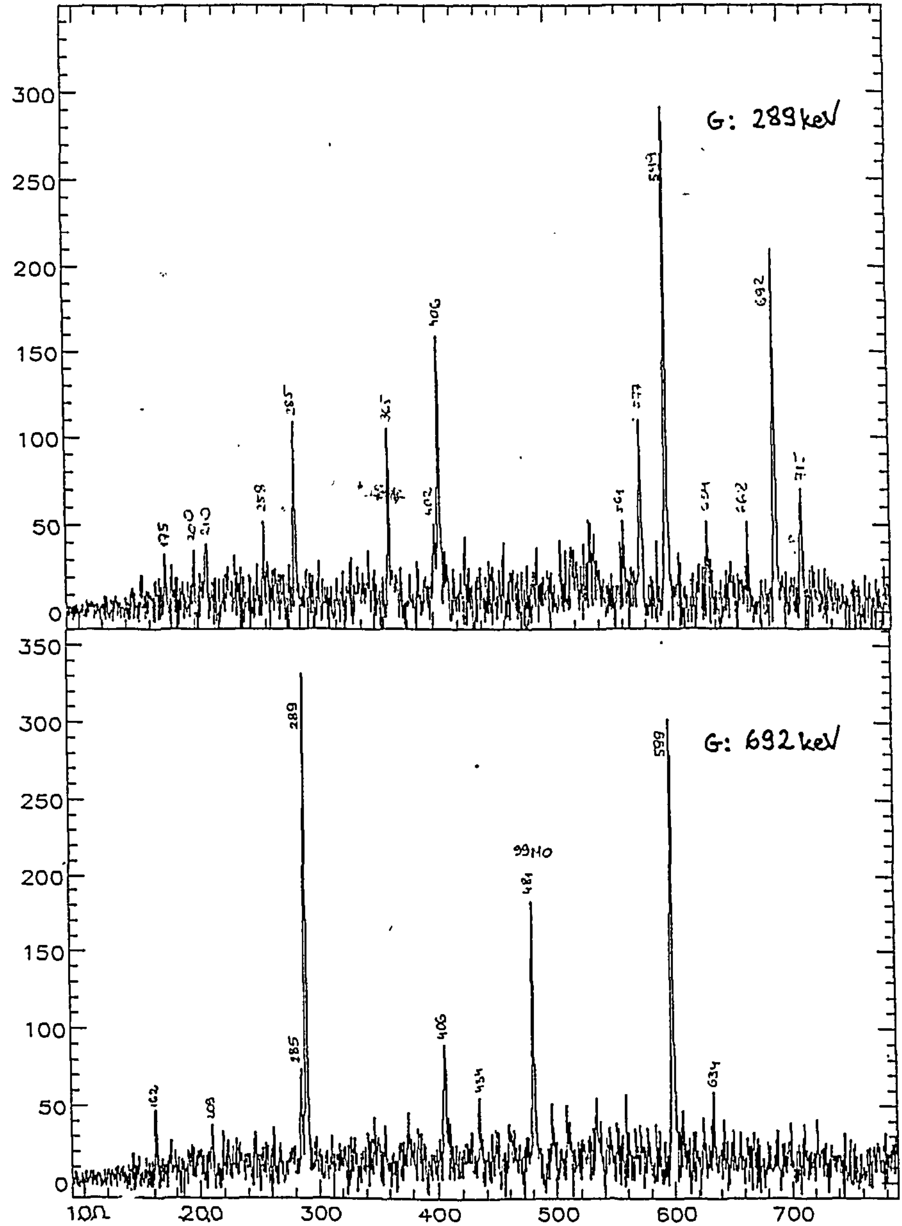
G: 289keV
175
200
210
258
285
365
402
406
561
577
599
634
662
692
717
0
50
100
150
200
250
300
G: 692keV
162
209
285
289
406
434
99Mo
481
599
634
0
50
100
150
200
250
300
350
100
200
300
400
500
600
700

DCO - analysis

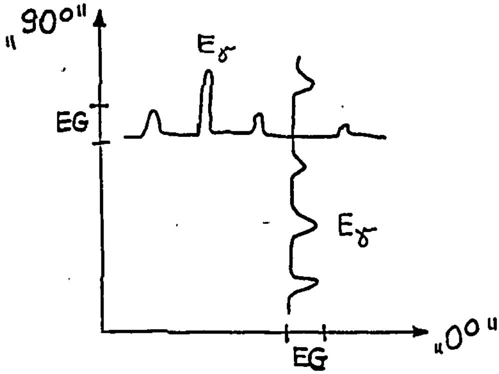

$$R = \frac{I_\gamma(E_\gamma \text{ in } 0^\circ, EG(90^\circ))\ \varepsilon(E_\gamma \text{ in } 90^\circ)\,\varepsilon(EG(0^\circ))}{I_\gamma(E_\gamma \text{ in } 90^\circ, EG(0^\circ))\ \varepsilon(E_\gamma \text{ in } 0^\circ)\ \varepsilon(EG(90^\circ))}$$

E_γ \ EG	599	562	399	482	692
599	—	.977	.948	1.272	3.029
562	.914	—	.908	1.437	
399	.921	.959	—	1.269	
482	.597	.593	.586	—	
692	.265				
289	.542				1.731

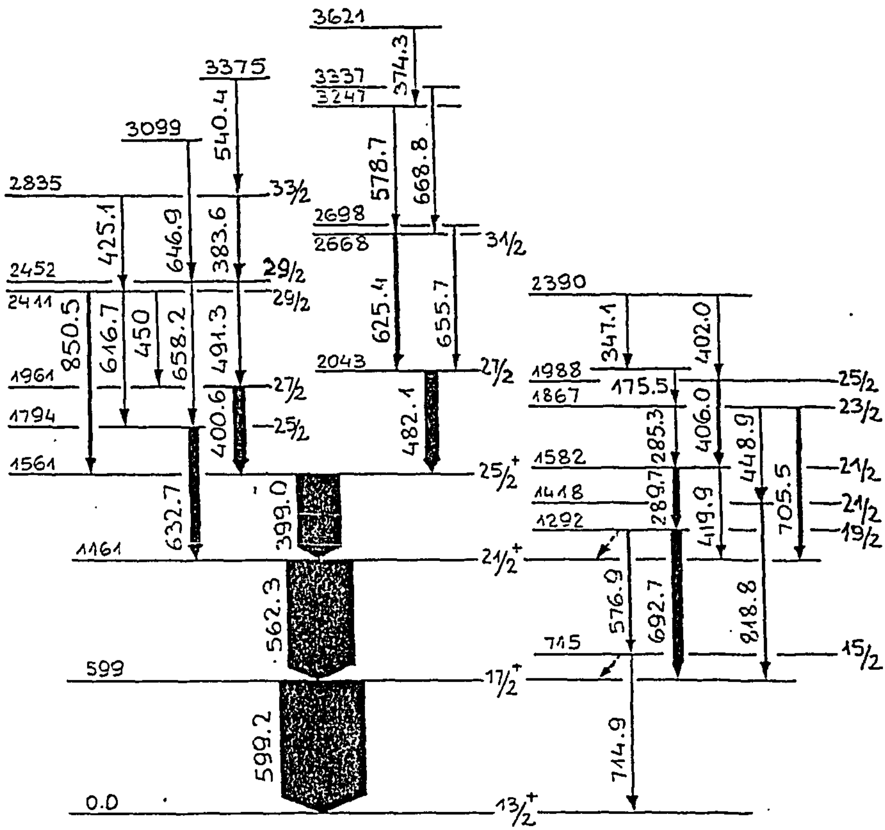
3621
3337
3247
374.3
3375
540.4
3099
668.8
578.7
2835
33/2
2698
2668
31/2
425.1
646.9
383.6
2452
29/2
2411
29/2
850.5
616.7
450
658.2
491.3
625.4
655.7
2043
27/2
1961
27/2
1794
25/2
400.6
482.1
1561
25/2+
632.7
399.0
1161
21/2+
562.3
599
17/2+
599.2
0.0
13/2+
2390
347.1
402.0
1988
25/2
175.5
1867
23/2
285.3
406.0
448.9
1582
21/2
1418
21/2
1292
19/2
289.7
419.9
705.5
576.9
692.7
918.8
715
15/2
714.9

$^{199}_{84}Po_{115}$

IN-BEAM SPECTROSCOPY OF EXOTIC NUCLEI WITH OSIRIS AND BEYOND

H. Grawe and R. Schubart in collaboration with D. Alber, R. Alfier, D.B. Fossan[1], J. Heese, H. Kluge, K.H. Maier, M. Schramm

Hahn-Meitner-Institut and Freie Universität Berlin, FRG
[1] SUNY Stony Brook, NY, USA

ABSTRACT

The experimental techniques and recent results of nuclear structure studies in-beam close to ^{100}Sn are reviewed. The structure of the nuclides ^{97}Ag, ^{100}Cd and ^{104}Sn, so far the nuclei of closest approach to ^{100}Sn with known excited states, is discussed within the spherical shell model. The basic shell model parameters of ^{100}Sn, single particle binding energies and two-body matrix elements, as deduced from the shell model analysis, are summarized. From the available structure information conclusions are drawn for the design and expected phenomena of future experiments towards the far-from-stability doubly magic ^{100}Sn.

KEYWORDS

Nuclei far from stability, experimental techniques, ^{100}Sn shell structure, single particle energies, residual interaction.

1) INTRODUCTION

The structure studies of nuclei far from stability will enter into a new phase with the current development of experimental techniques, 4π γ-ray spectrometers combined with efficient filter detectors for neutrons, charged particles and mass separated residues, radioactive ion beam facilities and exploitation of new types of nuclear reactions. In the near future it will be possible to detect nuclear structure details in these nuclei on the same level of statistical reliability as nowadays for the less exotic nuclei, which will open the field for the detection of unexpected phenomena. In expectation of the new experimental techniques there have been recently various exciting theoretical predictions especially for medium mass N=Z nuclei, where proton and neutron shell gaps are mutually reinforced. Collective oblate rotation and stable octupole deformation are predicted close to A = 70 [Bengtsson 1984, Nazarewicz 1990], and new regions of super- and hyperdeformation are expected at A=90 and 130 [Ragnarsson 1990, Garret, Olson 1991]. The doubly magic nucleus ^{100}Sn is situated in the center of this area and provides an excellent study field for single particle energies and the residual interaction specifically between protons and neutrons, on which the above mentioned predictions depend very sensitively and which cannot be studied elsewhere. Moreover, the Sn isotopic chain between the doubly magic ^{100}Sn and ^{132}Sn allows to study the spherical shell model throughout a full major shell for N/Z ratios from 1 to 1.6.

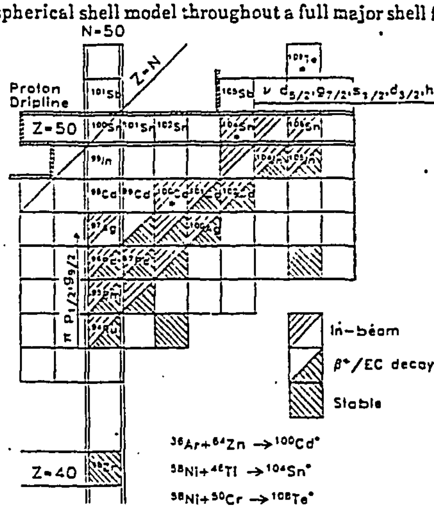

Table 1: Evaporation residue cross sections

Nucleus	Exit channel	σ^{exp} [mb]	σ^{CAS} [mb]	$\sigma^{exp}/\sigma_{tot}$ [%]
Reaction ^{58}Ni+^{46}Ti 230 MeV 2 mg/cm^2				
^{101}Cd	2pn	6.5(22)	7.4	1.6
^{100}Cd	2p2n	7.2(30)	6.4	1.8
^{99}Ag	3p2n	4.7(24)	5 6	1.2
^{97}Ag	αp2n	1.0(5)	0.5	0.3
^{99}Pd	4pn	38(10)	35	9 6
^{97}Pd	α2pn	16(5)	43	4.0
Reaction ^{58}Ni+^{50}Cr 245 MeV 2 mg/cm^2				
^{104}Sn	2p2n	5(3)	5	1.0
^{105}In	3p	35(10)	31	7
^{104}In	3pn	65(13)	48	13
^{103}In	3p2n	8(4)	9	1.6
^{104}Cd	4p	86(37)	62	17
^{103}Cd	4pn	48(12)	29	10

Fig. 1. Nuclidic chart of the ^{100}Sn region. Nuclei with excited states known from β+/EC decay and in-beam spectroscopy are drawn in different hatching. The closest stable nuclei, compound systems used in the present work and the proton dripline are shown, too.

We will give therefore in this paper a review of the nuclear structure information, which is known from in-beam studies of exotic nuclei as close to ^{100}Sn as presently possible. By means of a shell model analysis of the existing data conclusions are drawn for the shell model parameters of the yet inaccessible ^{100}Sn. In Fig. 1 a section of the nuclidic chart is shown, which demonstrates the key position of the N = Z = 50 shell closure.

(i) The proton dripline crosses the N=Z line, offering the last chance to study the T=0 proton-neutron (πν) interaction in identical orbitals, and the only one for the high spin $g_{9/2}$ shell and its spin-orbit partner $g_{7/2}$.

(ii) The dominating role of these orbitals at the Fermi surface allows to study microscopically the development of quadrupole degrees of freedom.

(iii) The $\pi g_{9/2} \rightarrow \nu\, g_{7/2}$ transformation provides a pure and undistorted case to investigate the Gamow-Teller decay and the source of its hindrance [Plochocki et al. 1991].

(iv) Finally dripline effects and proton decay can be studied under spherical shell model conditions. However, β^+/EC decay studies are hampered by the dripline. So in-beam spectroscopy is in some cases the only possible method.

2) EXPERIMENTAL DETAILS

The decay of neutron deficient compound nuclei (see Fig. 1) proceeds predominantly via charged particle emission, while the neutron evaporating exit channels leading to the most neutron deficient residues are only weakly populated. In table 1 examples of cross sections for various reactions and residual nuclei are listed and compared to predictions from the CASCADE code [Pühlhofer 1977]. Experimental values were determined from an analysis of the radioactive decay for strong exit channels and from relative intensities in the total $\gamma\gamma$-spectrum for the weaker channels. Typically about 30 residual nuclei are populated at the 1% level of the total fusion-evaporation cross section. This requires a highly selective setup to identify and study the most neutron deficient nuclei.

In Fig. 2 the OSIRIS spectrometer in its "isospin-detector" setup is shown, which was used in the present series of experiments. 12 HPGe detectors in BGO shields at 90°± 25° with a total photopeak efficiency of 0.55% at 1.33 MeV are combined with a 7 segment neutron detector at 0° with 12% efficiency for evaporation neutrons. The neutron detector is optimized to fit the 12 detector version of OSIRIS and is part of the 2π neutron multiplicity filter [Alber et al. 1988]. In the forward hemisphere the target is surrounded by an array of 4 silicon surface barriere ΔE detectors in the form of a trapezium and 250μm thickness building a cut off pyramid covering 25-30% of 4π depending on the target position. This determines proton and α particle multiplicities. Further details on the OSIRIS spectrometer and the ΔE detector array are given by Lieder et al. (1984) and Alber et al. (1986), respectively. Experiments were performed at the accelerator combination VICKSI of the Hahn-Meitner-Institute.

3) RESIDUE IDENTIFICATION AND LEVEL SCHEMES

The identification of unknown γ-ray cascades by means of the charged particle and neutron multiplicity information is illustrated in Fig. 3. Ratios of $\gamma\gamma$ coincidence intensities gated with two- and single-fold proton coincidences $I(\gamma\gamma 2p)/I(\gamma\gamma 1p)$ for different exit channels are shown in Fig. 3a for the reaction $^{58}Ni + ^{46}Ti$ at 230 MeV of the ^{58}Ni beam. Besides the average experimental values for individual nuclei also theoretical values as obtained from the well known multiplicity formula [Habs et al. 1979] with the detector efficiency from a fit are indicated (solid lines). As only true proton events were analyzed small corrections must be applied to the theoretical values in the case of additional α evaporation. In Fig. 3b the average experimental values for the ratio $I(\gamma\gamma n)/I(\gamma\gamma)$, which is independent from neutron detector cross talk due to scattering, is shown for several evaporation residues and the reaction $^{58}Ni + ^{50}Cr$ at 245 MeV. For both, protons and neutrons, the intensity ratios are distinctly grouped within their error bars according to their multiplicity and in good agreement with the theoretically expected values. Even for weakly populated exit channels as ^{104}Sn (see Fig. 3b and Table 1) a safe multiplicity assignment is possible.

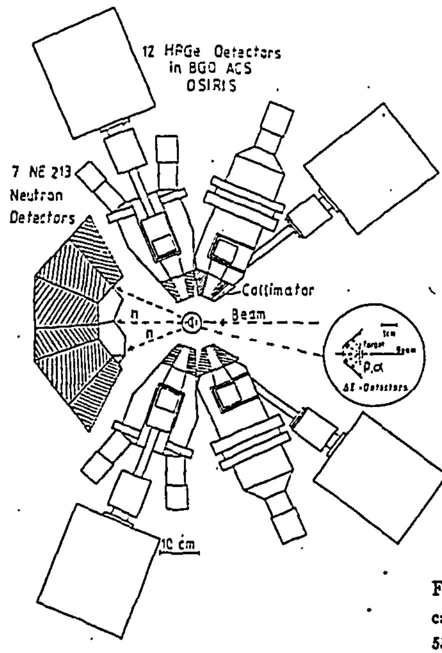

Fig.2. The OSIRIS isospin-spectrometer with neutron and charged particle multiplicity filters.

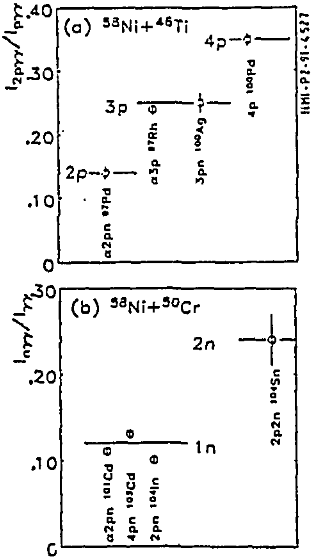

Fig. 3a. Charged particle multiplicity identification of residual nuclei in the reaction $^{58}Ni + ^{46}Ti$ at 230 MeV.
b. Neutron multiplicityidentification in the reaction $^{58}Ni + ^{50}Cr$ at 250MeV.

With the method described above the following nuclei close to ^{100}Sn have been identified for the first time in-beam (see Fig. 1); ^{97}Ag [Alber et al. 1990] ,^{100}Ag [Alfier et al. 1991], ^{100}Cd, ^{101}Cd [Alber et al. 1987], ^{104}In, ^{104}Sn [Schubart et al. 1991]. Excited states in the odd-odd ^{100}Ag and ^{104}In were known before from β^+/EC decay of ^{100}Cd [Rykaczewski et al. 1989] and ^{104}Sn [Szerypo et al. 1990], populating mainly low spin states. In the heavy ion in-beam spectroscopy of these nuclei, however, not a single γ-ray already known from the decay studies was observed, which stresses the importance of exit channel identification.

Level schemes were constructed mainly from the analysis of nγγ coincidences, which are least contaminated by the strong exit channels with only charged particle evaporation. To demonstrate the quality of the data even for weakly populated residues in Fig. 4a a nγγ coincidence spectrum with gate on the 1259 keV transition in ^{104}Sn is shown. Level sequences are determined in the order of decreasing γ-ray intensities, from cross over transitions and lifetime information. Generally, the neutron deficient nuclei discussed here are populated too weakly to possibly analyze DCO ratios for multipolarity determination. Spin and parity assignments are therefore mainly taken from systematics. Supplementary information, however, can be drawn from electronic lifetime measurements (see Fig. 4b) and Doppler shift (or broadening) making use of E1, E2 and M1 strength values known to be typical for the ^{100}Sn region. In particular:

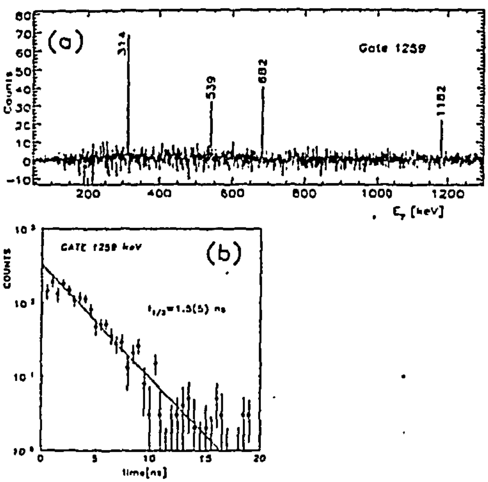

Fig. 4a. nγγ coincidence spectrum for ^{104}Sn with gate on the 1259 keV.
b. Time delay spectrum for the 1259 keV transition.

(i) Doppler shifted (or broadened) γ-rays below 700 keV are likely to be M1 transitions due to the dominating proton π $g_{9/2}$ orbital (see e.g. Piel et al. (1990)).

(ii) E2 transitions are weak close to the double shell closure, i.e. non Doppler shifted γ-rays and ns isomers are mainly E2 (or E1) transitions.

The level schemes shown in Figs. 5,7,8 have been constructed along these lines.

4) SHELL MODEL ANALYSIS AND NUCLEAR STRUCTURE CLOSE TO ^{100}Sn

The N = 50 isotone ^{97}Ag with three proton holes in the doubly-magic ^{100}Sn core, so far is the closest experimental approach to ^{100}Sn with known excited states. Therefore the basic shell model parameters as single particle binding energies (spe) and the two-body matrix elements (tbme) of the residual interaction cannot be determined empirically from experimental levels of the ^{100}Sn ± one- and two- particle (hole) neighbors. Several previous shell model investigations of N = 50 [Alber et al. 1990, Gloeckner, Serduke 1974, Blomquist, Rydström 1985, Ji, Wildenthal 1988, Alber et al. 1989] and N = 49 [Gross, Frenkel 1976] isotones, however, have resulted in a reliable empirical set of spe and tbme within a proton (π) and neutron (ν) $p_{1/2}$, $g_{9/2}$ model space. Little is known experimentally about the $\pi\nu$ and $\nu\nu$ residual interaction for the open N>50 shell with the $\nu d_{5/2}$, $g_{7/2}$, $s_{1/2}$ and $d_{3/2}$ orbitals (see Fig. 1). A realistic set of tbme has been derived in a π $p_{1/2}$, $g_{9/2}$ $\nu d_{5/2}$, $g_{7/2}$, $s_{1/2}$, $d_{3/2}$ space from nuclcon-nucleon phase shifts using the Sussex and Yale codes [Skouras, Dedes 1977] and was successfully applied to N=51 nuclei around ^{90}Zr.

In our shell model analysis of N$\geq$50, Z$\leq$50 nuclei close to the double shell closure we have adopted the following assumptions:

(i) We have used a hypothetical ^{100}Sn core and a $\pi(p_{1/2})$, $g_{9/2}$ $\nu d_{5/2}$, $g_{7/2}$, $s_{1/2}$, $d_{3/2}$ model space to calculate positive parity levels. We have omitted the least bound $\nu h_{11/2}$ intruder state. For N>51 nuclei the π $p_{1/2}$ orbital was omitted and the $\pi g_{9/2}{}^2$ interaction accordingly renormalised leaving the π^{-2} spectrum unchanged.

(ii) the $\pi\pi$ interaction was taken from a seniority conserving set of empirical tbme derived for N=50, 51 nuclei in a $p_{1/2}$, $g_{9/2}$ proton space [Gloeckner, Serduke 1974]. The proton-neutron ($\pi\nu$) interaction for $\pi(p_{1/2}, g_{9/2})$ $\nu d_{5/2}$ was taken from the known multiplets in ^{90}Y and ^{92}Nb for the diagonal part, and from the average of the two sets of realistic tbme derived from the Sussex and Yale codes [Skouras, Dedes 1977], for the remaining model space. The latter was used also for the $\nu\nu$ interaction. To account for the different model spaces used in the derivation of empirical and realistic tbme, we allowed for a general scaling factor and shift of the realistic diagonal matrix elements. It was found that only the $\nu\nu$ tbme had to be increased by 40% with a general shift of 0.33 MeV, which enters only into the calculation of absolute g.s. binding energies.

(iii) With this given residual interaction the single particle binding energies relative to a ^{100}Sn core can be calculated from those relative to ^{90}Zr using Racah algebra (c.f. Blomquist, Rydström (1985), de Shalit, Talmi (1963)). Taking the ^{90}Zr values from experiment [Blok et al. 1976] the following spe are derived for ^{100}Sn: $\varepsilon(\pi p_{1/2}{}^{-1})$ = 3.38 MeV, $\varepsilon(\pi g_{9/2}{}^{-1})$ = 3.00 MeV, $\varepsilon(\nu d_{5/2})$ = -11.13 MeV, $\varepsilon(\nu g_{7/2})$ = -10.93 MeV, $\varepsilon(\nu s_{1/2})$ = -8.33 MeV, $\varepsilon(\nu d_{3/2})$ = -8.24 MeV.

(iv) For the calculation of E2 matrix elements effective charges e_π=1.75 and e_ν=1.50 have been used as derived from E2 transitions and moments around ^{90}Zr [Gloeckner, Serduke 1974, Raghavan et al. 1985].

With these model assumptions we have calculated levels and g.s. binding energies in N=50, 51 isotones [Alber et al. 1989, 1990], Sn isotopes with A$\leq$ 107, Q_{EC} values for even N=50, Sn and Cd nuclei [Plochocki et al. 1991], Gamow-Teller distributions for even N=50 parent nuclei [Plochocki et al. 1991], selected quadrupole moments and B (E2) values in ^{100,101,102}Cd [Alber et al. 1987]. Only part of these results will be discussed in the context of this paper (Figs. 5-8).

In Fig. 5 the experimental level scheme of $^{97}_{47}$Ag$_{50}$ with three proton holes in the ^{100}Sn core is compared to a pure $\pi(p_{1/2}, g_{9/2})^{-n}$ shell model calculation (SM-PG) and a π $g_{(9/2)}{}^{-n}$ approach (SM-G)

[Alber et al. 1990]. Both theoretical approaches reproduce the experiment equally well, justifying the assumptions made in (i, ii) for the ππ interaction.

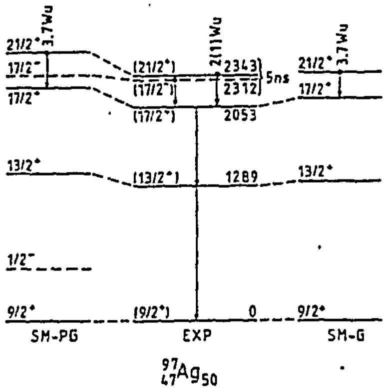

Fig. 5. Experimental and shell model level scheme for the N = 50 nucleus ^{97}Ag.

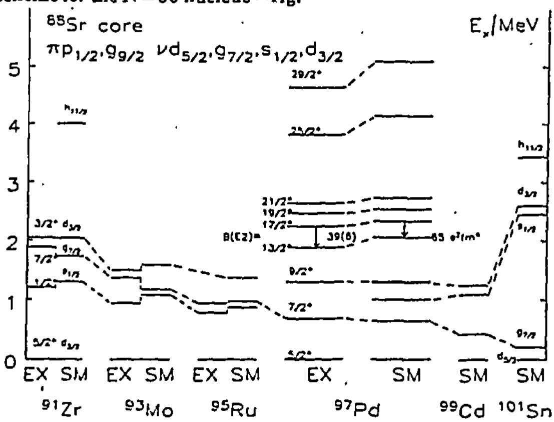

Fig. 6. Shell model calculation for neutron single particle states in N = 51 nuclei. Values are from Piel et al. (1990), Nuclear Data Sheets (1972, 1983, 1990)

A crucial test of the πν interaction is provided by the development of the neutron single particle binding energies going from ^{90}Zr to ^{100}Sn. In Fig. 6 for the odd N = 51 isotones the experimentally known lowest $I^\pi = 1/2^+$, $3/2^+$ and $7/2^+$ states relative to the $I^\pi = 5/2^+$ ground states are compared to the shell model results. The most prominent feature is the dramatic decrease of the $\nu g_{7/2}$-$\nu d_{5/2}$ splitting from over 2 MeV in ^{91}Zr to almost degeneracy in ^{101}Sn, which is also seen experimentally up to ^{97}Pd. This unique behavior is due to the strongly interacting $\pi g_{9/2}$ $\nu g_{7/2}$ spin-orbit partners and cannot be reproduced by a schematic interaction as e.g. MSDI with common strength parameters for all πν multiplets. The shell model calculation accounts also very well for the level scheme [Piel et al. 1990] and the B(E2) strength from the $I^\pi = 17/2^+$ isomer in ^{97}Pd, measured in the present series of experiments [Alber et al. 1990]. This establishes confidence in the ^{100}Sn single particle binding energies (iii).

To demonstrate the appropriate choice of the νν interaction (ii) (and the neutron spe) the experimental and theoretical level schemes for ^{104}Sn and ^{106}Sn are shown in Fig. 7. The experimental level splitting clearly corroborates the increased νν interaction strength. Also, due to the near-degeneracy of the $\nu d_{5/2}$ and $\nu g_{7/2}$ orbital no subshell effect at N = 56 is observed. ^{104}Sn is situated, at the proton drip line. This may explain the constancy or even slight increase in the B(E2, $6^+ \rightarrow 4^+$) as compared to ^{106}Sn and the failure to reproduce this value theoretically for ^{104}Sn.

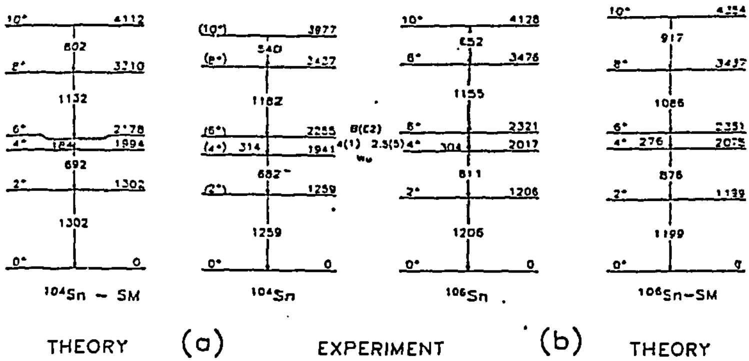

Fig. 7. Experimental and shell model level scheme for ^{104}Sn and ^{106}Sn. Experimental data for ^{106}Sn are fromAzaiez et al. (1989), Andrejtscheff et al. (1989).

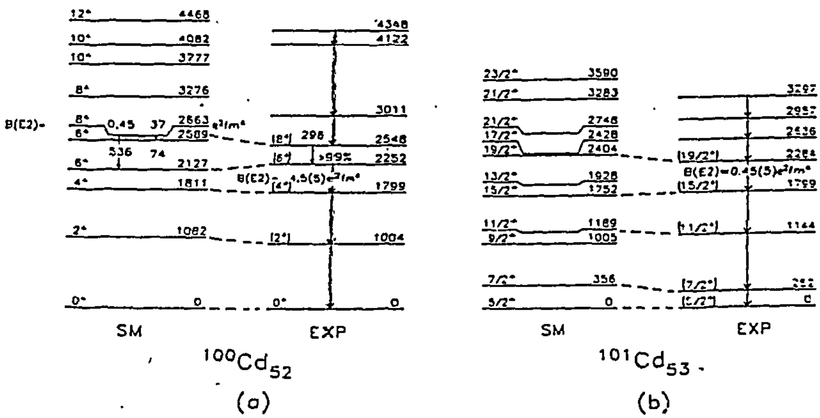

Fig. 8. Experimental and shell model level scheme for ^{100}Cd and ^{101}Cd.

Finally, to test proton and neutron excitations simultaneously we show in Fig. 8 the experimental level schemes of ^{100}Cd and ^{101}Cd in comparison to shell model predictions. The pure proton $\pi(g_{9/2})^{-2}$ character of the $I^\pi=8^+$ isomer in ^{100}Cd, as proven by the g-factor $g=1.24(6)$, the neutron character of the experimentally observed $I^\pi=6^+$ state leading to the isomerism and the missing γ-ray branch to the proton $I^\pi=6_2^+$ state is nicely reproduced in the shell model. The absolute value of the isomeric B(E2) strength between these states of entirely different intrinsic structure is underestimated in theory.

5) SUMMARY AND FUTURE EXPERIMENTS TOWARDS ^{100}Sn

With the present knowledge of the shell structure around ^{100}Sn as resulting from the analysis of the available experimental data sound predictions can be made for nuclei yet inaccessible, that can be tested in future experiments. In Fig. 9 the experimental single particle structure ("EXP") is compared to theoretical predictions from the generalized Woods-Saxon (WS) and the folded Yukawa (FY) potentials [Leander et al. 1984]. Considerable deviations are found for some orbitals and the neutron shell gap. The ^{100}Sn ground state is bound by 3.0 MeV against proton decay and predictions for ^{99}In and ^{101}Sn can be read from the figure. With the new generation of 4π γ-arrays implemented with filter detectors for evaporated particles and recoiling residues the nuclei ^{98}Cd, ^{99}Cd and ^{102}Sn will be accessible, probing the ππ, πν and νν residual interaction, respectively. As can be seen in Fig. 9 protons are unbound in ^{101}Sb; ^{105}Sb provides the last experimental access to the position of the proton levels beyond Z = 50. Typical cross sections for the production of these nuclei employing stable beams and targets in fusion - evaporation reactions are between 50μb and 1mb. A word of caution might be appropriate as to the experimental equipment. Most of these crucial probe nuclei are predicted to have isomers in the ns to μs region. This may limit the applicability of recoil mass separators and seems to favor an upgraded version of the setup described in section 2.

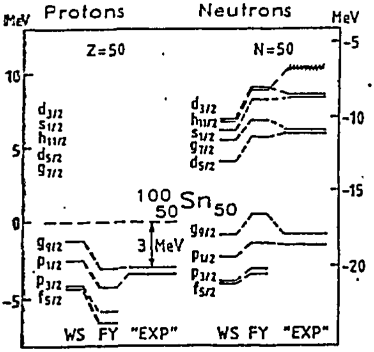

Fig. 9. Single particle levels for a ^{100}Sn core as deduced from the present shell model analysis. Theoretical values for the universal Woods-Saxon (WS) and folded Yukawa potentials (FY) are from Leander et al. (1984).

A further approach towards a spectroscopy of ^{100}Sn requires radioactive ion beams. The intensities foreseen for secondary beams produced by the facilities presently discussed [Garret, Olson 1991, Haas et al. 1990] restrict fusion-evaporation residue production to cross sections below 100μb. Therefore relativistic heavy ion beams may be more promising to reach the ultimate goal ^{100}Sn.

References

Alber, D., H. Grawe, H. Haas, B. Spellmeyer, Ein 2π-Detector für Protonen und α-Teilchen zum Einbau in OSIRIS (1986), Annual Report 1986, HMI-B Nr. 441, p. 127

Alber, D., H. Grawe, H. Haas, B. Spellmeyer, X. Sun (1987), In-beam study of neutron -deficient

^{100}Cd, Z. Physik A-Atomic Nuclei 327, 127 and to be published

Alber, D., H. Grawe, H. Haas, B. Spellmeyer, (1988), A 2n neutron multiplicity filter for in-beam γ-ray spectroscopy of neutron deficient nuclei, Nucl. Instr. and Meth. in Physics Research A263, 401

Alber, D., H.H. Bertschat, H. Grawe, H. Haas, B. Spellmeyer, (1989), Nuclear structure studies of the neutron deficient N = 50 nucleus ^{96}Pd, Z. Phys. A-Atomic Nuclei 332, 129

Alber, D., H.H. Bertschat, H. Grawe, H. Haas, B. Spellmeyer, X. Sun (1990), First in-beam observation of ^{97}Ag - The three-proton-hole spectrum in ^{100}Sn, Z. Physik, A-Atomic Nuclei 335, 265

Alfier, R., D. Alber, H. Grawe, H. Kluge, K.H. Maier, R. Schubart, D.B. Fossan, W.F. Piel, jr., (1991), In-beam spectroscopy of the neutron deficient nucleus ^{100}Ag, HMI preprint, to be published

Andrejtscheff, W., L.K. Kostov, P. Petkov, Y.S. Savane, C. Stoyanov, P. von Brentano, J. Eberth, R. Reinhardt, K.O. Zell (1989), Electric quadrupole transition strengths of the type $6_1^+ \rightarrow 4_1^+$ in $^{106\text{-}112}$Sn, Nucl. Phys. A505, 397

Azaiez, A., S. Andriamonje, J.F. Chemin, M. Fidah, J.N. Scheurer, M.M. Aleonard, G. Bastin, J.P. Thibaud, F. Beck, G. Costa, J.F. Bruandet, F. Liatard (1989), High spin states in neutron deficient ^{106}Sn and ^{108}Sn isotopes, Nucl. Phys. A501, 401

Bengtsson, R., P. Möller, J.R. Nix, J.Y. Zhang (1984), Nuclear shapes and shape transitions, Phys. Scr. 29, 402

Blok, H.P.-, L. Hulstman, E.J. Kaptein, J. Blok (1976), Investigation of ^{91}Zr by high resolution (d,p), (p,p') and (p,d) reactions, Nucl. Phys. A273, 142

Blomquist, J., L. Rydström (1985), Shell model discription of the N = 50 isotones between ^{88}Sr and ^{100}Sn, Phys. Scr. 31, 31

Garret, J.D., D.K. Olson, eds. (1991), A proposal for physics with exotic beams at the Holifield Heavy Ion Research Facility, Physics Division ORNL, Oak Ridge, Tennessee

Gloeckner, D.H., F.D.J. Serduke (1974), Shell model study of N = 50 nuclei, Nucl. Phys. A220, 477

Gross, R., A. Frenkel (1976), Effective interaction of proton and neutrons in the $2p_{1/2}$ - $1g_{9/2}$ subshells, Nucl. Phys. A267, 85

Haas, H., H. Ravn, A. Schempp, B.W. Allardyce, B. Jonson, C. Rolfs (1990) in: Radioactive Nuclear Beams, ed. W.D. Myers, J.M. Nitschke, E.B. Norman, Word Scientific, Singapore, p. 59

Habs, D., F.S. Stephens, R.M. Diamond (1979), A proposal for a crystal ball detector system, LBL Berkeley, CA, USA, preprint PUB-5020

Ji, S., B.H. Wildenthal (1988), Effective interaction of N = 50 isotones, Phys. Rev. C37, 1256 and C38, 2849

Leander, G.A., J. Dudek, W. Nazarewicz, J.R. Nix, Ph. Quentin (1984), Single particle levels in the doubly magic ^{132}Sn and ^{100}Sn nuclei, Phys. Rev. C30, 416

Lieder, R.M., H. Jäger, A. Neskakis, T. Venkova, C. Michel (1984), Design of a BGO Anti-Compton spectrometer and its use in nuclear spectroscopy, Nucl. Instr. and Meth. 220, 363

Nazarewicz, W. (1990), Low energy octupole and dipole modes in nuclei, Nucl. Phys. A520, 333c

Nuclear Data Sheets (1972) B8, 477; (1983) 38, 1; (1990) 60, 835

Piel, W.F., jr, D.B. Fossan, R. Ma, E.S. Paul, N. Xu, J.B. McGrory (1990), High spin structure of N = 51 ^{96}Rh and ^{97}Pd: A shell model study, Phys. Rev. C41, 1223.

Płochocki, A., K. Rykaczewski, T. Batsch, J. Szerypo, J. Zylicz, R. Barden, O. Klepper, E. Roeckl, D. Schardt, H. Gabelmann, P. Hill, H. Ravn, T. Thorsteinsen, I.S. Grant, H. Grawe, P. Manakos, L. D. Skouras (1991), Gamow-Teller Beta decay of the very neutron-defficient N=50 nuclide ^{98}Cd, GSI preprint GSI-91-31 and Z. Physik A, in print.

Pühlhofer, F. (1977), On the interpretation of evaporation residue mass distributions in heavy-ion induced fusion reactions, Nucl. Phys. A280, 267

Raghavan, P., M. Senba, Z.Z. Ding, A. Lopez-Garcia, B.A. Brown, R. S. Raghavan (1985), E2 effective charge of $g_{9/2}$ nucleons derived from quadrupole moments of high-spin isomers in ^{88,90,91}Zr and ^{90,92,93}Mo, Phys. Rev. Lett. 54, 2592

Ragnarsson, I. (1990) in: Proc. of the Workshop on the Science of intense radioactive ion beams, ed. J.B. McClelland, D.J. Vieria, LNL Report LA-11964, p.199

Rykaczewski, K., A. Plochocki, J. Zylicz, I.S. Grant, H. Gabelmann, R. Barden, D. Schardt, O. Klepper, E. Roeckl, G. Nyman (1989), The Gamow-Teller β-decay of ^{100}Cd, Z. Physik A-Atomic Nuclei 332, 275

Schubart, R., D. Alber, R. Alfier, C. Bach, D.B. Fossan, H. Grawe, H. Kluge, K.H. Maier, M. Schramm, M. Waring, L. Wood (1991), In-beam spectroscopy of ^{104}Sn, Z. Physik A-Atomic Nuclei 340, 109

de Shalit, A., I. Talmi (1964), Nuclear Shell Theory, Academic Press, New York, USA, ch. 37,

Skouras, L.D., C. Dedes (1977), Even-parity states of ^{95}Tc. Phys. Rev. C15, 1873

Szerypo, J., R. Barden, L. Kalinowski, R. Kirchner, O. Klepper, A. Plochocki, E. Roeckl, K. Rykaczewski, D. Schardt, J. Zylicz, (1990), Low-lying levels in ^{104}In and a problem of spin-mixing in hyperfine fields, Nucl. Pyhs. A507, 357

46

Z. Phys. A Hadrons and Nuclei 340, 109-110 (1991)

Zeitschrift für Physik A Hadrons and Nuclei
© Springer-Verlag 1991

Short note

In-beam spectroscopy of ^{104}Sn

R. Schubart[2], D. Alber[2], R. Alfier[2], C. Bach[2], D.B. Fossan[1], H. Grawe[2], H. Kluge[2], K.H. Maier[2], M. Schramm[2], M. Waring[1], and L. Wood[2]

[1] SUNY Stony Brook, NY, USA
[2] Hahn-Meitner-Institut and Freie Universität Berlin, Federal Republic of Germany

Received June 6, 1991

Abstract: The very neutron deficient nucleus ^{104}Sn has been identified in in-beam spectroscopy using the reaction ^{50}Cr(^{58}Ni, 2p2n) and neutron and charged particle multiplicity filter detectors. Excited states up to $I \approx 10$ and $E_x = 4$ MeV were observed and the level scheme is discussed in the frame work of the spherical shell model.

The spectroscopic approach to the extremely neutron deficient doubly magic ^{100}Sn has made substantial progress recently. ^{97}Ag [1] and ^{100}Cd [2] have been studied in-beam and ^{98}Ag in the β^+/EC decay of ^{98}Cd [3]. From these studies fairly good knowledge of the proton-proton-(ππ) and proton-neutron (πν) residual interaction and single particle binding energies was obtained. Much less is known about the neutron-neutron (νν) interaction in the light semimagic Sn isotopes. Due to the near-degeneracy of the $\nu d_{5/2}$ and $\nu g_{7/2}$ orbitals at Z=50 the N=56 subshell closure disappears [4,5] and therefore little is known on the $\nu g_{7/2}{}^2$ and $\nu g_{7/2}\,d_{5/2}$ interaction. The experimental situation is complicated by the fact that the Sn isotopes with A<105 touch the proton drip line so that they cannot be populated by β^+/EC decay.

In the present work we have searched for light Sn isotopes populated in the reaction ^{50}Cr+^{58}Ni at 245 and 250 MeV energy of the Ni beam from the tandem-cyclotron combination VICKSI at the Hahn-Meitner-Institute. The target was a 2.1 mg/cm^2 foil of ^{50}Cr enriched to >97% on a 23 mg/cm^2 Au backing. The γ-rays were detected in the 6 and 12 detector version of OSIRIS [6] with the detectors positioned at 90° and 90° ±25°, respectively. Evaporation neutrons were measured in a 16 respective 7 segment close packed detector array made from hexagons and pentagons [7].

An array of four 400 μm thick 300 mm^2 large SSB ΔE-detectors served as a multiplicity filter for charged particles, discriminating also between evaporation protons and α-particles [8]. Further details on the experiments and data handling are published elsewhere [1,2].

In Fig. 1 a nγγ spectrum with gate on an unassigned 1259 keV transition is shown. The γ-rays (I) 1259, 682, 314, 1182, 539 keV are in mutual coincidence, coincident with protons but not with α-particles. In Fig. 2 the intensity ratios I(nγγ)/I(γγ) are shown for several known residual nuclei populated in the present experiment and compared to the values for the new and unassigned γ-ray cascade (I). The values for a second yet unassigned cascade (II) 1272, 522, 314, 321, 817 keV are also shown. Clearly the first cascade (I) belongs to a 2n exit channel, whereas all other γ-ray cascades are 1n. Starting with the compound nucleus $^{108}_{52}$Te$_{56}$ possible assignments are restricted to ^{104}Sn$_{54}$, ^{103}In$_{54}$ and ^{105}Sn$_{55}$, ^{104}In$_{55}$ for cascades (I) and (II), respectively, as the heavier isotones are unlikely to be populated with measurable cross section, and the lighter isotones are known. ^{104}In, with a dominating 1197keV transition, has been identified in the present series of experiments from proton multiplicity M_p=3, whereas due to the low population cross section no definite M_p can be given for cascades (I) and (II). Further evidence comes from the Doppler shift observed in the 90±25° detectors. The γ-rays of cascade (I) are unshifted as expected for E2 (or E1) transitions. The γ-rays of cascade (II), except for the 1272 and 522 keV transitions are Doppler shifted, which is expected for fast M1 transitions as known for all odd-A In and Sn isotopes.

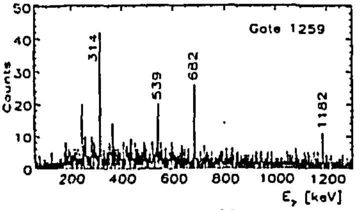

Fig. 1 Prompt nγγ spectrum with gate on the 1259 keV transition

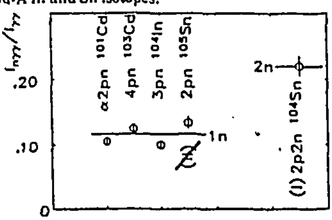

Fig. 2 Intensity ratios I(nγγ)/I(γγ) averaged over γ-ray cascades for exit channels of different neutron multiplicities.

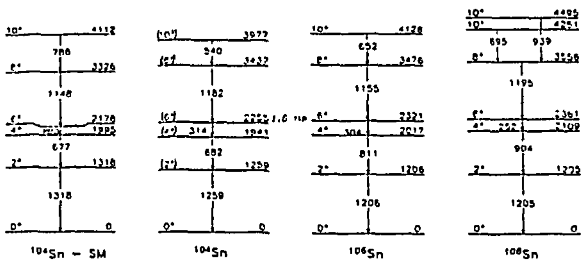

Fig. 3 Experimental level scheme for ^{104}Sn in comparison to ^{106}Sn and ^{108}Sn and a shell model calculation.

Therefore cascade (I) is assigned to ^{104}Sn and (II) consequently to ^{105}Sn. This assignment is further corroborated by the bombarding energy dependence of the relative intensites. We also made a search for the residues from the main target contaminants ^{12}C and ^{16}O with the result, that none of the known residual nuclei with proton multiplicity M_p = 2,3 and neutron multiplicity M_n = 1,2 (and M_α = 0) contains the γ-ray cascade (I) under discussion. The observed Doppler shifts exclude an assignment of the respective γ-rays to the light contaminants, as the corresponding shifts should be 50% larger. The population cross section was determined from the coincidence intensities relative to strongly populated prompt exit channels for which the cross section was determined from β^+/EC decay intensities [2]. The experimental value σ = 5(3) mb compares well with the CASCADE [9] prediction, σ = 5 mb, when averaged over the 40 MeV energy loss of the 245 MeV ^{58}Ni ions in the target. The level scheme as shown in Fig. 3 was constructed in the sequence of decreasing intensity of γ-rays and continues the trend seen in the systematics of the heavier even Sn isotopes [10,11]. Due to the low production rate the analysis of γγ angular correlation data was not feasible. The tentative spin assignments given in Fig. 3 are therefore taken from systematics. They are consistent with the Doppler shift results and the half life $t_{\frac{1}{2}}$ = 1.5(5) ns measured with the centroid shift method for the 1259 keV γ-ray, which is ascribed to the 314 keV $(6^+) \rightarrow (4^+)$ primary transition.

For comparison the yrast levels of the even Sn isotopes with neutron number N = 56 and 58 are shown on the right side of Fig. 3. Evidently there is no break in the general trend at N = 56, corroborating previous evidence [4,5] that the $\nu d_{5/2}$ and $g_{7/2}$ orbitals are nearly degenerate in ^{100}Sn. In the left part of Fig. 3 we present the result of a shell model calculation for ^{104}Sn. Experimentally little is known about the νν residual interaction for a ^{90}Zr or ^{100}Sn core. We have modified the neutron-neutron two-body matrix elements (TBME) of Skouras and Dedes [12], by scaling the average of their two sets of TBME with a factor of 1.4 to reproduce the correct level splitting in $^{92,94}Zr$ and ^{106}Sn. To account for ground state binding energies the diagonal TBME were shifted by + 310 keV. Single particle energies (s.p.e.) relative to ^{100}Sn, $\varepsilon(\nu d_{5/2})$ = -11.13, $\varepsilon(\nu g_{7/2})$ = -10.93, $\varepsilon(\nu s_{1/2})$ = -8.33 and $\varepsilon(\nu d_{3/2})$ = -8.24 MeV were calculated from the experimental ones in ^{91}Zr [13] using the $\pi g_{9/2}$ νj proton-neutron interaction as listed in ref. [12] for j = $g_{7/2}$, $s_{1/2}$, $d_{3/2}$ and from experiment (^{92}Nb) for j = $d_{5/2}$.

The present choice of TBME for the ππ, πν and νν interaction gives a satisfactory description of the N = 51 isotones, the N = 52 nucleus ^{100}Cd [2] and $^{104,106}Sn$ including the ground state binding energies. Nevertheless it should be regarded only as a starting point for a comprehensive shell model study of nuclei close to ^{100}Sn between the N = 50 isotone and Z = 50 isotope series. Furthermore it should be noted, that the correct level sequence of the $I^\pi = 2^+, 4^+, 6^+$ states is only obtained if the $s_{1/2}$ and $d_{3/2}$ subshells are included to bring the $I^\pi = 4^+$ state below the 6^+ state with predominant $(\nu d_{5/2} g_{7/2})_{6^+}$ structure.

In conclusion the spectroscopy of the lightest Sn isotopes, though hampered by low reaction yields and limited in the amount of accessible data, contributes substantially to basic shell model parameters as single particle energies and the neutron-neutron residual interaction owing to the simple structure of these nuclei.

References:

1) D. Alber et al.: Z. Physik A-Atomic Nuclei 335, 265 (1990)
2) D. Alber et al.: Z. Physik A-Atomic Nuclei 327, 127 (1987) and submitted to Z. Phys. A.
3) K. Rykaczewski et al.: to be published in Z. Physik
4) W.F. Piel et al: Phys. Rev. C 41, 1213 (1990)
5) J. Vanhorenbeeck et al.: Phys. Rev. C 39, 1528 (1989)
6) R.M. Lieder et al.: Nucl. Instr. and Meth. 220, 363 (1984); W. Gast et al.: to be published
7) D. Alber et al.: Nucl. Instr. and Meth. in Phys. Res. A263, 401 (1988)
8) D. Alber et al.: Annual Report 1986, HMI-B Nr. 441, p.127
9) F. Puhlhofer: Nucl. Phys. A 280, 267 (1977)
10) G. Auger et al.: Z. Phys. A-Atoms and Nuclei 296, 319 (1980)
11) E. Andersson et al.: Z. Phys. A-Atoms and Nuclei 299, 105 (1981)
12) L.D. Skouras, C. Dedes: Phys. Rev. C 15, 1873 (1977)
13) A.P. Blok et al.: Nucl. Phys. A 273, (1976) 142

multiplicity

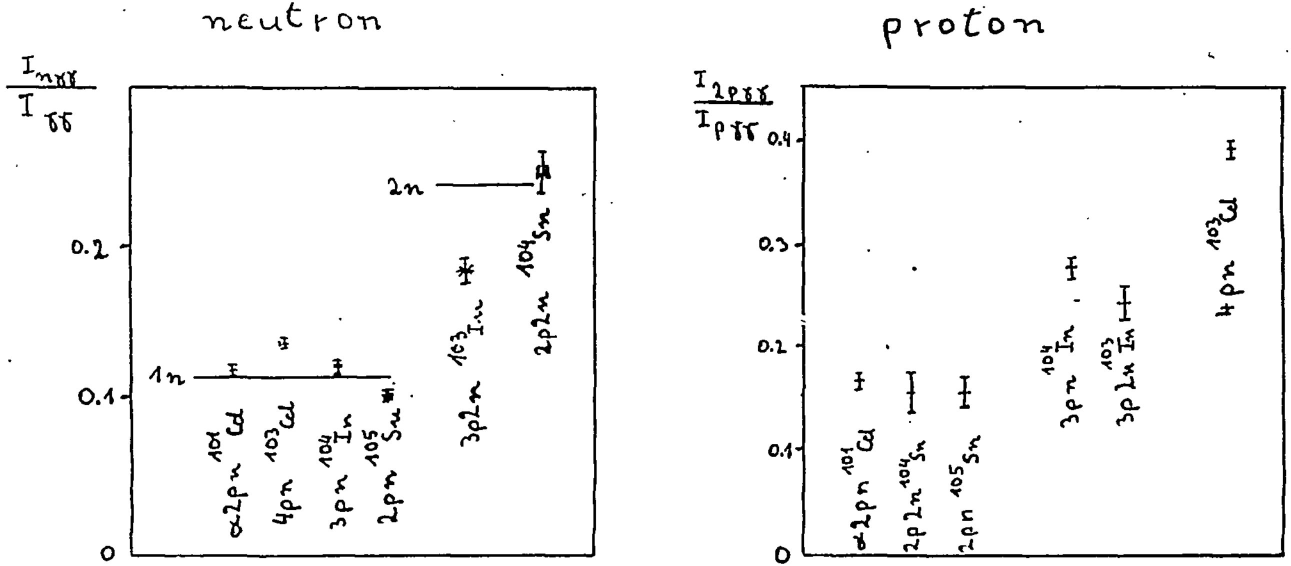

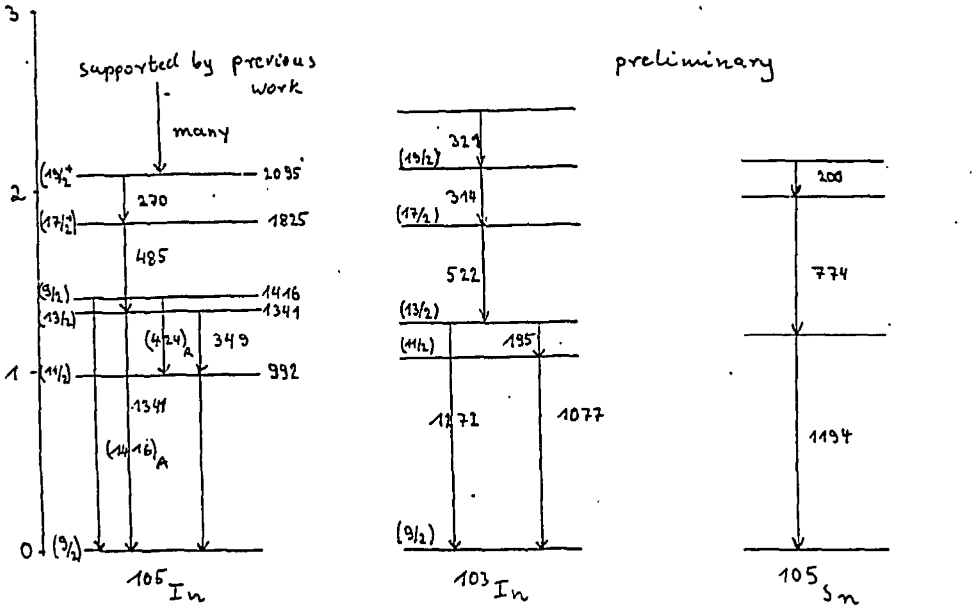

supported by previous work
many
preliminary
270
485
1341
(1416)A
(424)A
349
2095
1825
1416
1341
992
329
314
522
195
1272
1077
200
774
1194
105In
103In
105Sn

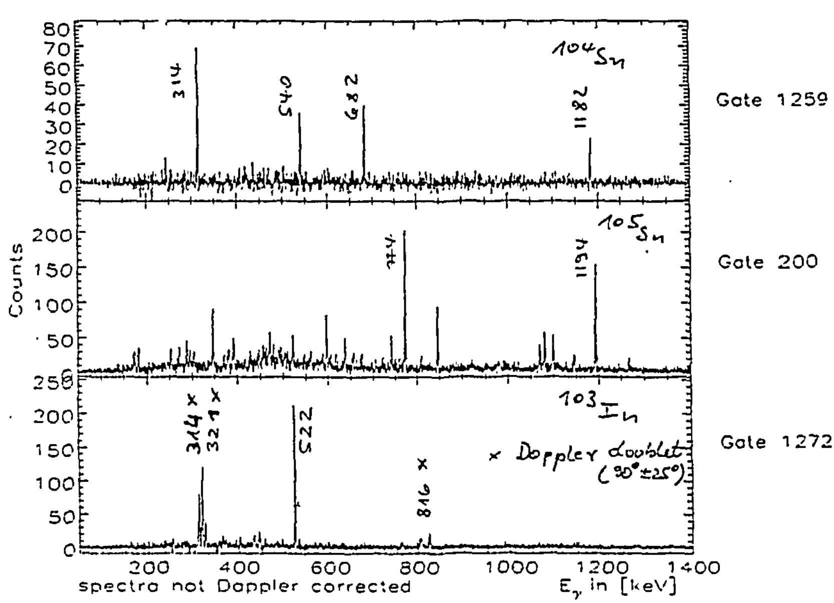

104Sn
Gate 1259
105Sn
Gate 200
103In
Gate 1272
× Doppler doublet (90°±25°)
Counts
spectra not Doppler corrected
Eγ in [keV]

4 Grawe 8.12.1932

Theoretical Predictions Z = 82

Bengtsson, Nazarewicz
Z. Phys. A 334, 269 (89)

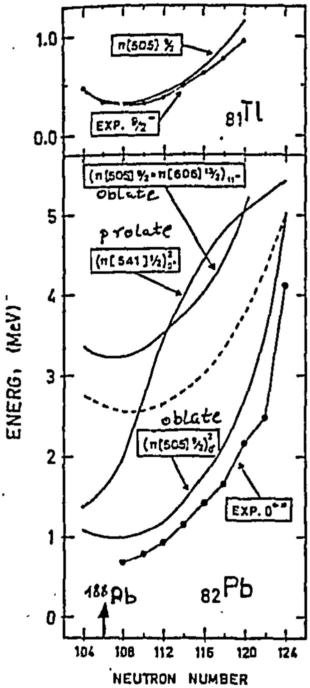

EPS calculation

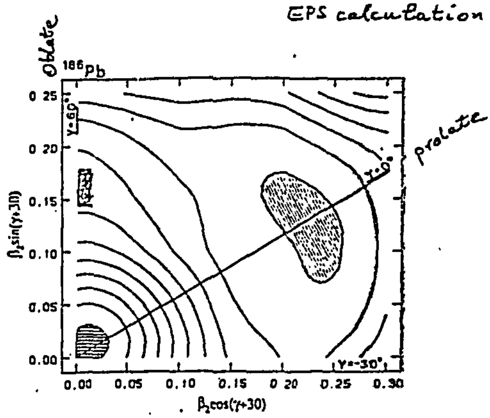

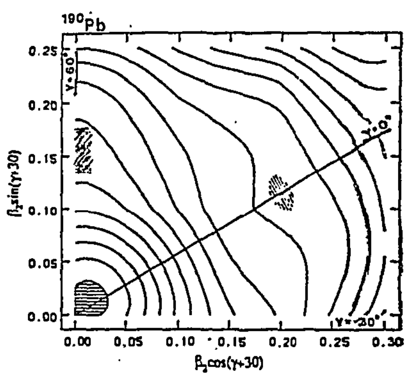

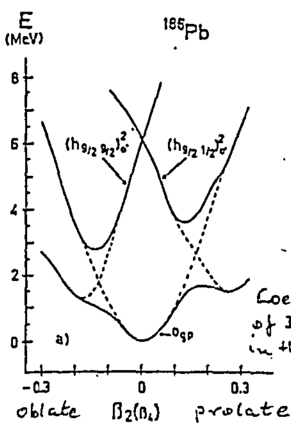

Coexistence
of 3 shapes
in the g.s. region

Questions:

- Isomerism
- Deformation
- Intruder States

In-beam results

Orsay : Nucl. Phys. A 530, 437 (1991), A 323, 495 (1979)
HMI ($T_{1/2}$) : Z. Phys. A 322, 83 (1985)

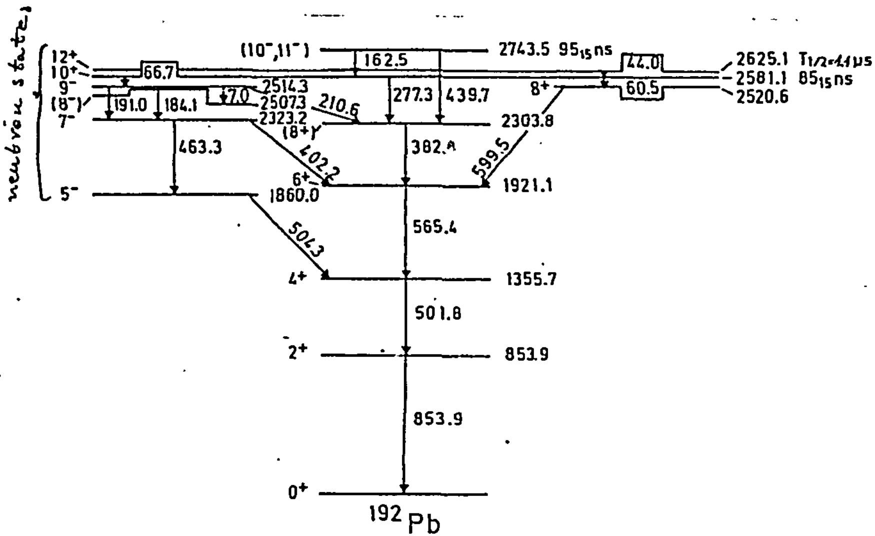

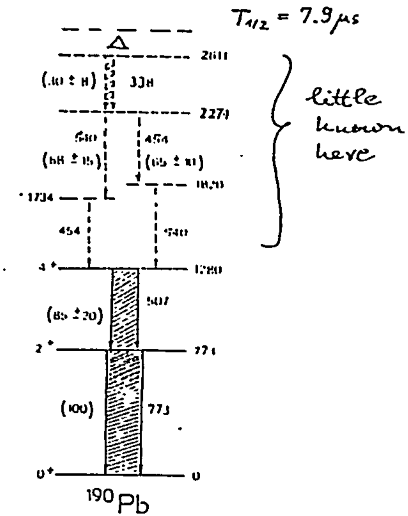

$(10^-, 11^-)$
(8^+) } proton states

2_1^+ states deformed / spherical (?)

euven : Refs: Phys. Rev. C $\underline{35}$, 1861 (1987)

Phys. Rev. Lett. $\underline{52}$, 1974 (1984)

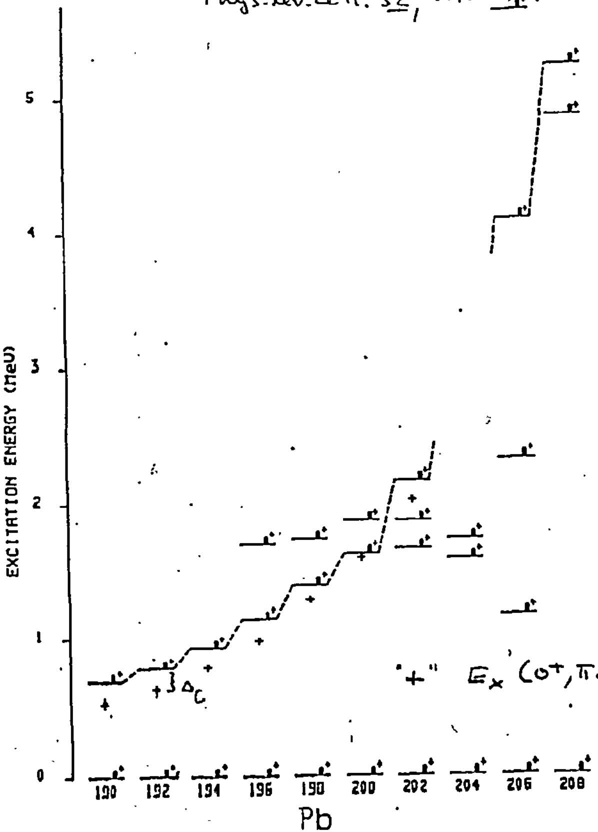

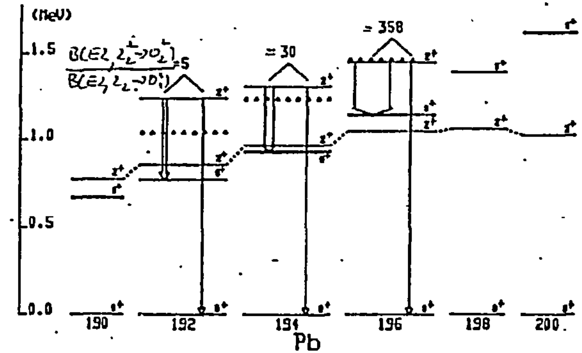

$E_0(2^+, sph) = 1050$ keV $(^{196}Pb - ^{200}Pb)$

$E_0(2^+, def) = E_x(0^+, 2p2h) + E_x(2^+, {}^{A-4}Pt)$

corresponding boson number

"+" $E_x(0^+, \pi 2p2h, {}^{A}Pb) = E_x(1/2^+, \pi 2p\text{-}1h, {}^{A+1}Bi) + E_x(9/2^-, \pi 1p\text{-}2h, {}^{A-1}Tl)$

$+ \ \Delta_c$

≈ 155 keV

α-Decay Systematics

Coenen et al. Phys. Rev. Lett. 54, 1783 (1985)

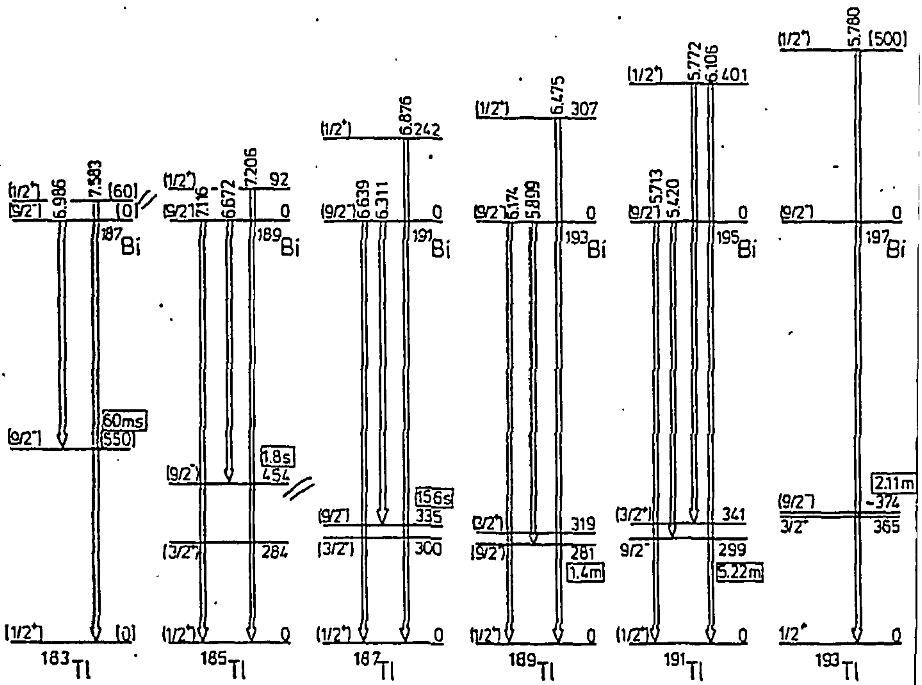

e.g.

$$E_x(0^+, {}^{186}Pb) = E_x(1/2^+, {}^{187}Bi) + E_x(9/2^-, {}^{185}Tl)$$

$$60\ keV + 454\ keV$$

$$= 514\ keV$$

Systematics Pb - Isotopes

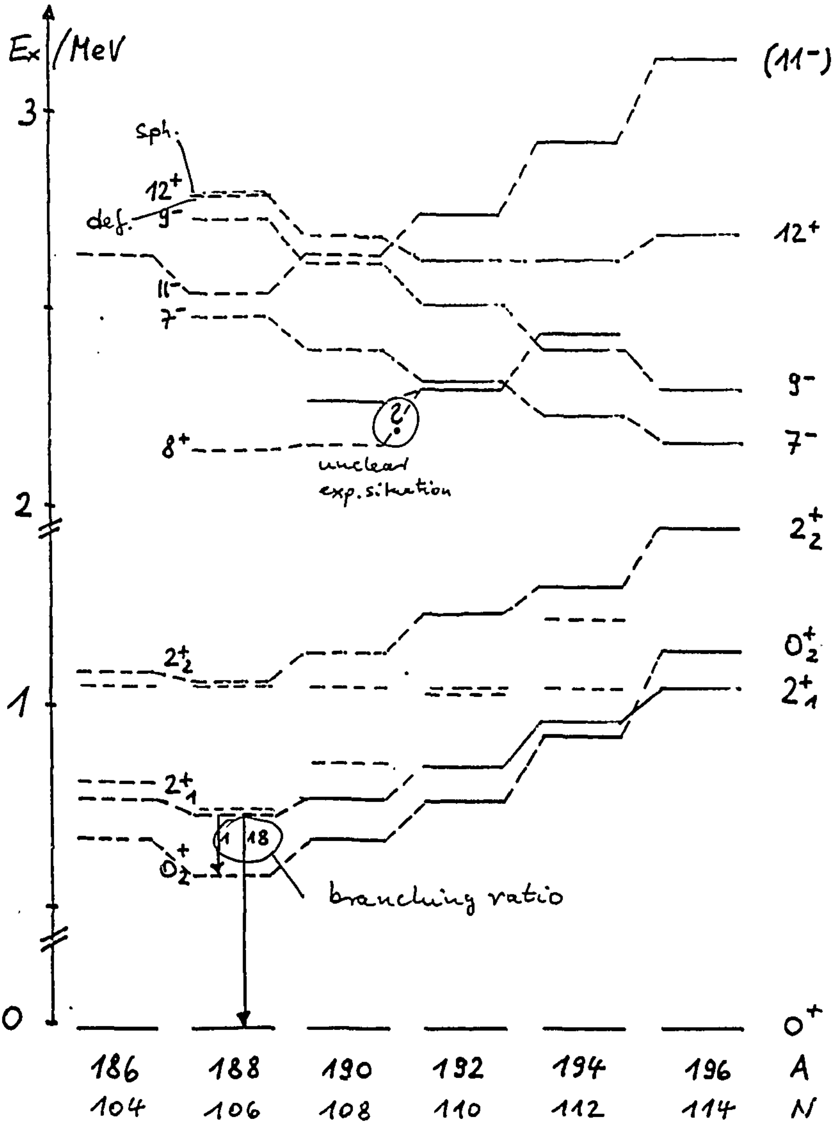

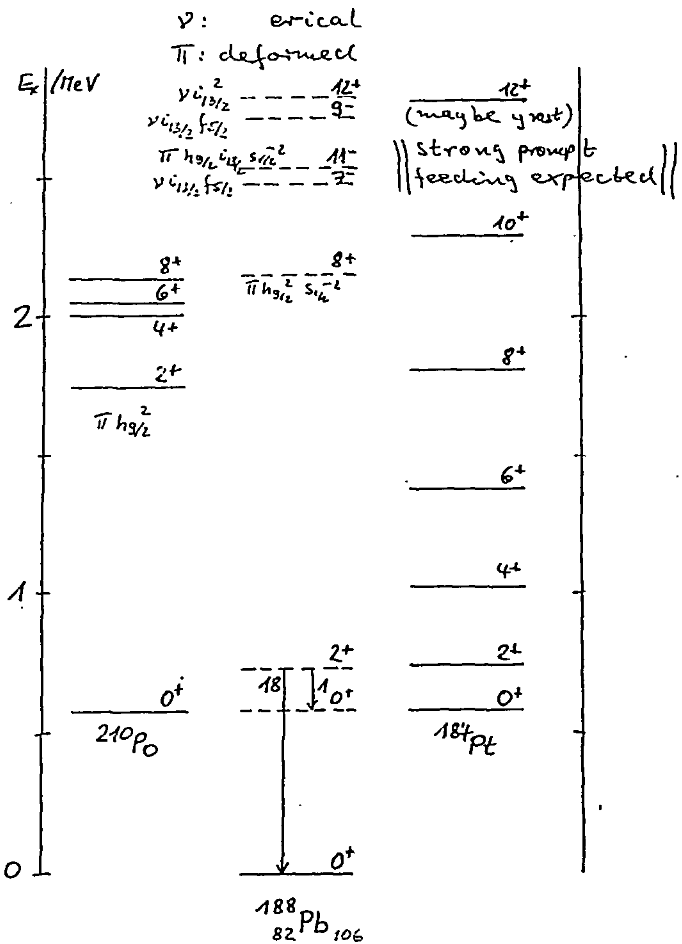
ν: erical
π: deformed
E_x /MeV
$\nu i_{13/2}^2$ 12+
$\nu i_{13/2} f_{5/2}$ 9−
$\pi h_{9/2} i_{13/2} s_{1/2}^{-2}$ 11−
$\nu i_{13/2} f_{5/2}$ 7−
$\pi h_{9/2}^2 s_{1/2}^{-2}$ 8+
$\pi h_{9/2}^2$
18
1
^{210}Po
$^{188}_{82}Pb_{106}$
^{184}Pt
(maybe yrast)
strong prompt feeding expected

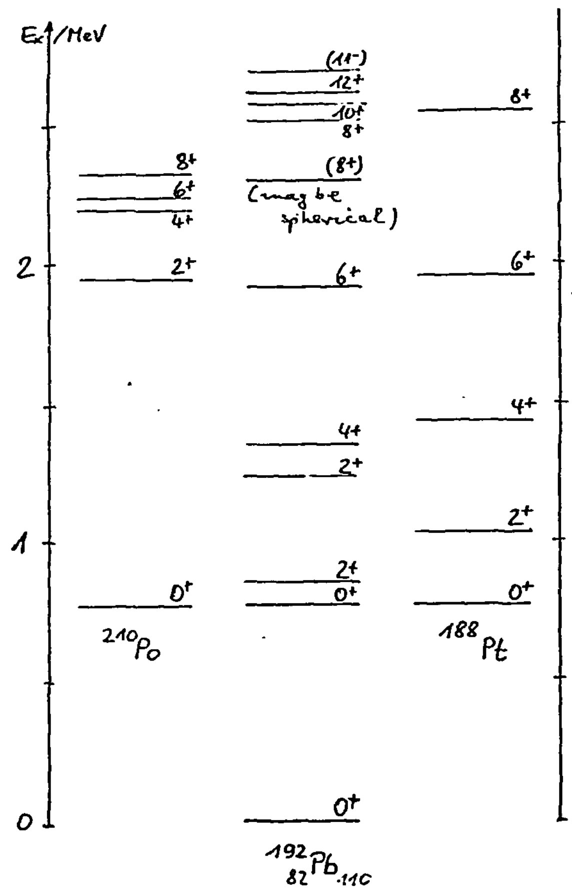
E_x /MeV
(11−)
(8+)
(maybe spherical)
^{210}Po
$^{192}_{82}Pb_{110}$
^{188}Pt

Systematics E2- and M1- Operator for $\nu i_{13/2}$ in Pb isotopes

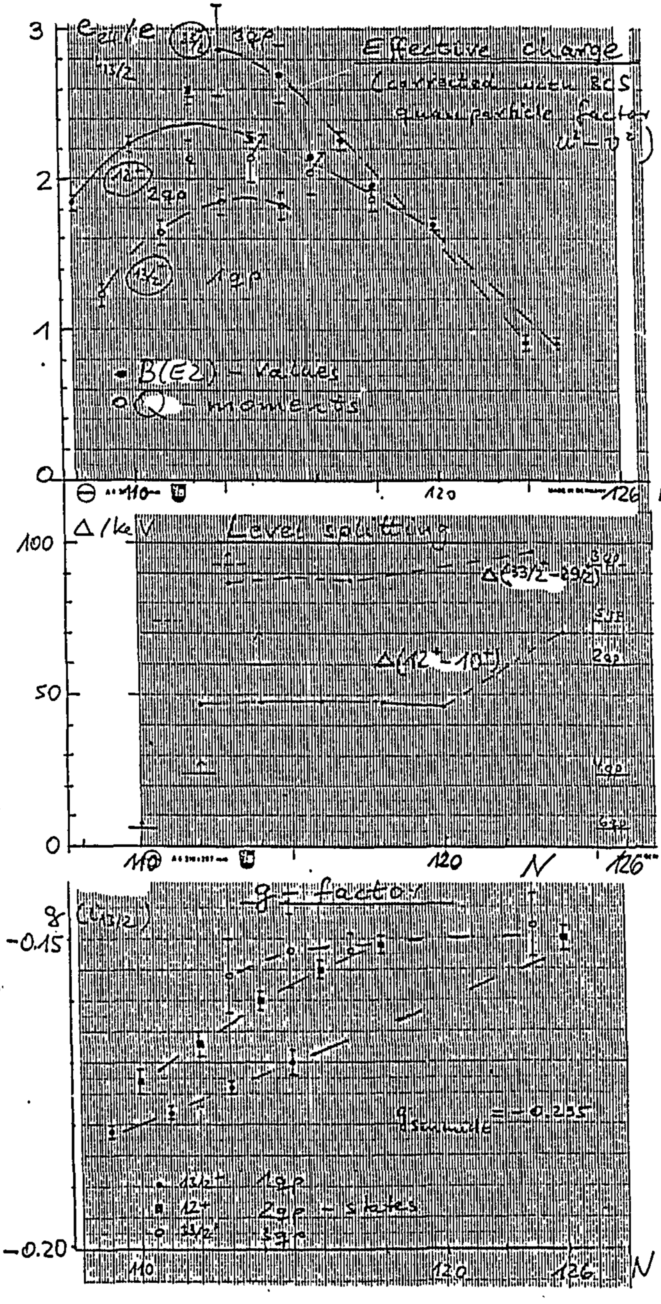

Mass charge and angular momentum transfer in ^{106}Cd + 255 MeV ^{54}Fe collisions studied by γ-γ coincidences.

R.B., C.T. Zhang, P. Kleinheinz, R. Menegazzo, M. Lach
IKP der KFA - Jülich
K.H. Maier, H. Grawe, M. Schramm, R. Schubart
HMI Berlin
S. Hofmann - GSI Darmstadt

TARGET: 1.2 mg/cm^2 90.7% ^{106}Cd + 15 mg/cm^2 ^{208}Pb

BEAM: 255 MeV ^{54}Fe (1.12 × V_c)

300 ns pulse separation

standard γ-γ coincidence measurement

+ radioactivity measurement (continued for ~400 days after bombardment)

OSIRIS + X-ray detector + neutron detector

$\left.\begin{matrix}\gamma\text{-}x \\ \gamma\text{-}n\end{matrix}\right\}$ coincidences used for identification

^{92}Mo + 255 ^{60}Ni

Purdue University - Argonne NL

Phys.Lett. B 251 2 (1990) 245

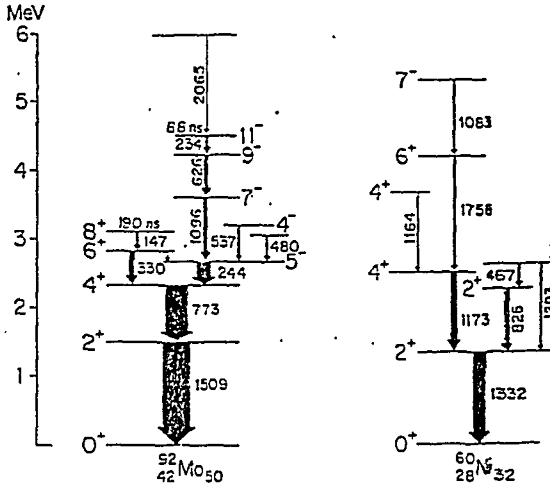

Fig. 2. The ^{92}Mo and ^{60}Ni level schemes. The widths of the transition arrows are proportional to the measured γ-ray intensities and they illustrate the relative population of individual levels by inelastic scattering.

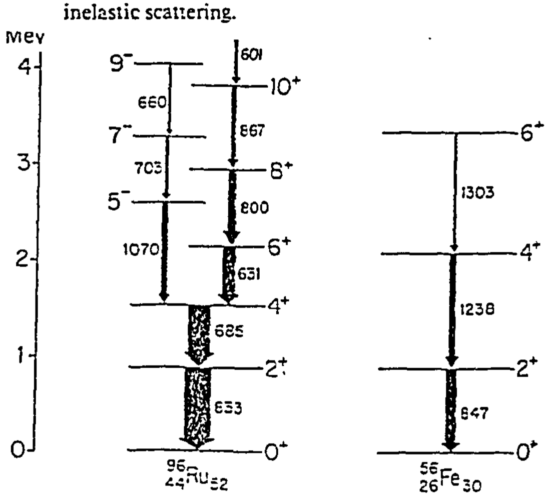

Fig. 3. The ^{96}Ru and ^{56}Fe level schemes, illustrating the relative population of individual levels in the α-transfer process.

(2)

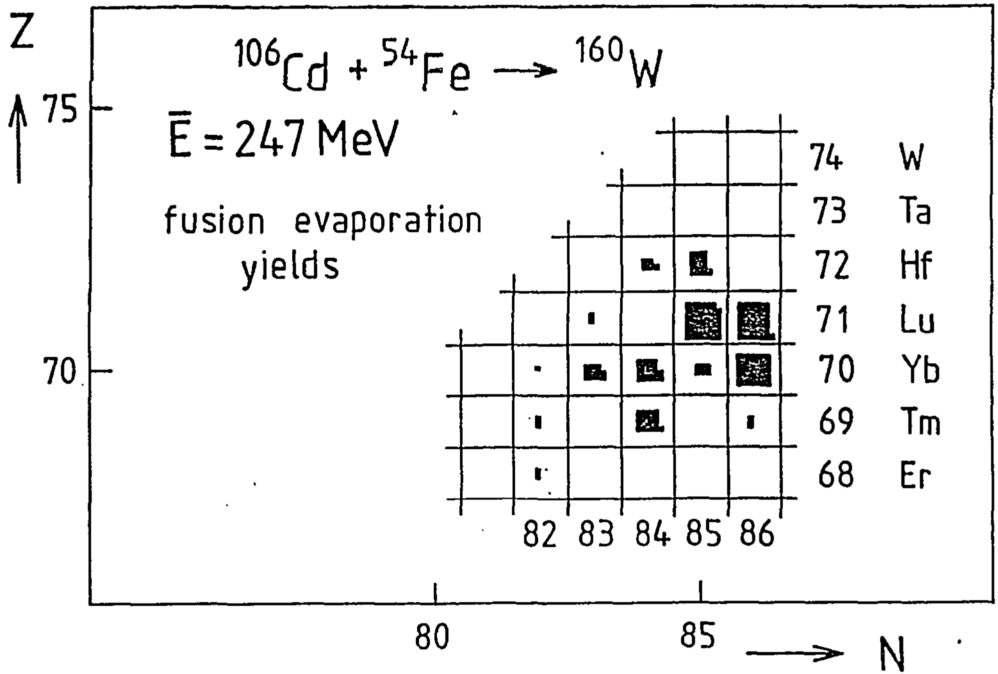

$^{106}Cd + ^{54}Fe \longrightarrow ^{160}W$
$\bar{E} = 247$ MeV
fusion evaporation yields
Z
75
70
74 W
73 Ta
72 Hf
71 Lu
70 Yb
69 Tm
68 Er
82 83 84 85 86
80
85
N

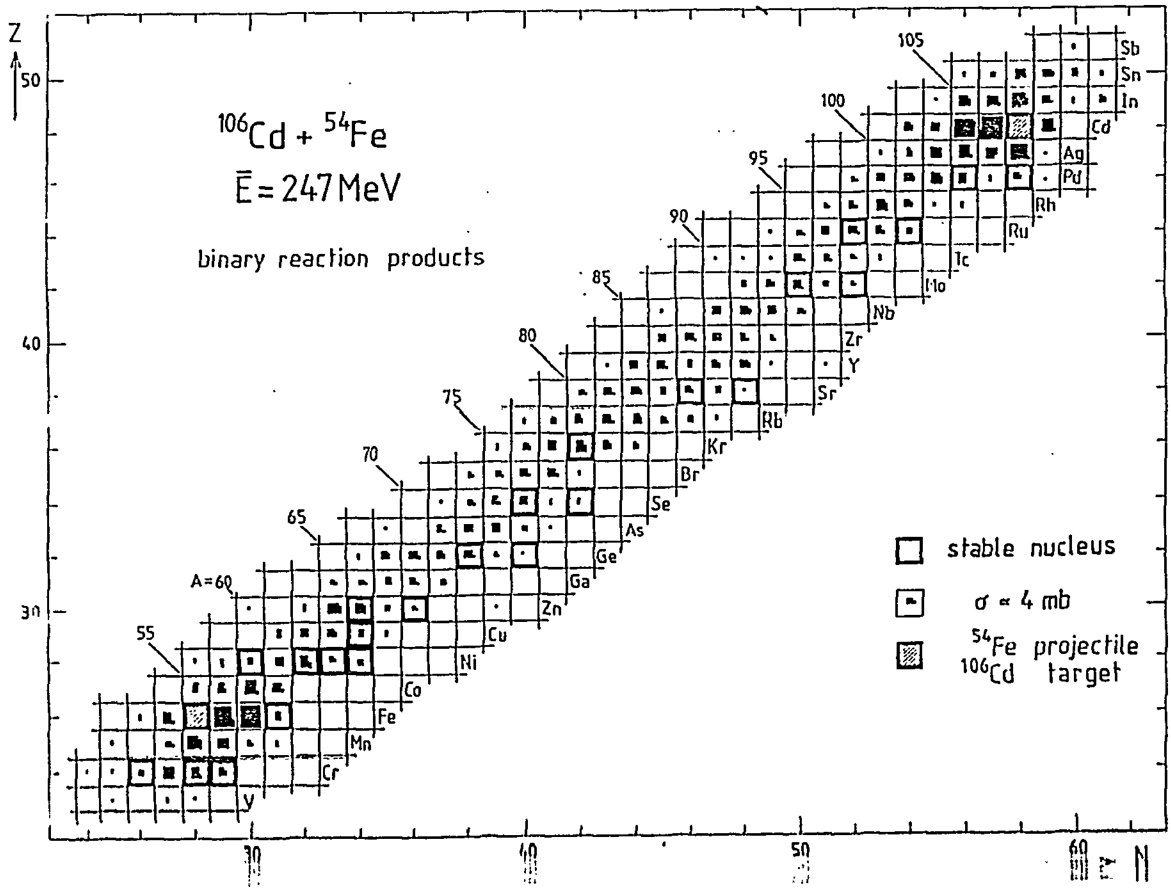

$^{106}Cd + ^{54}Fe$
$\bar{E} = 247$ MeV
binary reaction products
Z
50
40
30
N
30
40
50
60
A=60
55
65
70
75
80
85
90
95
100
105
V
Cr
Mn
Fe
Co
Ni
Cu
Zn
Ga
Ge
As
Se
Br
Kr
Rb
Sr
Y
Zr
Nb
Mo
Tc
Ru
Rh
Pd
Ag
Cd
In
Sn
Sb
stable nucleus
σ ≈ 4 mb
^{54}Fe projectile
^{106}Cd target

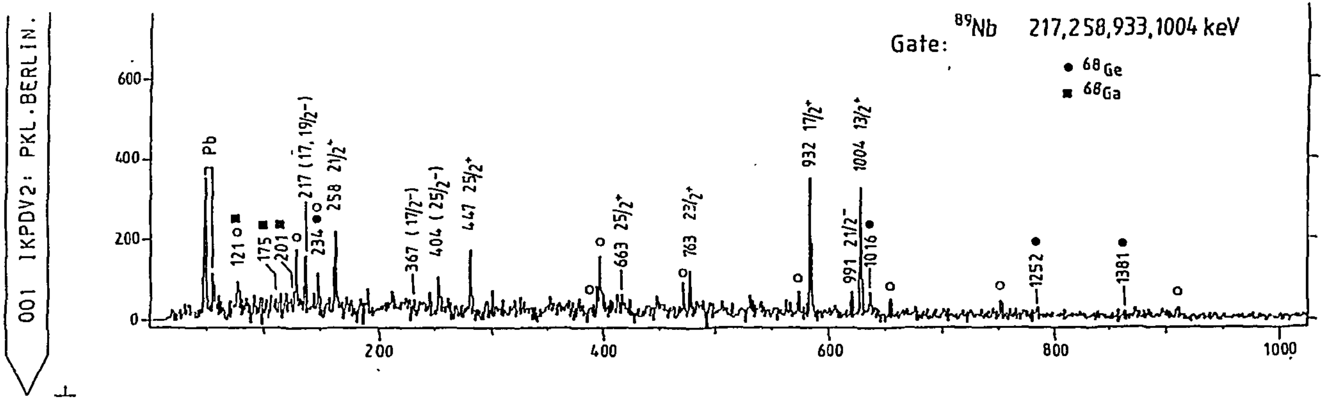

Gate: ^{89}Nb 217,258,933,1004 keV
● ^{68}Ge
■ ^{68}Ga
Pb
121
175
201
217 (17, 19/2⁻)
234
258 21/2⁺
367 (17/2⁻)
404 (25/2⁻)
447 25/2⁺
663 25/2⁺
763 23/2⁺
932 17/2⁺
991 21/2⁻
1004 13/2⁺
1016
1252
1381
0
200
400
600
800
1000
001 IKPDV2: PKL.BERLIN.

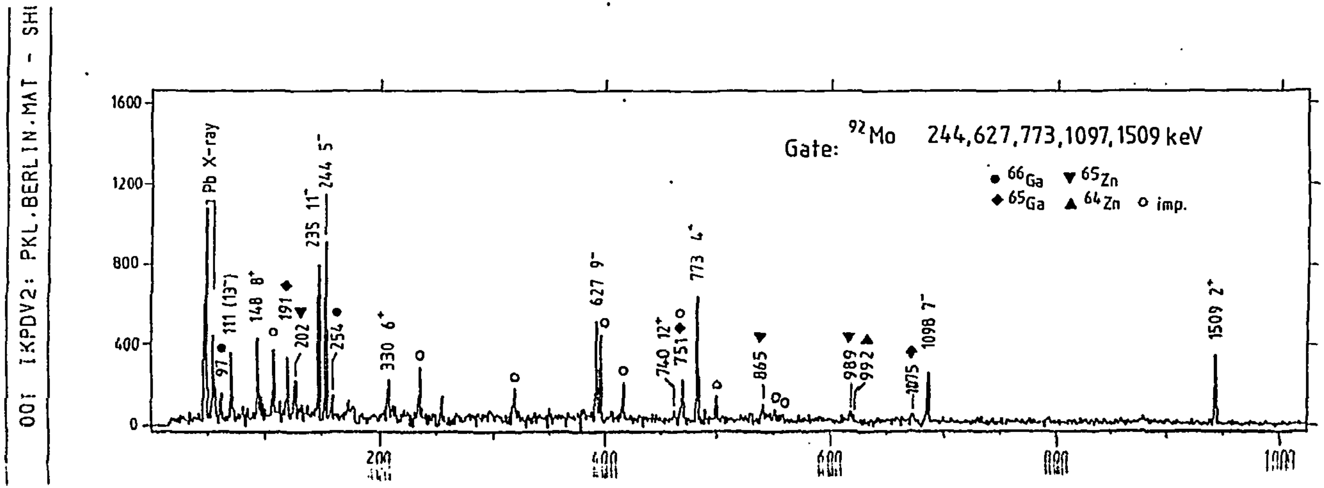

Gate: ^{92}Mo 244,627,773,1097,1509 keV
● ^{66}Ga ▼ ^{65}Zn
◆ ^{65}Ga ▲ ^{64}Zn ○ imp.
Pb X-ray
97
111 (13⁻)
148 8⁺
191
202
235 11⁺
244 5⁻
254
330 6⁺
627 9⁻
740 12⁺
751
773 4⁺
865
989
992
1075
1098 7⁻
1509 2⁺
0
400
800
1200
1600
200
400
600
800
1000
001 IKPDV2: PKL.BERLIN.MAT - SHI

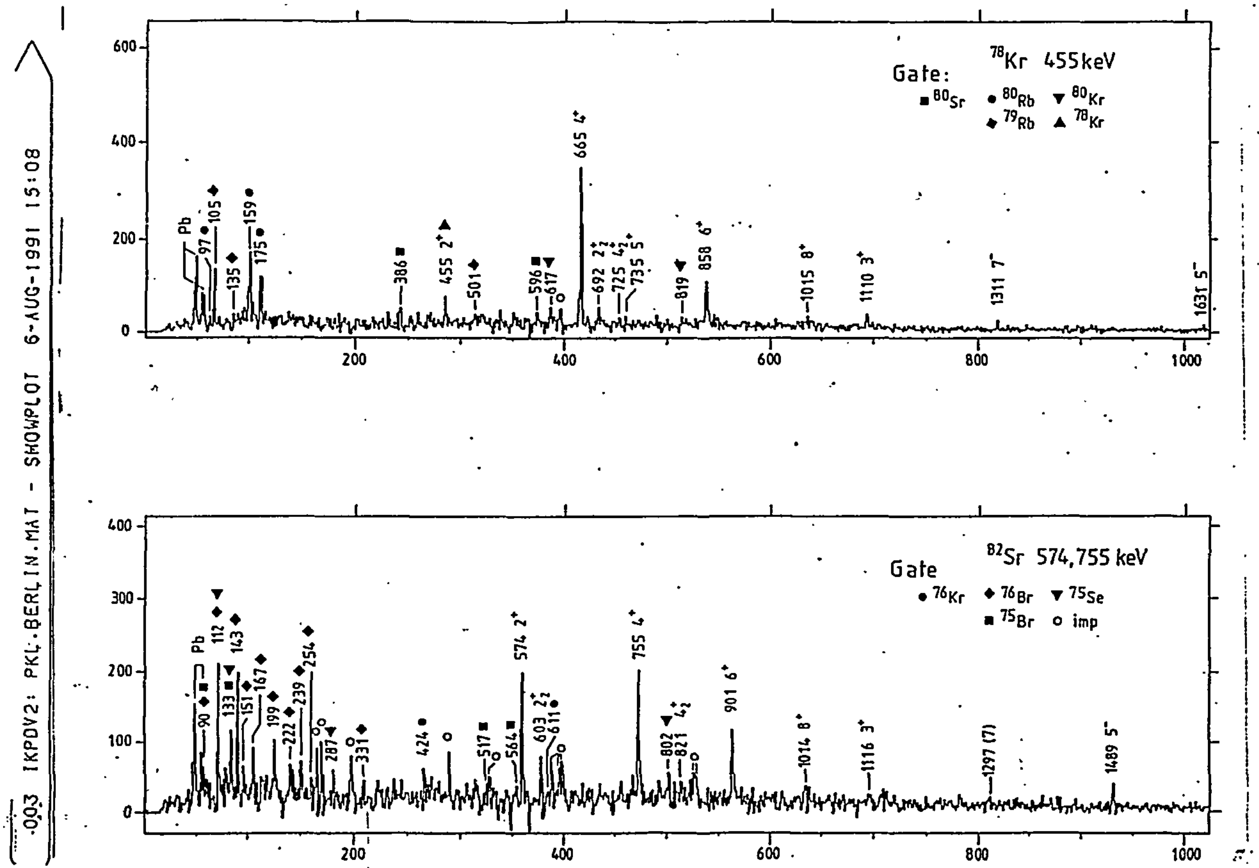
IKPDV2: PKL.BERLIN.MAT - SHOWPLOT 6-AUG-1991 15:08
003
Gate: ^{78}Kr 455keV
■ ^{80}Sr ● ^{80}Rb ▼ ^{80}Kr
◆ ^{79}Rb ▲ ^{78}Kr
Pb
97
105
135
159
175
386
455 2^+
501
596
617
665 4^+
692 2_2^+
725 4_2^+
735 5^+
819
858 6^+
1015 8^+
1110 3^+
1311 7^-
1631 5^-
Gate ^{82}Sr 574,755 keV
● ^{76}Kr ◆ ^{76}Br ▼ ^{75}Se
■ ^{75}Br ○ imp
Pb
90
112
133
143
151
167
199
222
239
254
287
331
424
517
564
574 2^+
603 2_2^+
611
755 4^+
802
821 4_2^+
901 6^+
1014 8^+
1116 3^+
1297 (7)
1489 5^-
0
100
200
300
400
600
800
1000

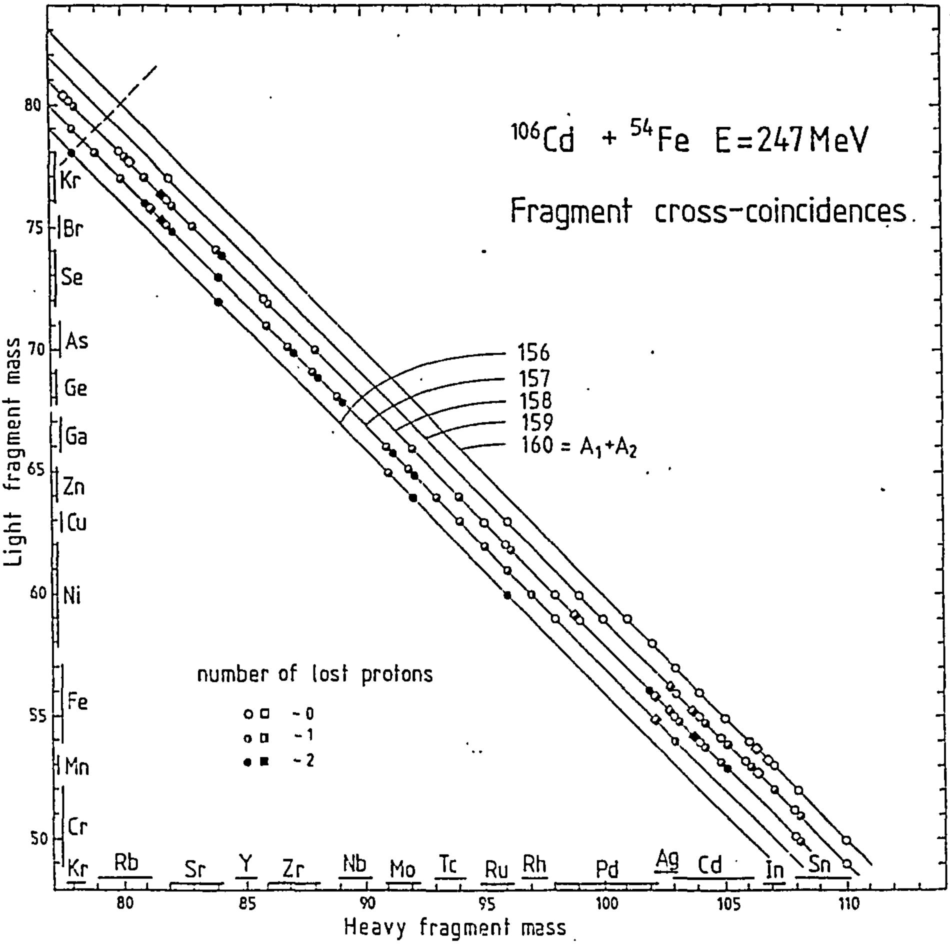

$^{106}Cd + ^{54}Fe$ E=247 MeV
Fragment cross-coincidences
156
157
158
159
$160 = A_1+A_2$
number of lost protons
- 0
- 1
- 2
Light fragment mass
Heavy fragment mass
Kr
Br
Se
As
Ge
Ga
Zn
Cu
Ni
Fe
Mn
Cr
Kr
Rb
Sr
Y
Zr
Nb
Mo
Tc
Ru
Rh
Pd
Ag
Cd
In
Sn
80
75
70
65
60
55
50
80
85
90
95
100
105
110

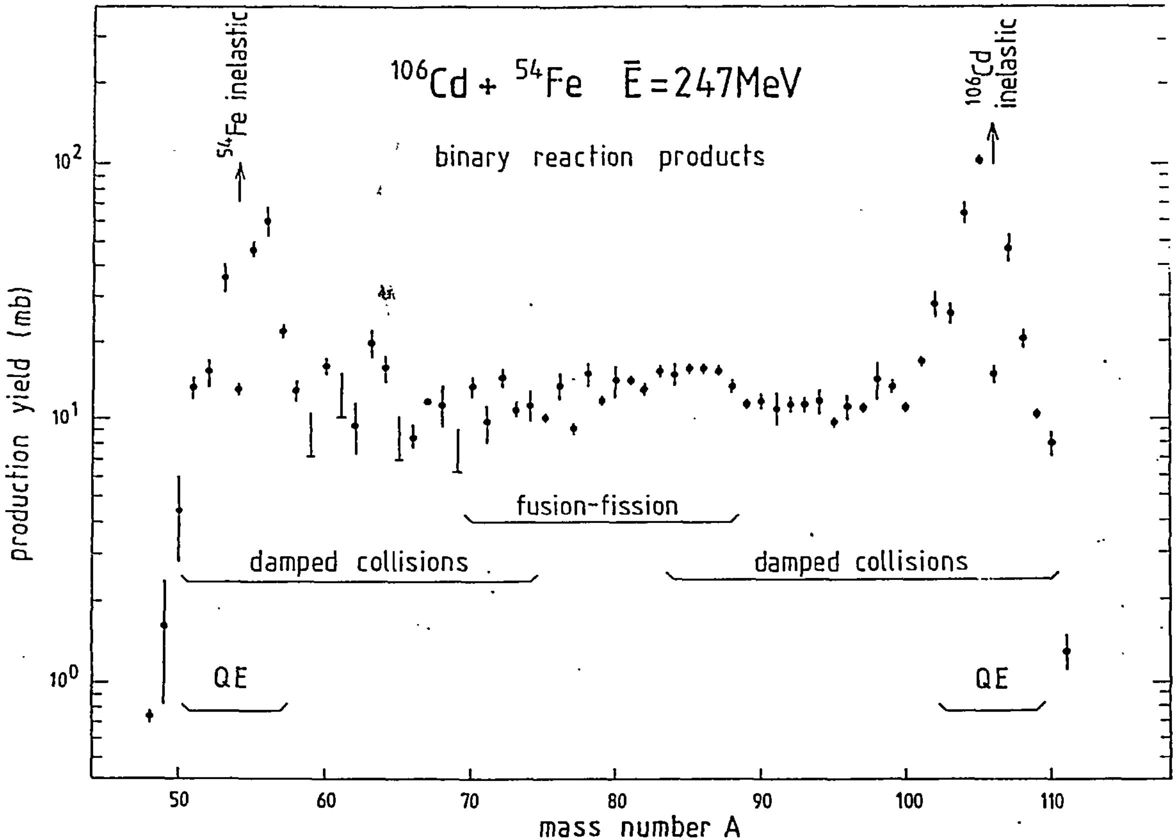

$^{106}Cd + ^{54}Fe \quad \bar{E} = 247 MeV$
binary reaction products
^{54}Fe inelastic
^{106}Cd inelastic
fusion-fission
damped collisions
damped collisions
QE
QE
production yield (mb)
10^2
10^1
10^0
50
60
70
80
90
100
110
mass number A

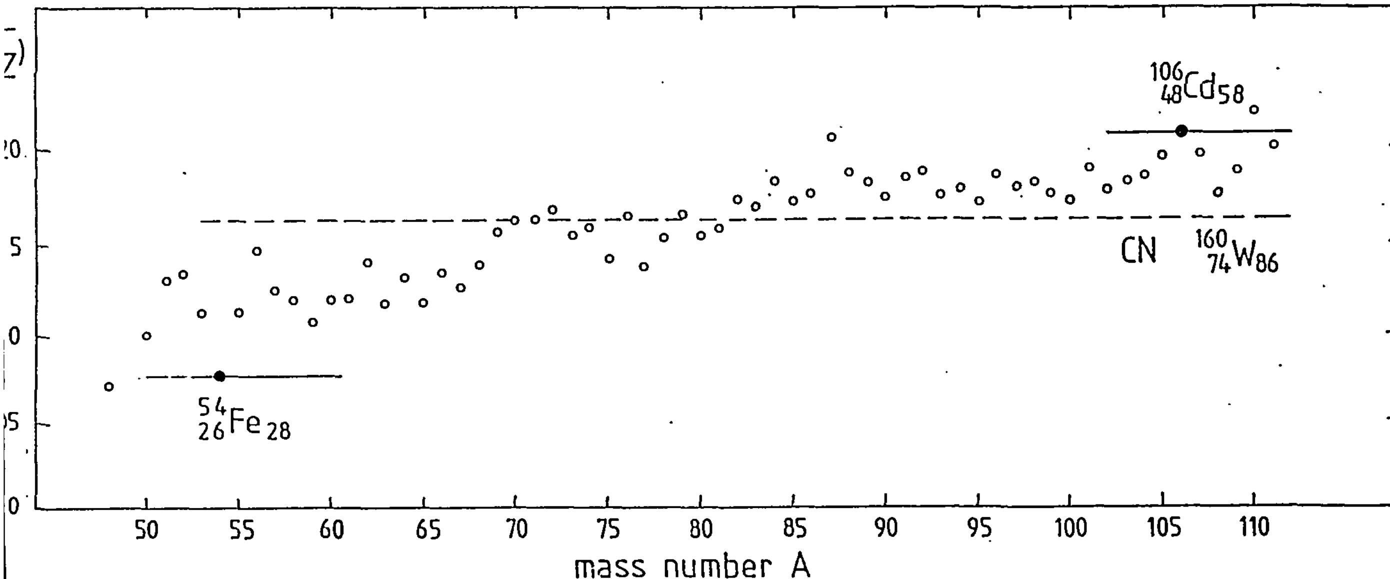

106 48 Cd 58
CN
160 74 W 86
54 26 Fe 28
50
55
60
65
70
75
80
85
90
95
100
105
110
mass number A

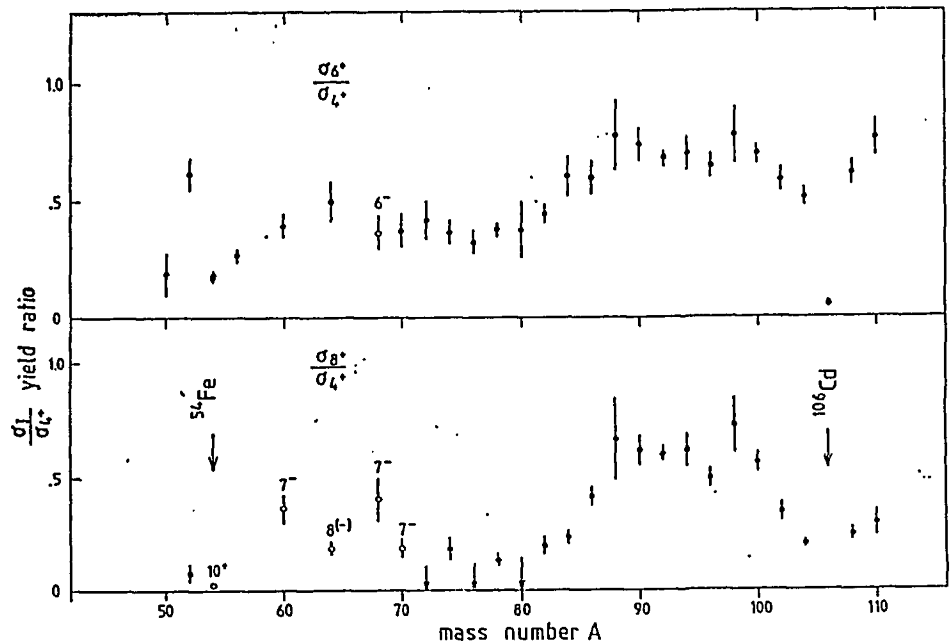

$\frac{\sigma_{6^+}}{\sigma_{4^+}}$
$\frac{\sigma_{8^+}}{\sigma_{4^+}}$
$\frac{\sigma_I}{\sigma_{4^+}}$ yield ratio
^{54}Fe
^{106}Cd
10^+
7^-
$8^{(-)}$
7^-
7^-
6^-
mass number A

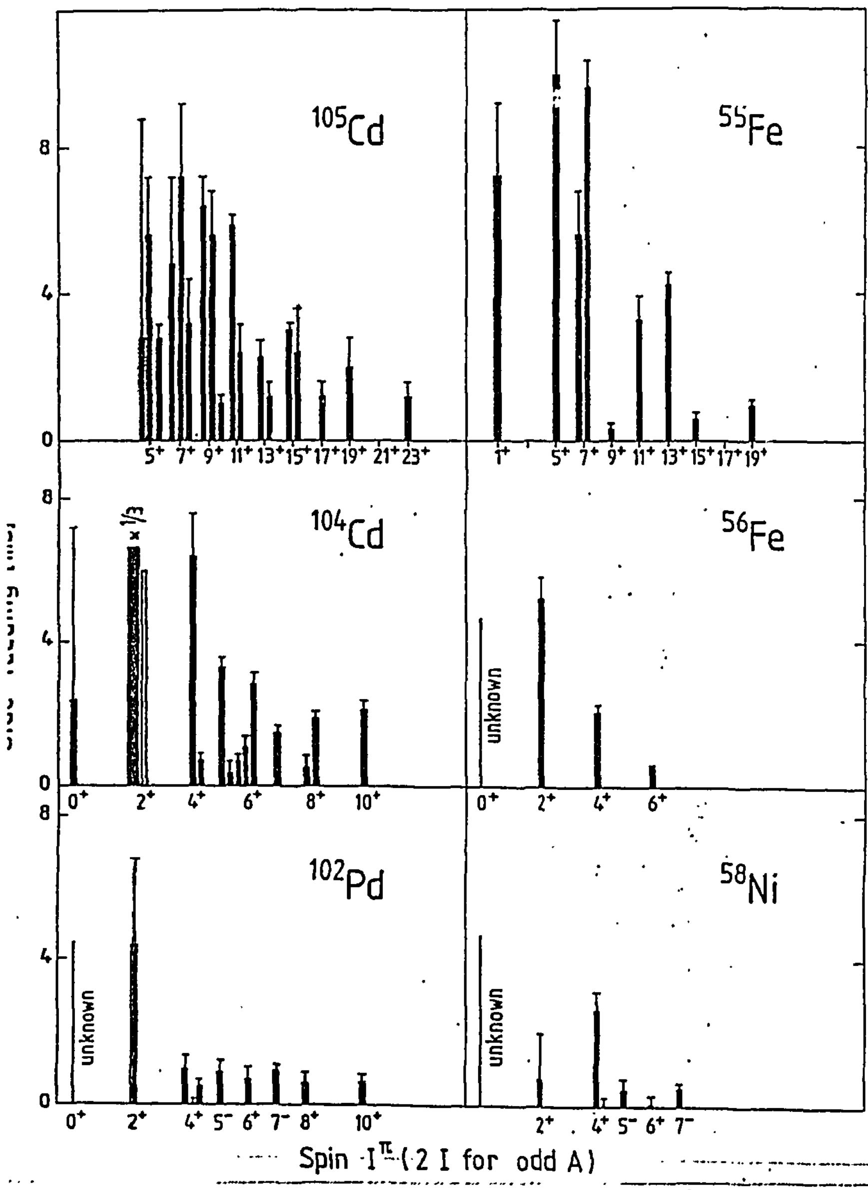

105Cd
55Fe
104Cd
56Fe
102Pd
58Ni
unknown
unknown
unknown
x 1/3
0
4
8
0+ 2+ 4+ 5− 6+ 7− 8+ 10+
5+ 7+ 9+ 11+ 13+ 15+ 17+ 19+ 21+ 23+
1+ 5+ 7+ 9+ 11+ 13+ 15+ 17+ 19+
Spin I^π (2 I for odd A)

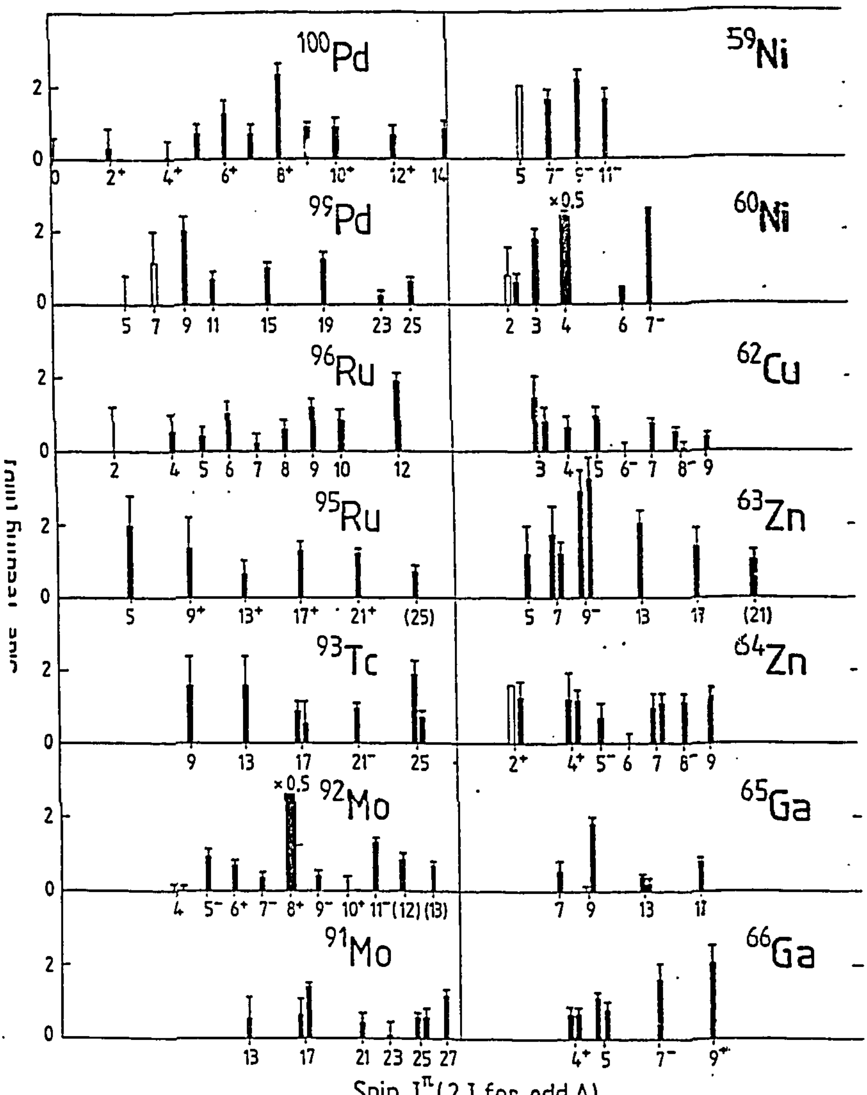

100Pd
59Ni
99Pd
60Ni
×0.5
96Ru
62Cu
95Ru
63Zn
93Tc
64Zn
×0.5
92Mo
65Ga
91Mo
66Ga
Spin I^{π} (2 I for odd A)

63

Quasielastic and deep inelastic Reactions with Heavy Ions in γ-Spectroscopy

Investigation of ^{208}Pb with

$^{82}Se + ^{208}Pb$ at 420 MeV

$^{64,62}Ni + ^{208}Pb$ at 380 (?) MeV

(Jan. 91)

Ref: Rehm et. al., Phys Rev C42 (1990) 2497

Types of Reactions

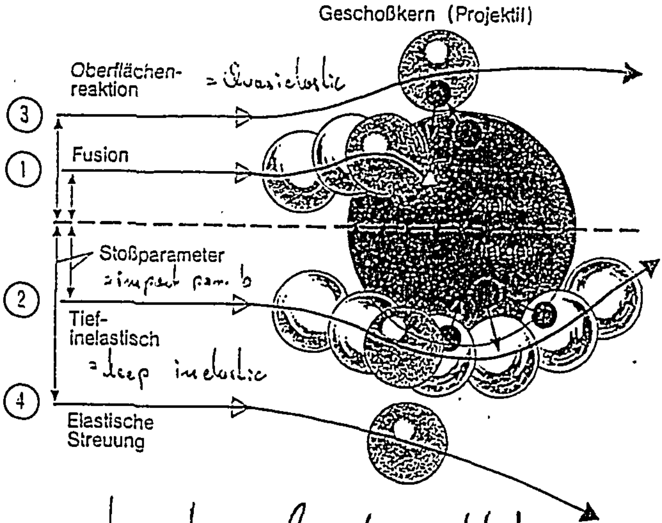

impact parameter $b \approx l$ (roughly)

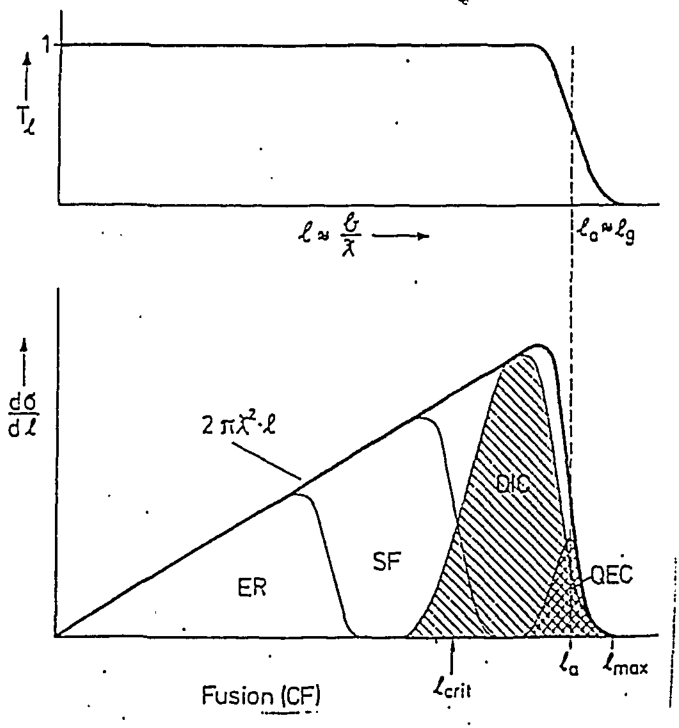

Angular distributions for $^{80}Se + ^{208}Pb$

assumption: n-pickup >> p-pickup

p-stripping > n-stripping...

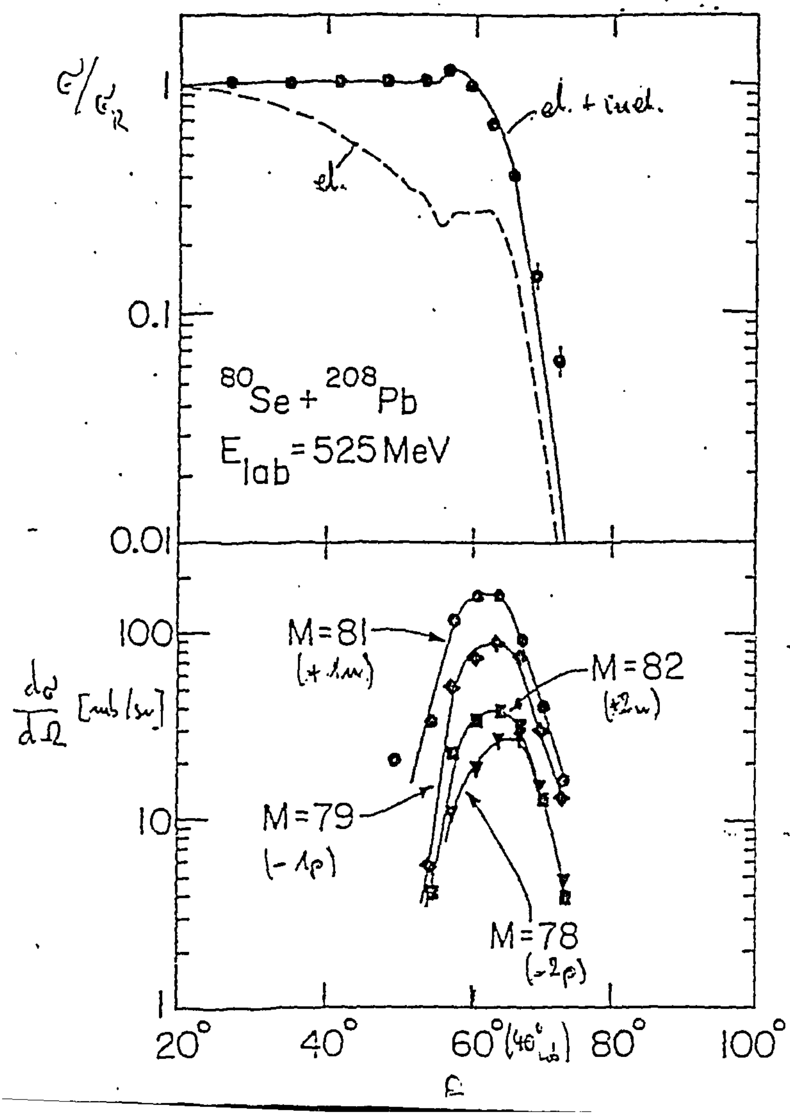

elastic + inelastic scattering

1n and 2n transfer react.

Rehm et al.

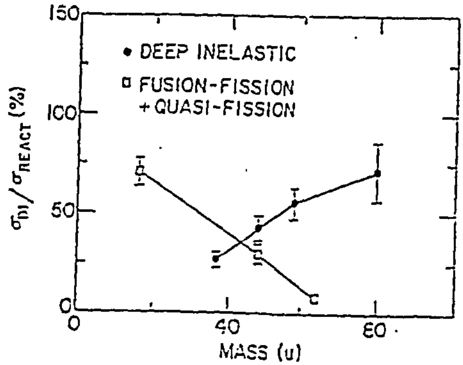

$\sigma_{DIC} + \sigma_{F} \approx const$

$\approx 70\%$

but: $f(E)$!

Def: quasielastic: $Q > -30$ MeV

deep inelastic: $Q < -30$ MeV

Angular Distribution:

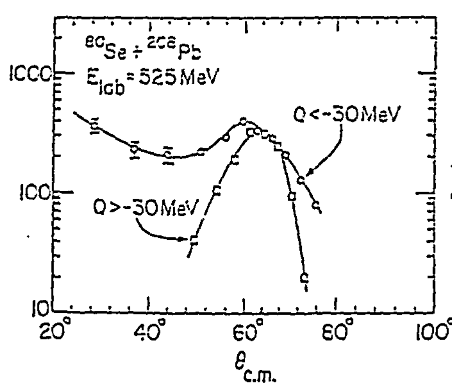

$\frac{d\sigma}{d\Omega}$

$\Downarrow$

40°_{lab}

Rehm et al

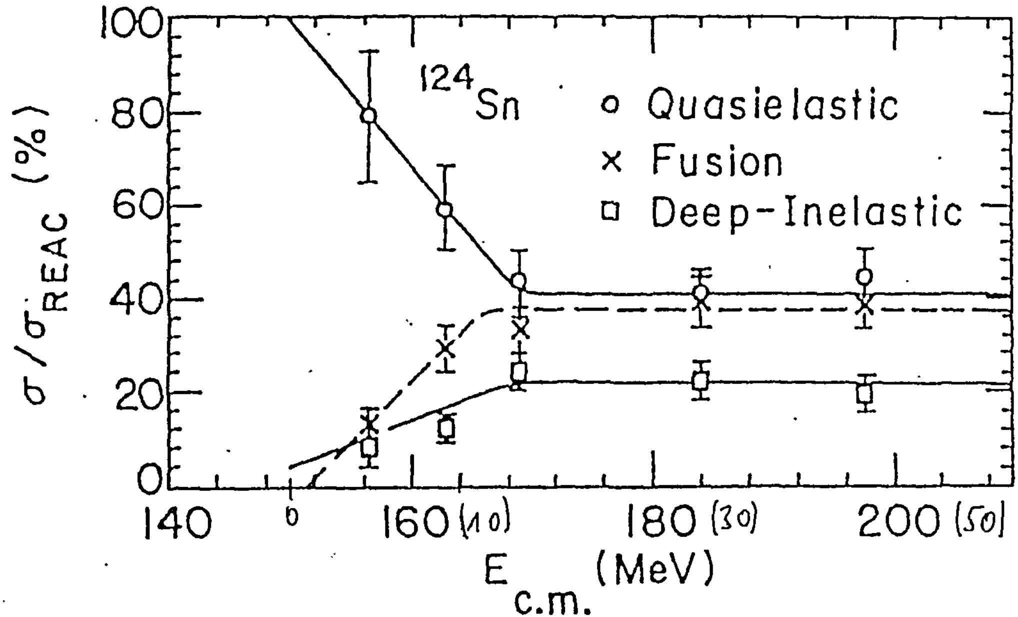

Fig. 3. Strength of fusion, deep-inelastic and quasielastic scattering as a fraction of the total reaction cross section for $^{58}Ni + ^{124}Sn$ at various energies. The lines serve to guide the eye.

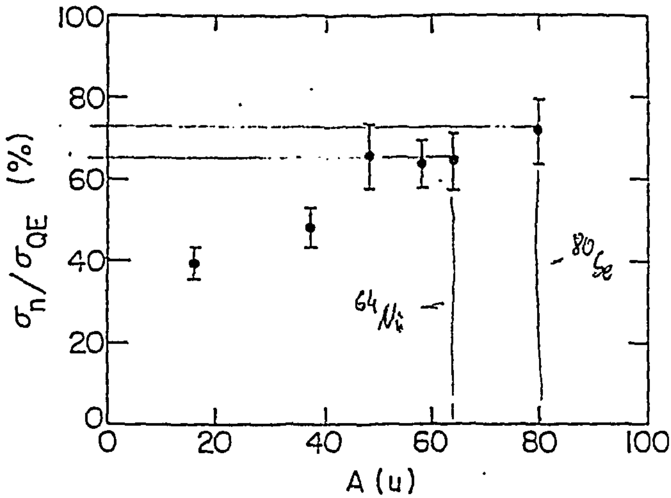

Rehm et al

FIG. 6. Relative contribution of neutron-transfer channels to the total quasielastic reaction strength for reactions induced by various projectiles on ^{208}Pb targets.

=> systematic investigation of n-transfer is important for the description of heavy-systems

Problems: - DWBA calculations become difficult (^{58}Ni + ^{208}Pb: 48 states had to be included)

- no Spectroscopic Factors known for high excitation energies

Problem: Models describe only σ_{react},

not σ_{QE}!

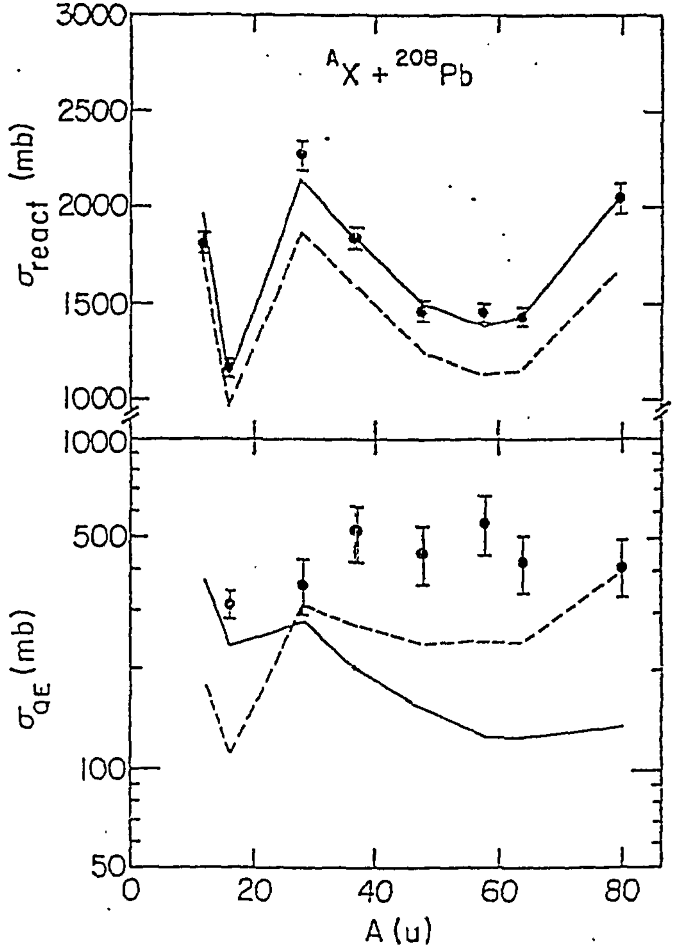

Rehm et al

FIG. 7. (a) Total reaction cross sections calculated using equations from Ref. 25 (solid lines) or Ref. 27 (dashed lines) in comparison with experimental values (dots) for systems involving various projectiles on ^{208}Pb targets. (b) Same as (a) but for

$\Rightarrow$ is there a simpler method to get cross-sections for E and θ ?

$$\sigma = \sum_{\substack{i \in \text{Proj} \\ j \in \text{Target}}} S_i(\text{Proj})\, S_j(\text{Target})\, \sigma_{ij\,\text{DWBA}}$$

near V_C : $\sigma_{ij\,\text{DWBA}}$ depends not on angular momenta

$$\Rightarrow \quad \sigma = \sum_i S_i(P) \sum_j S_j(T) \;\langle \sigma(Q) \rangle$$

For heavy-Ion-Reactions (rough):

$$\langle \sigma(Q) \rangle = f\,(Q_{gg}\,,\,E_w)$$

Q - matching:

⇒ all Q-Values in a certain window contribute to σ

$$\Rightarrow \langle \sigma(Q_{gg}) \rangle = \int_{-\infty}^{Q_{gg}} \sigma(Q)\, dQ$$

if $\sigma \sim e^{-Q^2/w^2}$

$$\Rightarrow \langle \sigma(Q_{gg}) \rangle = N \left[1 + \operatorname{erf} \left[\frac{Q_{gg} - Q_{OPT}}{w} \right] \right]$$

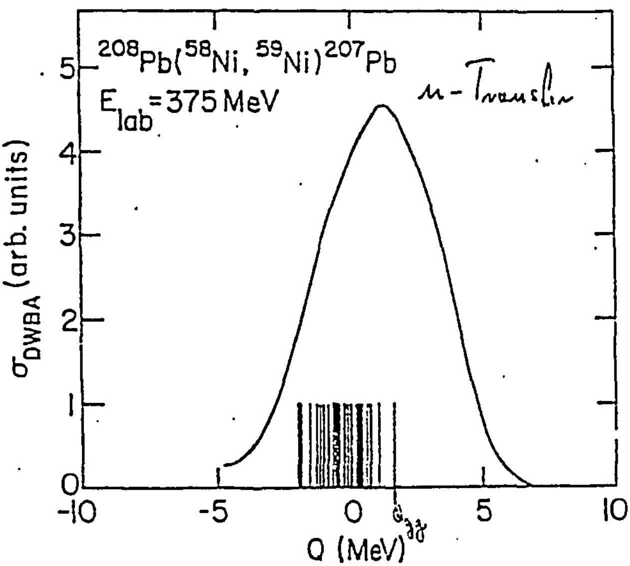

$W = f(E_n)$

FIG. 9. "*Q* window" obtained from DWBA calculations for the reaction $^{208}Pb(^{58}Ni, ^{59}Ni(\frac{1}{2}^-))^{207}Pb(\frac{1}{2}^-)$. The vertical lines correspond to the various known single-particle states which can be populated in the outgoing nuclei. See text for details.

corr.: – one-particle state density is large (gg-nuclei) otherwise overprediction of σ

– correction for E_B (n)

– $\Sigma\, \delta_i = f(A)$

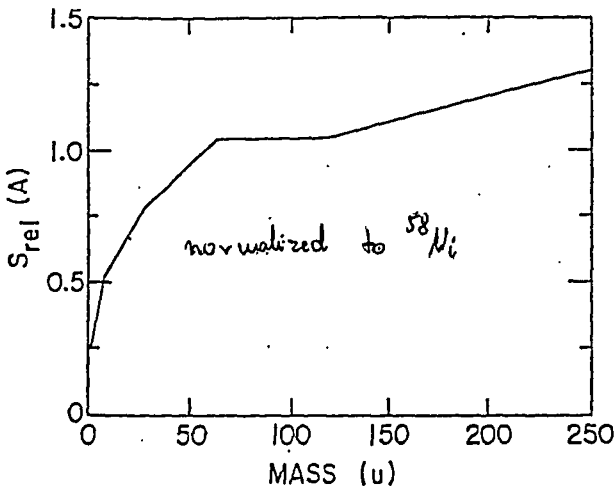

$$\Rightarrow \sigma(Q_{gg}) = \delta_p(A)\, \delta_T(A)\, N \left(1 + \mathrm{erf}\left[\frac{Q_{gg} - Q_{OPT}}{W}\right]\right)$$

with: $N = 1{,}73 \times 10^4$; $W = 5{,}8$ MeV ; $Q_{OPT} = 0$ (for 1-n-Transfer

÷ 1n

÷ 2n

− 1n

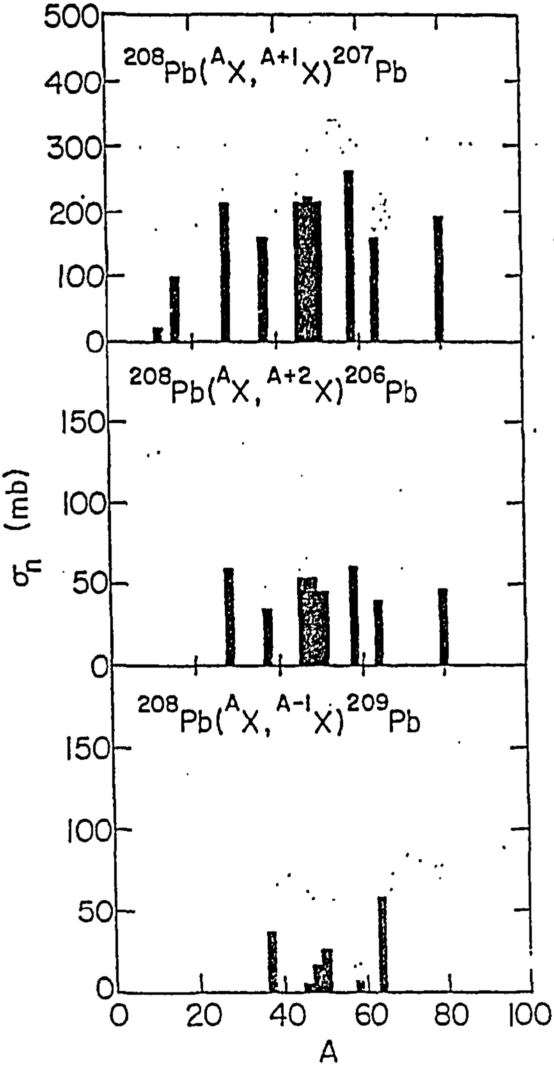

FIG. 8. (a) Energy- and angle-integrated cross sections for one-neutron-pickup cross sections induced by various projectiles on ^{208}Pb targets plotted as a function of the projectile mass. (b) Same as (a) but for two-neutron-pickup reactions. (c) Same as (a) but for one-neutron-stripping reactions.

Similar calculations for 2n-transfer show different results

but the same dependance $\sigma = f(Q_{gg})$

per transfer, σ decreases a factor 4 - 5

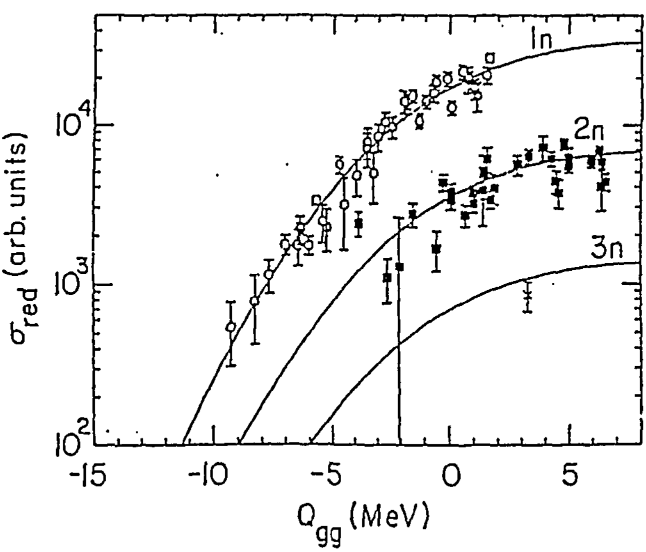

FIG. 12. Binding-energy-corrected one-, two-, and three-neutron transfer cross sections induced by various projectiles plotted as a function of the ground-state Q value Q_{gg}. Rehm et al

TABLE III. Energy- and angle-integrated cross sections for one-neutron transfer reactions induced by various projectiles on ^{208}Pb targets.

Reaction	E_{lab} (MeV)	Q_{gg} (MeV)	σ_{exp} (mb)	σ [Eq. (7)] (mb)	Ref.
(^{12}C,^{13}C)	97.9	−2.422	22	101	11
(^{16}O,^{17}O)	104	−3.227	100	106	12
(^{28}Si,^{27}Si)	225	−13.240	<0.5	0.2	8
(^{28}Si,^{29}Si)	225	1.105	214	174	8
(^{37}Cl,^{38}Cl)	250	−1.259	160	169	7
(^{37}Cl,^{36}Cl)	250	−6.374	38	30	7
(^{46}Ti,^{47}Ti)	297	1.506	210	205	9
(^{46}Ti,^{45}Ti)	297	−9.259	7	5	9
(^{48}Ti,^{49}Ti)	300	−0.775	225	204	9
(^{48}Ti,^{47}Ti)	300	−7.690	17	15	9
(^{50}Ti,^{51}Ti)	303	−0.992	205	191	9
(^{50}Ti,^{49}Ti)	303	−7.010	28	23	9
(^{58}Ni,^{59}Ni)	375	1.631	265	225	7
(^{58}Ni,^{57}Ni)	375	−8.265	11	11	7
(^{64}Ni,^{65}Ni) +Δm	380	−1.273	160	208	This work
(^{64}Ni,^{63}Ni) −Δm	380	−5.722	60	54	This work
(^{80}Se,^{81}Se) +Δm	525	−0.667	194	216	This work
(^{86}Kr,^{87}Kr)	695	−1.858	200	200	10
(^{152}Sm,^{153}Sm)	1311	−1.502	80	218	30
(^{152}Sm,^{151}Sm)	1311	−4.330	43	121	30
(^{232}Th,^{231}Th)	1314	0.307	370	367	30

Fig. 1:
Section of the nuclidic chart around ^{82}Se with population cross sections (*mb*) for β-unstable nuclei.

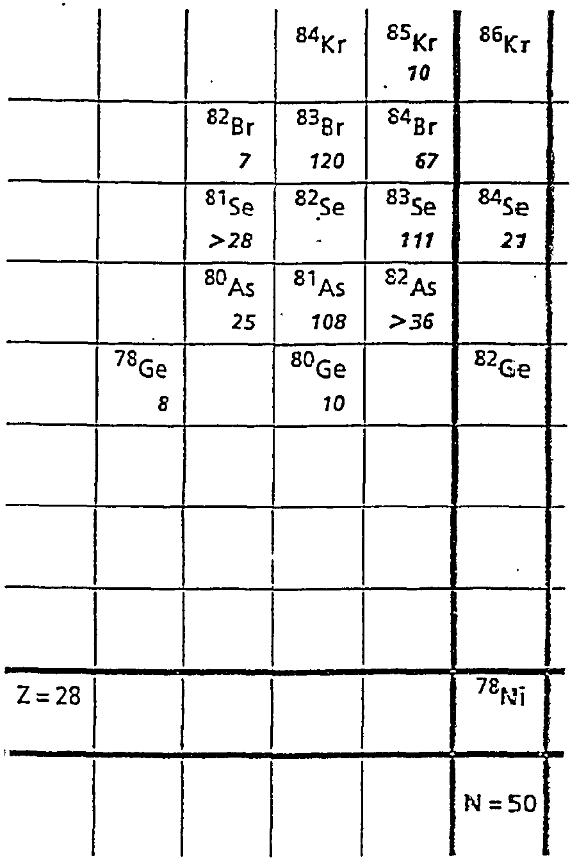

Table 1: Production cross sections for β- unstable projectile like nuclei in ^{208}Pb + 420 MeV ^{82}Se.

Reaction Channel			Q_{gg} [MeV]	σ [mb]
$^{208}Pb + {}^{82}Se \rightarrow$	$(-2n) \rightarrow$	$^{80}Se + {}^{210}Pb$	- 6.9	--
	$(-n) \rightarrow$	$^{81}Se + {}^{209}Pb$	- 5.3	>28 (6) a)
	$(+n) \rightarrow$	$^{83}Se + {}^{207}Pb$	- 1.5	111 (10)
	$(+2n) \rightarrow$	$^{84}Se + {}^{206}Pb$	+ 0.4	21 (4)
	$(-n-p) \rightarrow$	$^{80}As + {}^{210}Bi$	- 12.4	25 (6)
	$(-p) \rightarrow$	$^{81}As + {}^{209}Bi$	- 8.6	108 (35)
	$(+n-p) \rightarrow$	$^{82}As + {}^{208}Bi$	- 10.4	>36 (14) a)
	$(-n+p) \rightarrow$	$^{82}Br + {}^{208}Tl$	- 5.1	7 (1)
	$(+p) \rightarrow$	$^{83}Br + {}^{207}Tl$	+ 0.7	120 (100)
	$(+n+p) \rightarrow$	$^{84}Br + {}^{206}Tl$	+ 0.7	67 (18)
	$(+2p) \rightarrow$	$^{84}Kr + {}^{206}Hg$	+ 4.0	--
	$(-\alpha) \rightarrow$	$^{78}Ge + {}^{212}Po$	- 19.9	8 (1)
	$(-2p) \rightarrow$	$^{80}Ge + {}^{210}Po$	- 14.0	10 (3)

a) Lower limit, as only part of the decay intensity was observed

Isomers in ^{208}Pb-region

		210 Po $(6,8)^+$ $\pi h_{9/2}^2$		212 Po 8^+ $\nu g_{9/2}^2$ $\otimes \pi h_{9/2}^2$	
	208 Bi 10^- $\pi h_{9/2} \nu i_{13/2}^{-1}$	209 Bi $19/2^+$ $\nu g_{9/2} p_{1/2}^{-1} \pi h_{9/2}$			
206 Pb 12^+ $\nu i_{13/2}^{-2}$	207 Pb $13/2^+$ $\nu i_{13/2}^{-1}$	208 Pb 10^+ $\nu g_{9/2} i_{13/2}^{-1}$ $+ \pi h_{9/2} h_{11/2}^{-1}$		210 Pb $(6,8)^+$ $\nu g_{9/2}^2$	
	206 Tl 12^- $\pi h_{11/2}^{-1} \nu i_{13/2}^{-1}$	207 Tl $11/2^-$ $\pi h_{11/2}^{-1}$			
		420 MeV 82 Se $+ ^{208}$Pb			

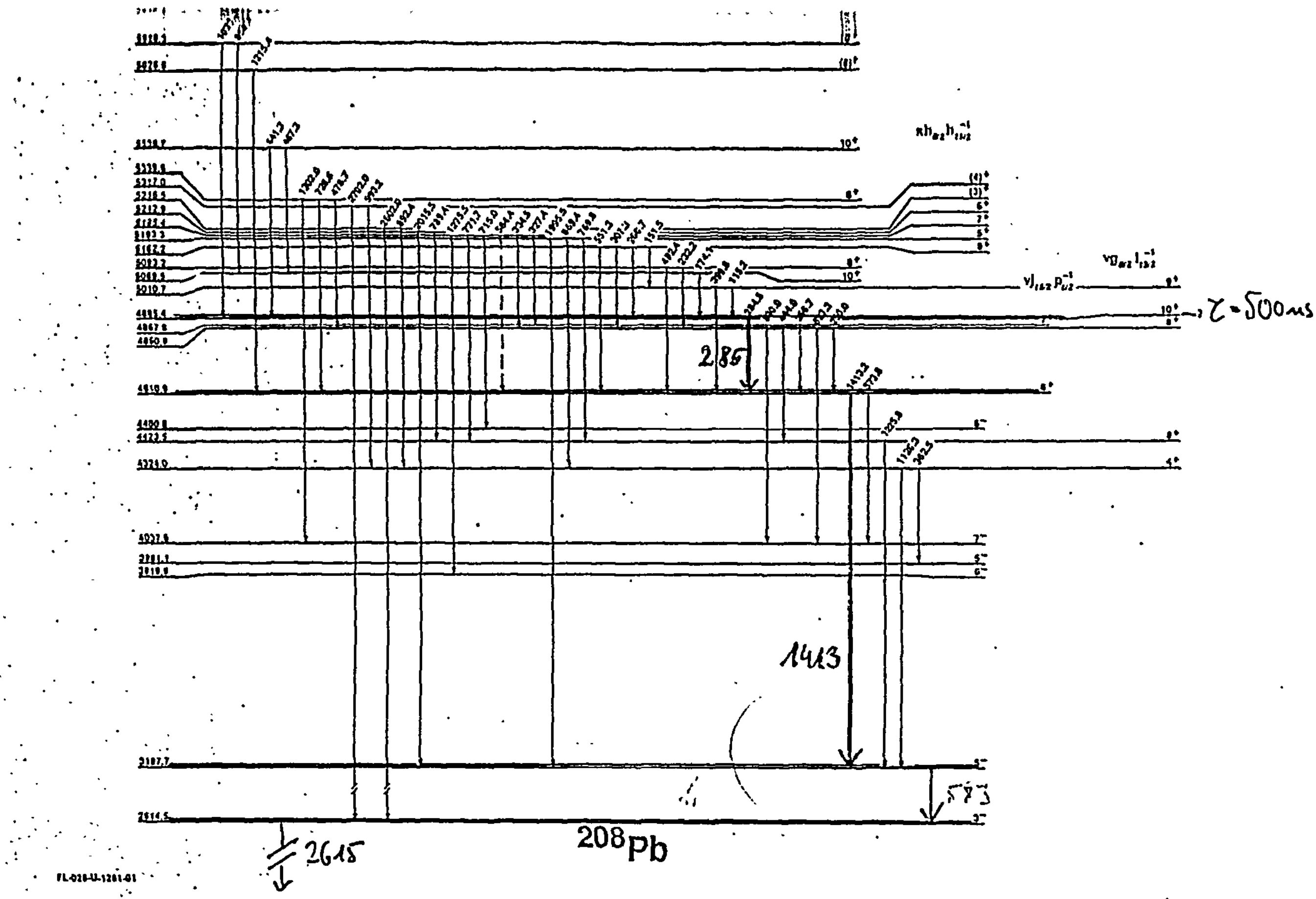

208Pb
2615
583
1413
286
τ = 500 ns
FL-020-U-1261-01

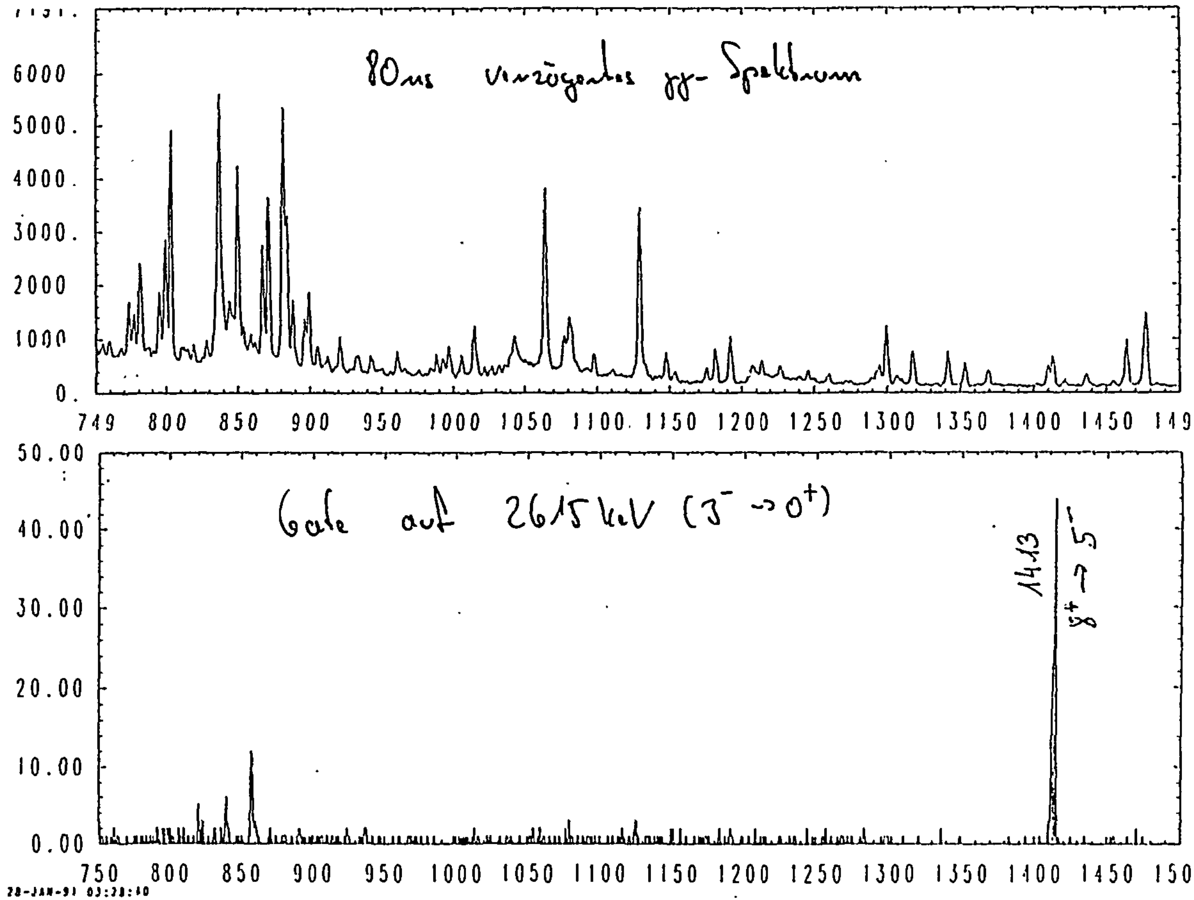
80ns verzögertes γγ-Spektrum
6000
5000.
4000.
3000.
2000.
1000
0.
749 800 850 900 950 1000 1050 1100 1150 1200 1250 1300 1350 1400 1450 1499
Gate auf 2615 keV (3⁻ → 0⁺)
1413
8⁺ → 5⁻
50.00
40.00
30.00
20.00
10.00
0.00
750 800 850 900 950 1000 1050 1100 1150 1200 1250 1300 1350 1400 1450 1500
28-JAN-91 03:28:10

Verzögertes
γγ-Spektrum
(~80 ms)

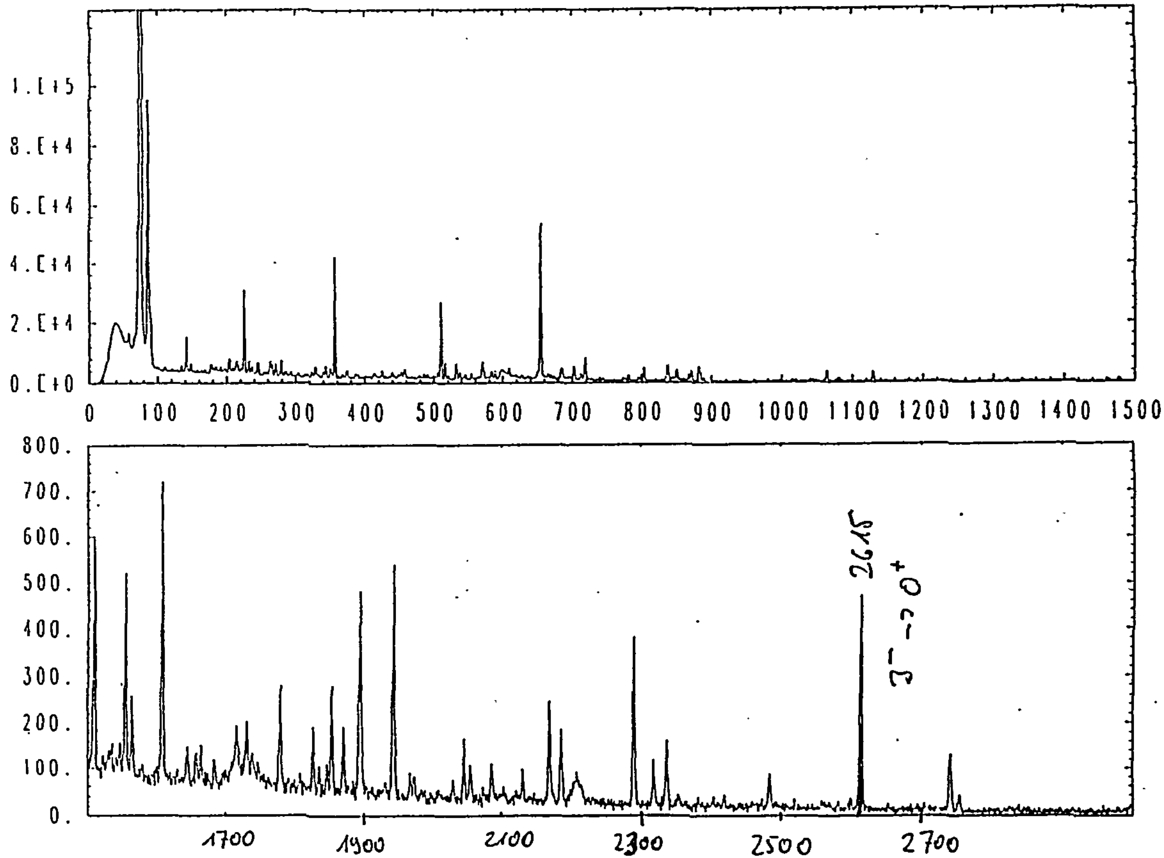

Parametrization of σ $\quad$ ($^{64}Ni + {}^{201}Pb$)

$$\sigma = \pi R^2 \left(1 - \frac{V}{E} \right)$$

$V_c = 212$ MeV $\quad$ with

$r_0 = 1{,}52(1)$ fm (measured)

$R = 15{,}61$ fm

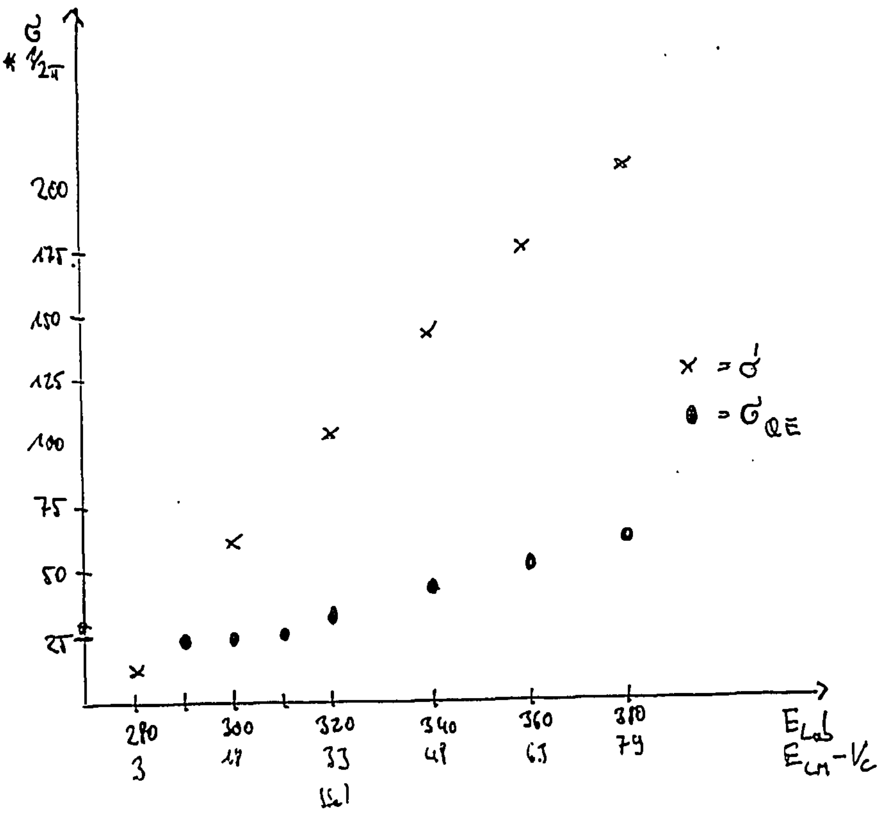

New and old Sn isomers produced in heavy-ion collisions

R.B.*, P.J. Daly, R. Meyer, Z. Grabowski, Ph. Benett

PURDUE UNIVERSITY, W. Lafayette IN

S. Lunardi

LNL Legnaro - Padova University

T.L. Khoo, R.V.F. Janssens, F. Carpenter .+. .....

ARGONNE NAT. LAB.

\+ IKP Jülich

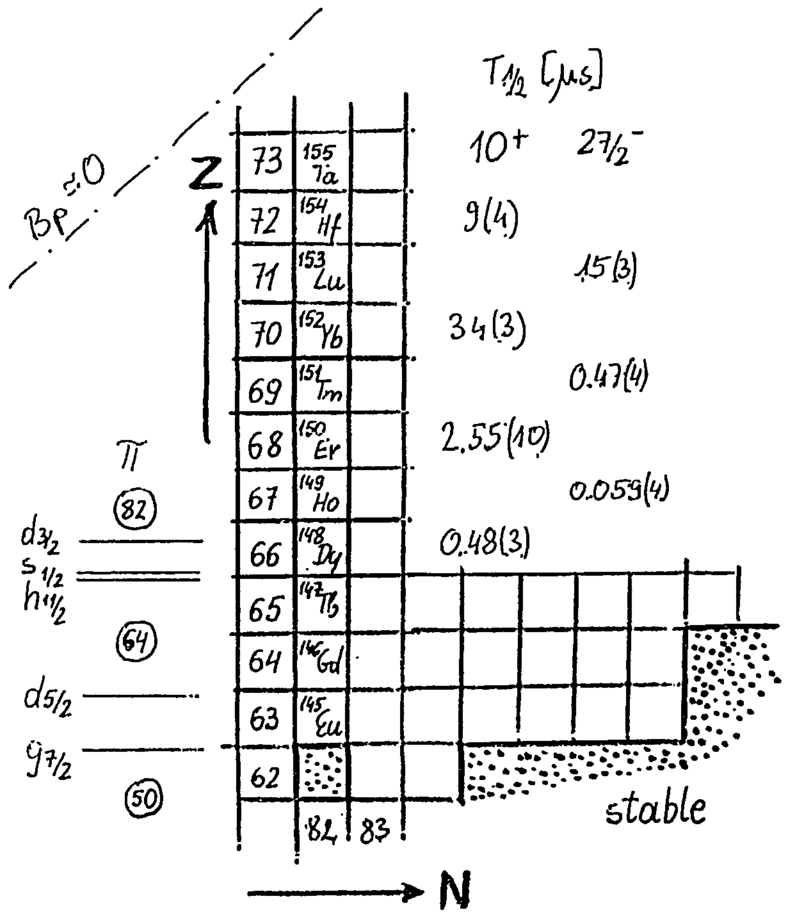

Bρ ≈ 0
Z
N
T1/2 [μs]
10+
27/2−
9(4)
15(3)
34(3)
0.47(4)
2.55(10)
0.059(4)
0.48(3)
73
155 Ta
72
154 Hf
71
153 Lu
70
152 Yb
69
151 Tm
68
150 Er
67
149 Ho
66
148 Dy
65
147 Tb
64
146 Gd
63
145 Eu
62
82
83
π
82
64
50
d3/2
s1/2
h11/2
d5/2
g7/2
stable

$$B(E2;\ 10^+ \to 8^+) = \left[\frac{6-n}{4}\right]^2 \frac{2025}{35321\,\pi} \left(e_{eff}\langle r^2\rangle\right)^2$$

$$B(E2;\ 27/2^- \to 23/2^-) = \left[\frac{6-n}{4}\right]^2 \frac{32400}{265837\,\pi} \left(e_{eff}\langle r^2\rangle\right)^2$$

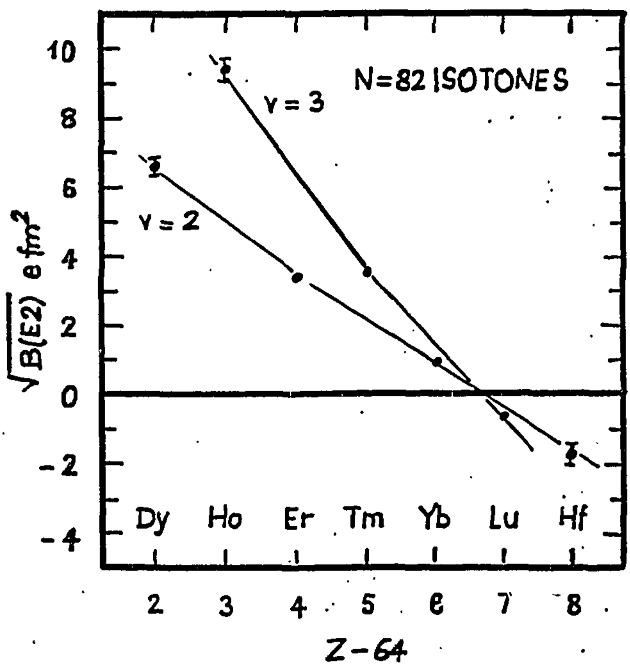

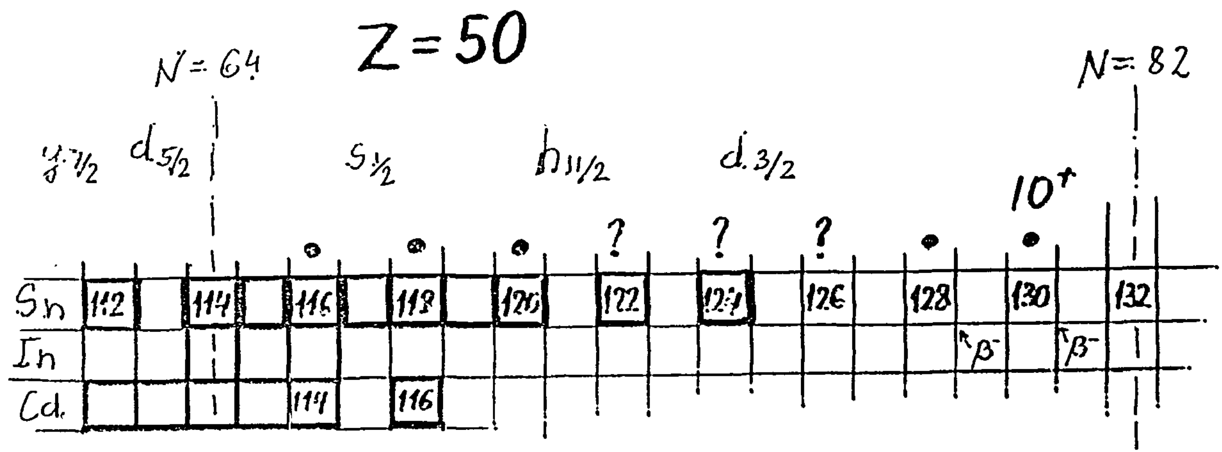

$^{114}Cd\ (\alpha, 2n)\ ^{116}Sn$ — $T_{1/2}\,(10^+) = 0.90(1)\,\mu s$ } Ishihara, Broda, Herskind

$^{116}Cd\ (\alpha, 2n)\ ^{118}Sn$ — $= 2.63(7)\,\mu s$ } Proc. Intl. Conf. Munich 1973

$^{116}Cd\ (^7Li, p2n)\ ^{120}Sn$ — $= 6.26(11)\,\mu s$ Lunardi et al. Z. Phys. A 328 487 (1987)

$^{128}In \rightarrow \beta^-\ ^{128}Sn$ — $= 2.69(23)\,\mu s$ } Fogelberg, Heide, Sau

$^{130}In \rightarrow \beta^-\ ^{130}Sn$ — $= 1.61(15)\,\mu s$ } Nucl. Phys. A352, 157 (1981)

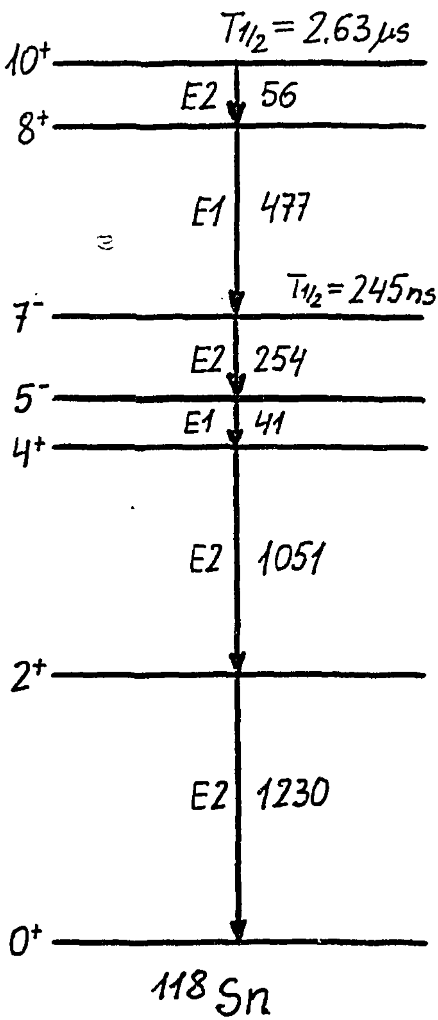

T1/2 = 2.63 μs
10+
E2 56
8+
E1 477
T1/2 = 245 ns
7-
E2 254
5-
E1 41
4+
E2 1051
2+
E2 1230
0+
118 Sn

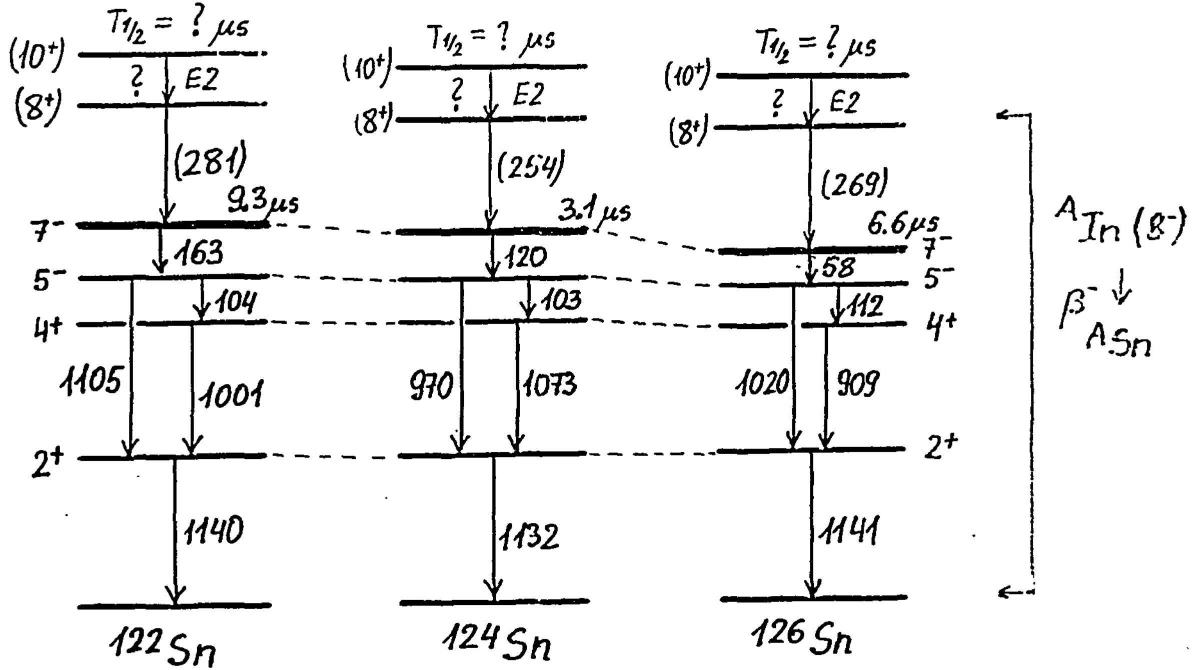

B. Fogelberg, P. Carle Nucl. Phys. A

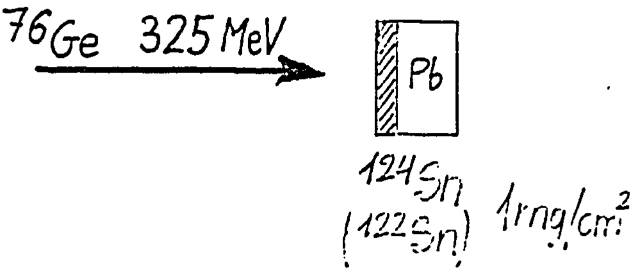

$V_B \simeq 280 MeV$

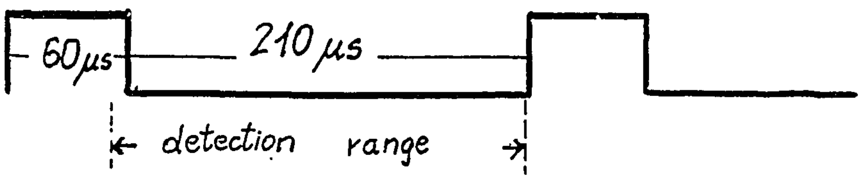

Argonne – Notre Dame array

12 Compton-supressed Ge
BGO ball

DATA: $E_\gamma * TIME$

$E_\gamma * TIME * T_{Ge\text{-}BGO}$ – delayed coincidence with BGO ball

$E_\gamma * E_\gamma$ off beam prompt coincidences

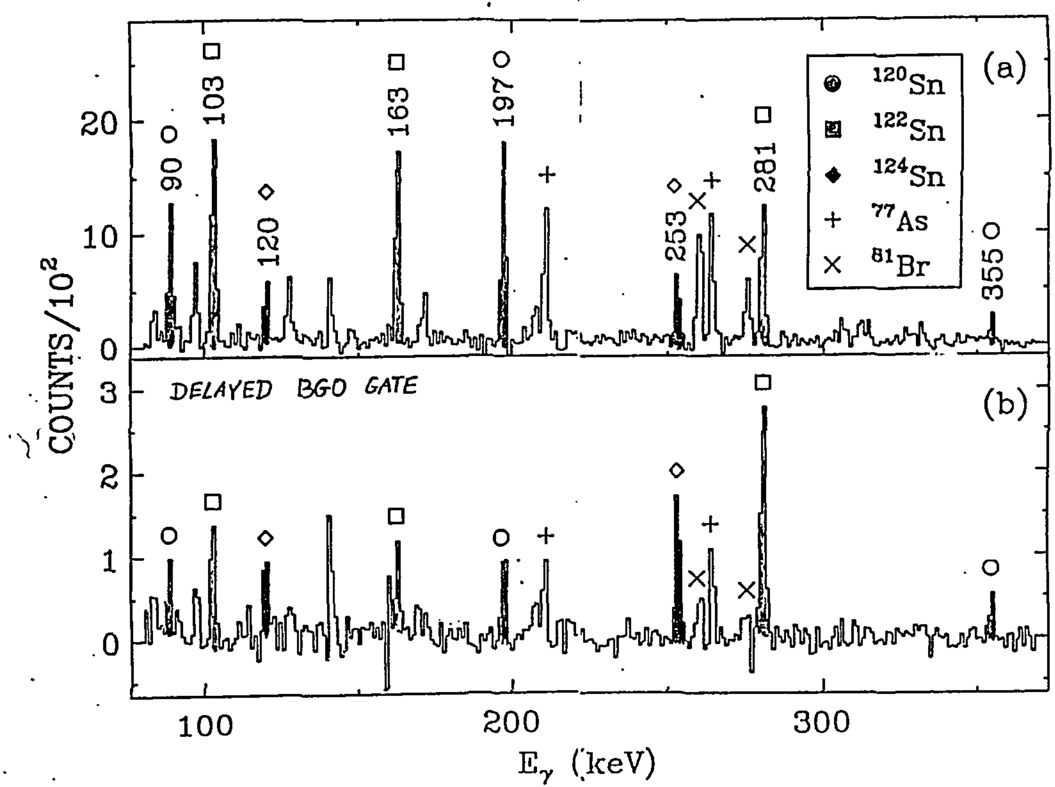

COUNTS/10²
E$_\gamma$ (keV)
(a)
(b)
DELAYED BGO GATE
90
103
120
163
197
253
281
355
^{120}Sn
^{122}Sn
^{124}Sn
^{77}As
^{81}Br

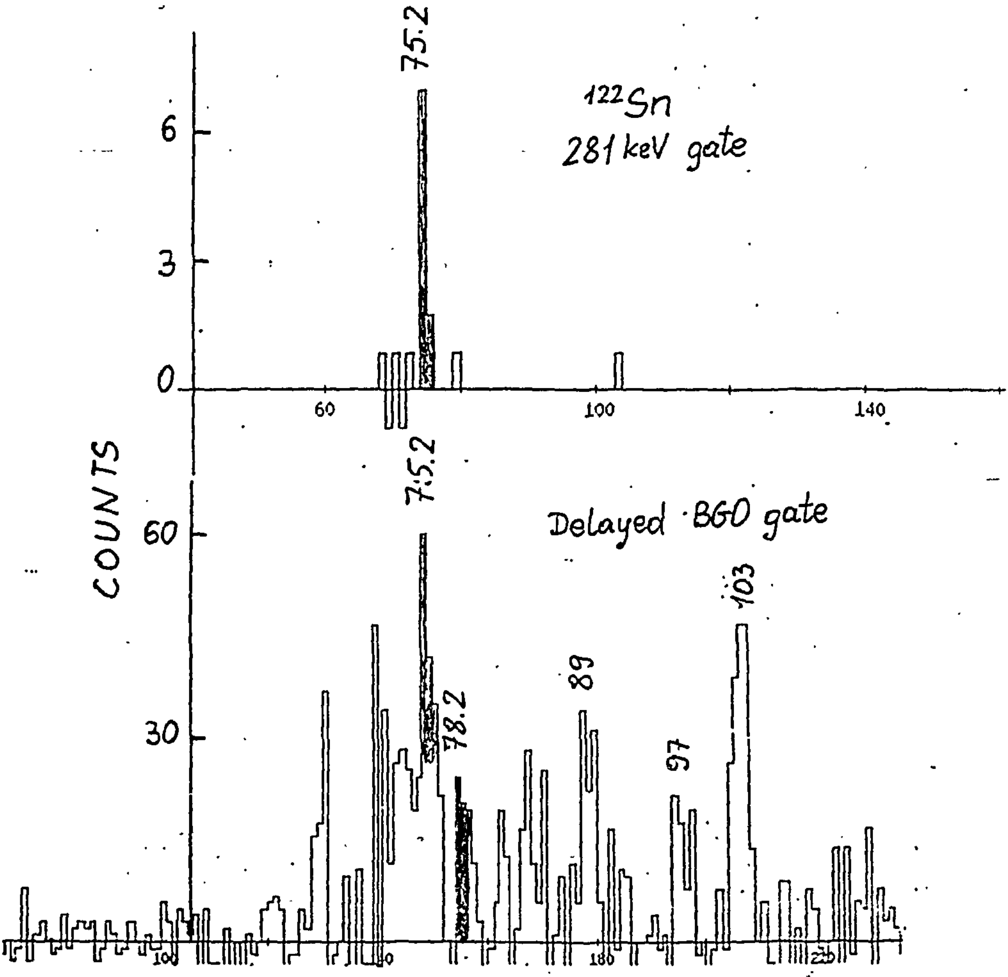

75.2
^{122}Sn
281 keV gate
6
3
0
60
100
140
COUNTS
7.5.2
Delayed BGO gate
60
103
89
78.2
30
97
100
180

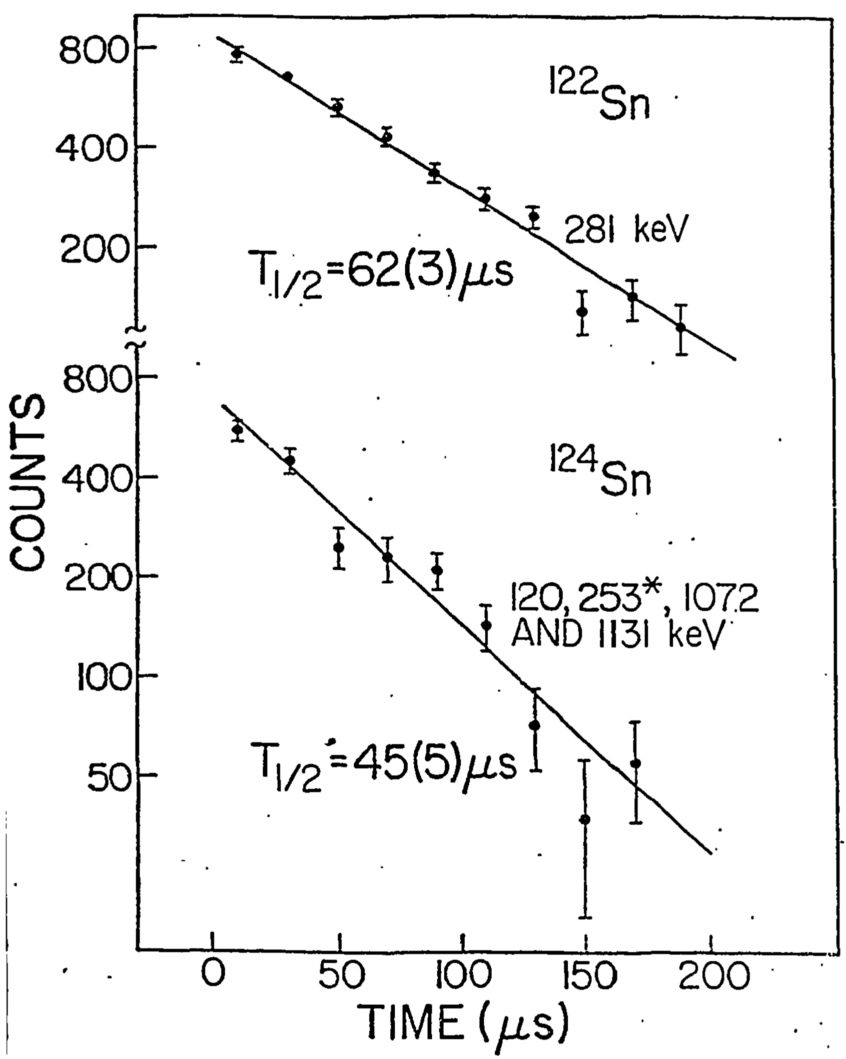

COUNTS
800
400
200
800
400
200
100
50
^{122}Sn
281 keV
$T_{1/2}$=62(3)μs
^{124}Sn
120, 253*, 1072
AND 1131 keV
$T_{1/2}$=45(5)μs
0
50
100
150
200
TIME (μs)

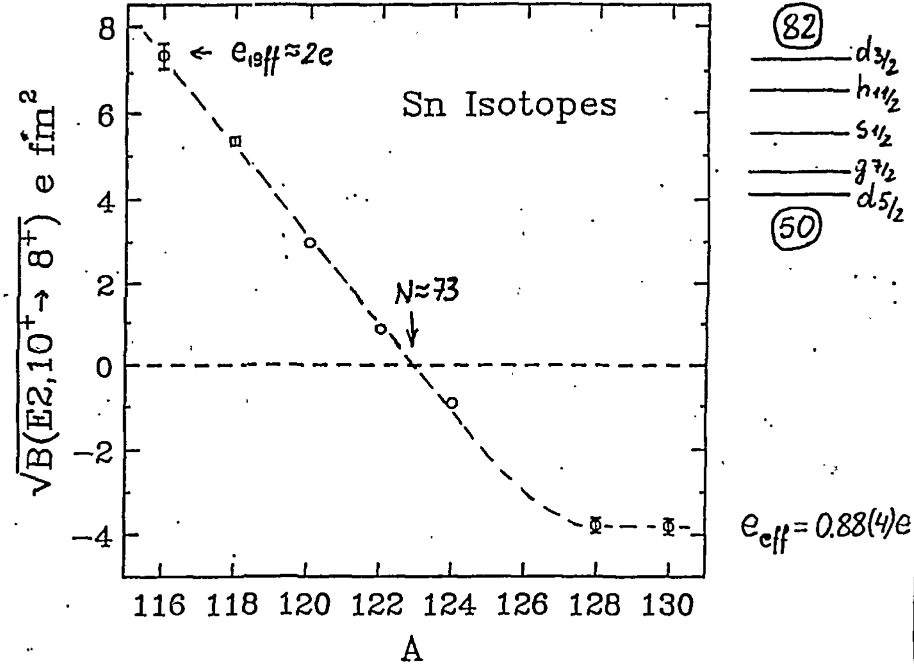

$$\sqrt{B(E2)} \sim (U^2 - V^2)\, e_{eff}$$

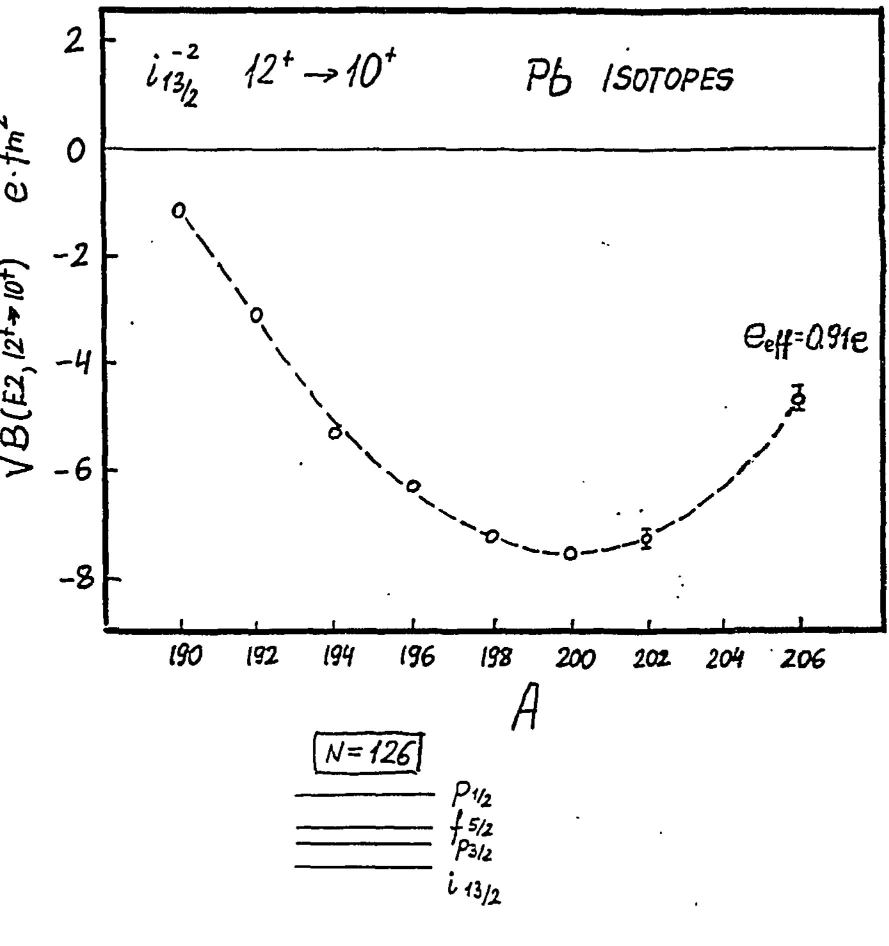

$i_{13/2}^{-2}$ $12^+ \to 10^+$
Pb ISOTOPES
$\sqrt{B(E2, 12^+ \to 10^+)}$ $e \cdot fm^2$
2
0
-2
-4
-6
-8
$e_{eff} = 0.91e$
190
192
194
196
198
200
202
204
206
A
N=126
$p_{1/2}$
$f_{5/2}$
$p_{3/2}$
$i_{13/2}$

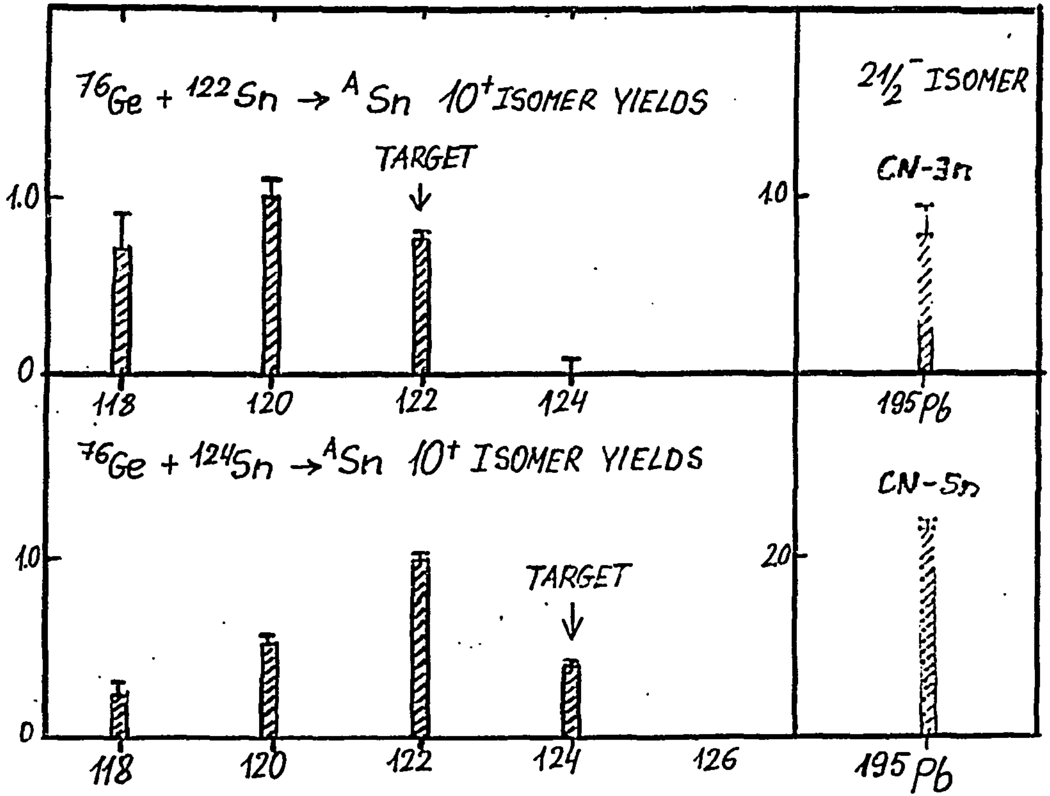

$^{76}Ge + ^{122}Sn \rightarrow {}^{A}Sn$ 10^{+} ISOMER YIELDS
TARGET
1.0
0
118
120
122
124
$21/2^{-}$ ISOMER
CN-3n
1.0
195 Pb
$^{76}Ge + ^{124}Sn \rightarrow {}^{A}Sn$ 10^{+} ISOMER YIELDS
TARGET
1.0
0
118
120
122
124
126
CN-5n
2.0
195 Pb

THE 2- TO 1-Phonon E3 TRANSITION Streng in ^{148}Gd

M. Piiparinen[1,2], P. Kleinheinz[3], J. Blomqvist[4], A. Virtanen[1], A. Ataç[2], D. Müller[2], J. Nyberg[2], T. Ramsøy[2], G. Sletten[2]

[1] Jyväskylä, [2] NBI Risø, [3] IKP Jülich, [4] MSI Stockholm

NORDBALL Plunger Measurement, June 1991

^{nat}CsI (^{19}F,4n) ^{148}Gd & ^{142}Sm

$$E_{^{19}F} = 73.5\,\mathrm{MeV}$$
$$E^{calc}_{Cb,\,Cs+F} = 73.6\,\mathrm{MeV}$$

1.3 mg CsI on 0.8 mg/cm² Au Target
6 mg/cm² Au Stopper

Nordball:

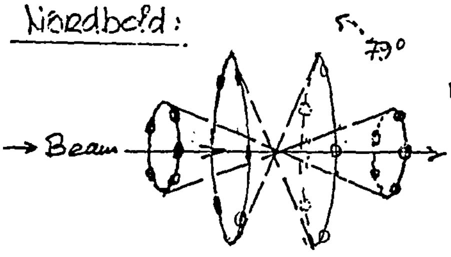

10 Detectors at 37°
10 Detectors at 79°
to Beam axis

Result
$$\tau^{12^+}_{143^\circ} = 85.0(49)\,\mathrm{ps}$$
$$\tau^{12^+}_{37^\circ} = 82.1(42)\,\mathrm{ps} \quad \rightsquigarrow \tau = 83(10)\,\mathrm{ps}$$

$$\rightsquigarrow \boxed{B(E3, 12^+ \to 9^-) = 1.00(14) \times 10^5\, e^2\mathrm{fm}^6 = 77(11)\,\mathrm{B_W}}$$

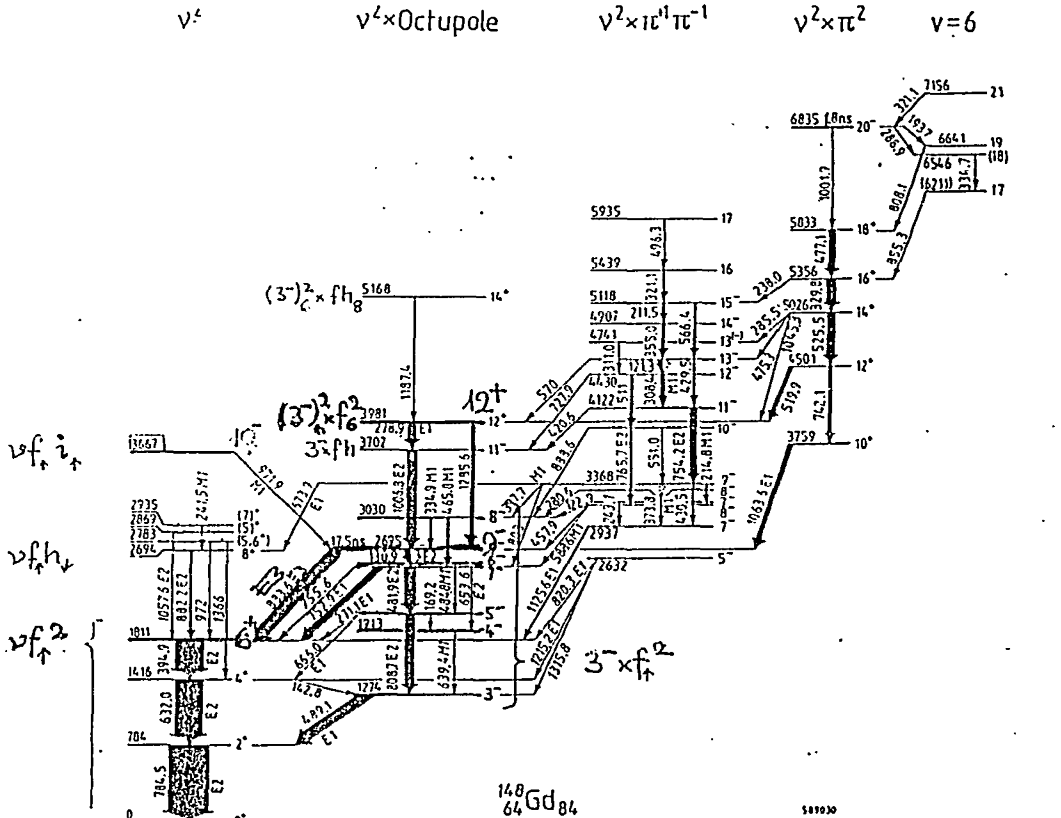

Piiparinen, Lunardi, de Angelis, et.al, ZPA 337(1990)387

$^{133}Cs(^{19}F,4n)^{148}Gd$ at 73.5 M

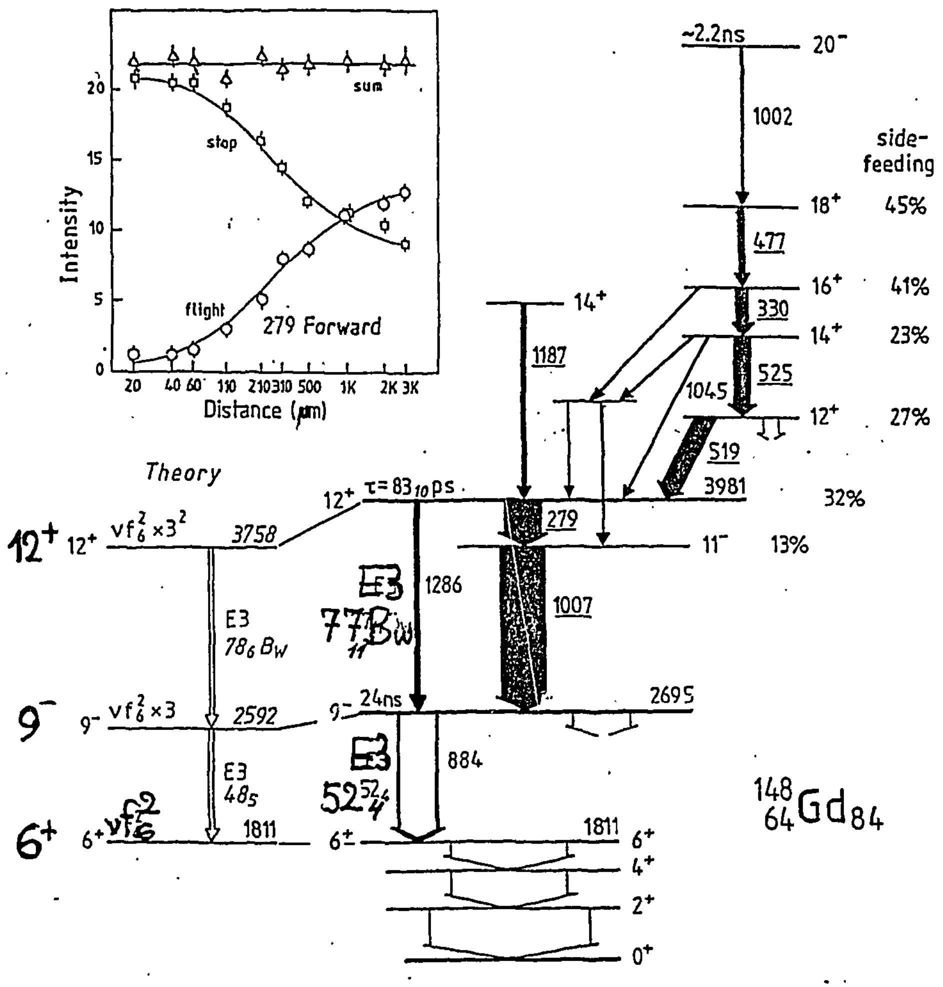

Fig. 1: Schematic partial level scheme of ^{148}Gd as observed in the present experiments. The filled γ–transitions were included in the decay time fit, individual timing data were obtained for the underlined γ's. Transitions without energies are symbolic & represent the inclusion in the fit of komplex known weak branches. Theoretical results are from ref. [2]. Insert: Fit to the data points for the 279 keV 12⁺ to 11⁻ transition measured in the 5 forward detectors at 37° to the beam direction.

The $\nu f_{7/2} \times 3^-$ Septet in $^{147}Gd_{83}$

$(i_{13/2}, f_{7/2} \times 3^-)$ Coupling

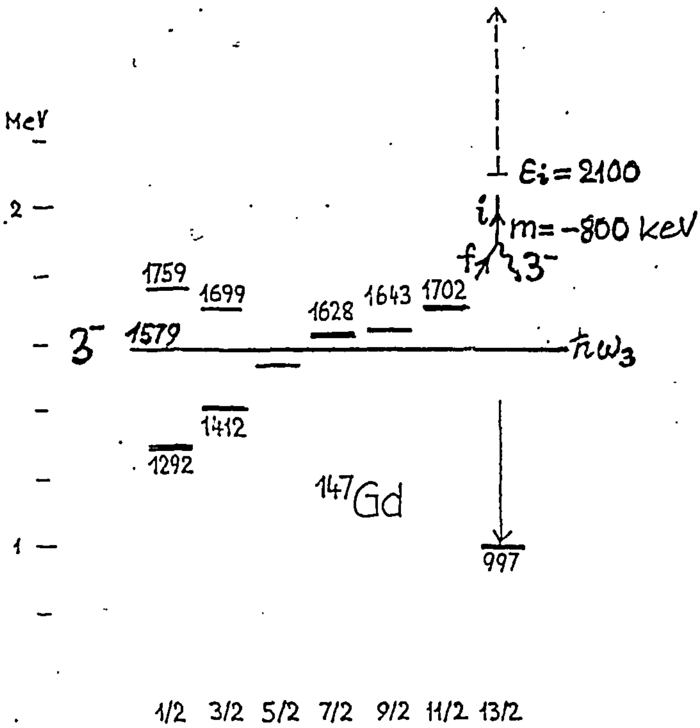

Lemma:

> The $f \times 3^-$ anharmonicities of $^{147}Gd_{83}$ fully determine the $f^2 \times 3$ anharmonicities in $^{148}Gd_{84}$

$\delta E_{13/2}$ treated exact by diagonalization

$\delta E_{<13/2}$ by first order perturbation theory

$(\nu f_{7/2} \times 3^-, \nu i_{13/2})$ - Mixing in N=83 Nuclei

and $^{sp}B(E3, \nu i_{13/2} \rightarrow \nu f_{7/2})$

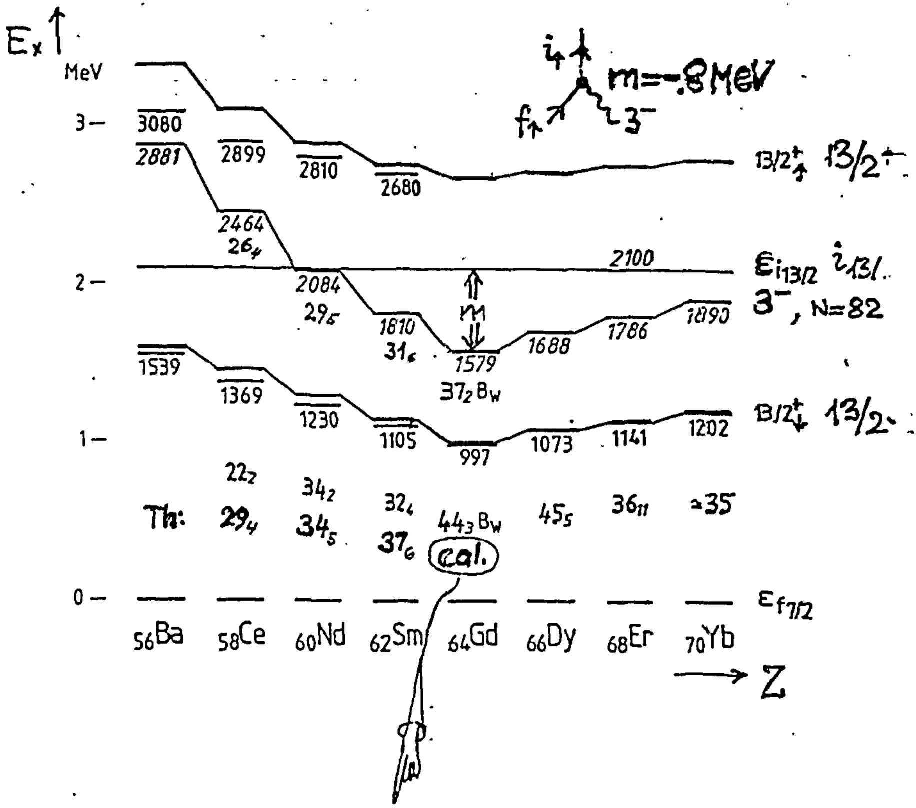

$$\left.\begin{array}{l} \Psi_{13/2\downarrow} = .81(\nu f \times 3) + .59(\nu i) \\ \text{Gd:}\quad B(E3, 3^- \rightarrow 0^+) = 37_2\ B_W \\ \qquad B(E3, 13/2\downarrow \rightarrow 7/2) = 44_3\ B_W \end{array}\right\} \rightsquigarrow B(E3, \nu i \rightarrow \nu f) = 8.1_{25}\ B_W$$

from Experiment

Piiparinen et al, IKP Jül. Z. Phys. A 337 (1990) 387

Harmonic energies for $\nu f^2 \times 3^-$ multiplet in ^{148}Gd

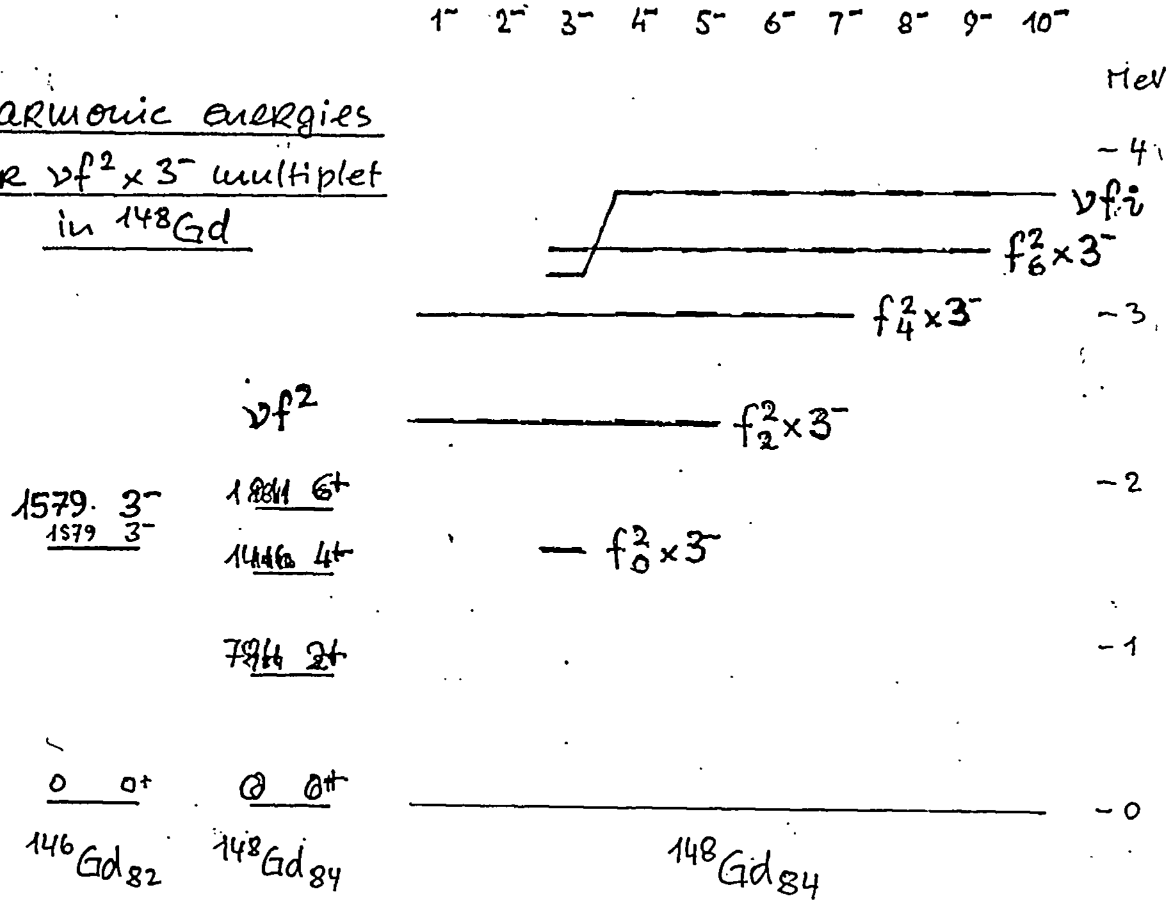

Recoupling

$$\boxed{[f_J^2\times 3]_I = \sum_j (-1)^{7+3+I}\sqrt{(2J+1)(2j+1)}\begin{Bmatrix} 7/2 & 7/2 & J\\ 3 & I & j\end{Bmatrix}[f\times(f\times 3)_j]_I}$$

Example: $\boxed{I=5^-}$ $f^2\times 3$ States in $^{148}Gd_{84}$

Harmonic	Anharmonic contr. from		$E^{th.}$ from diagonalization
ALL FROM DATA IN ^{147}Gd	$j=3/2$ to $11/2$ (1st ord. pert.)	$j=13/2$ (exact)	4156

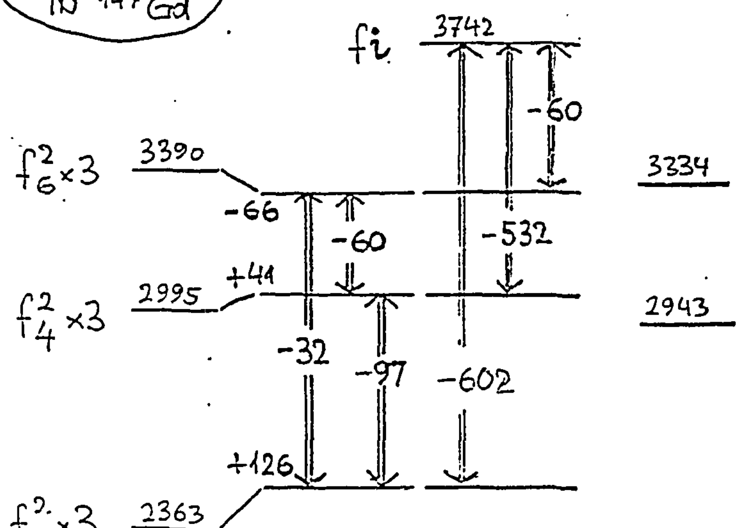

	SM	Exp.
$(\nu f^2\times 3)5_1^-$:	2432	2082

OBSERVED & CALCULATED

$\nu f_{7/2}^2 \times 3^-$ STATES IN ^{148}Gd

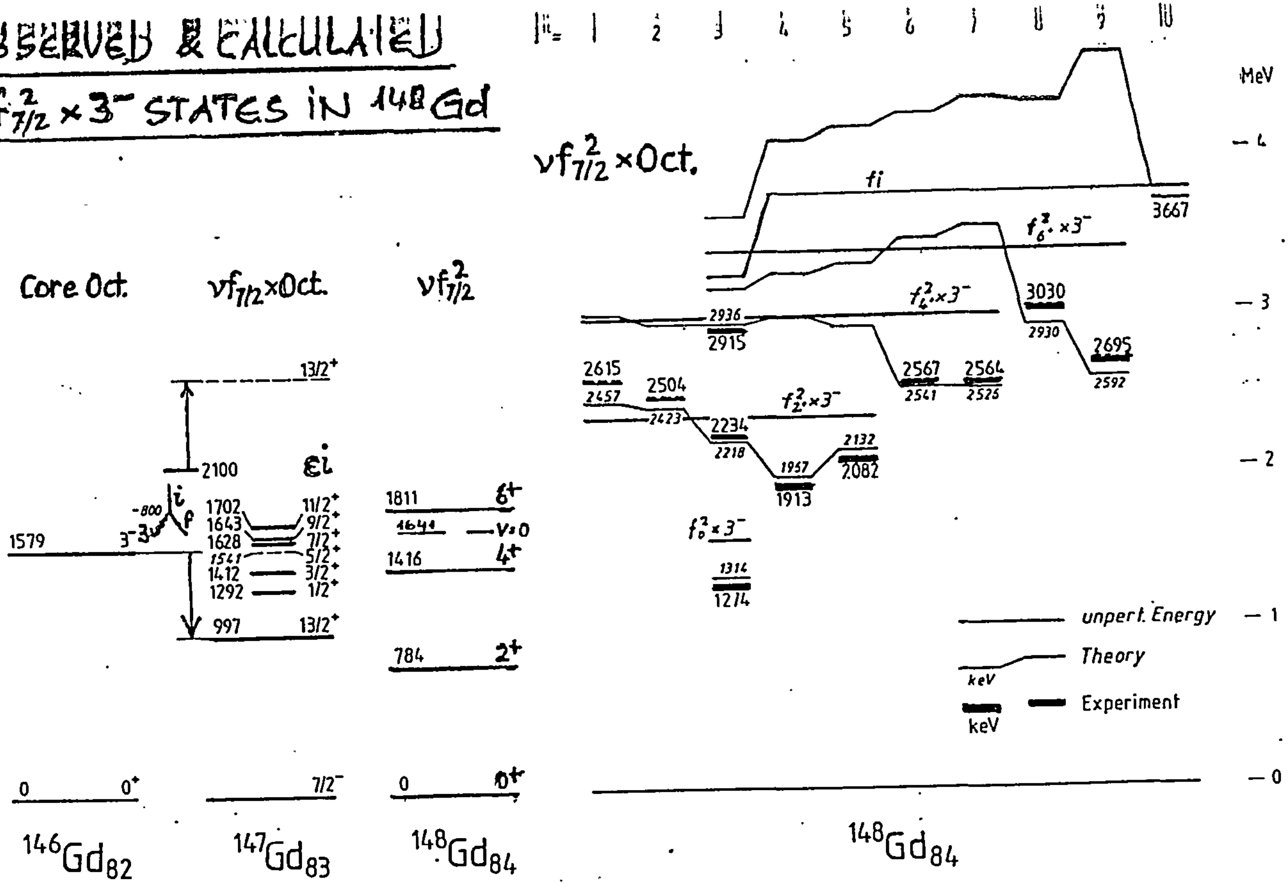

input data

E3 Transition Strengths (in Bw) of $f^2 \times 3^- \to f^2$ transitions

$\nu f^2_{7/2}$ $\qquad$ $\nu f^2_{7/2} \times$ Octupole

Ground-state E3 transitions:

Exp.(pp'): Theory

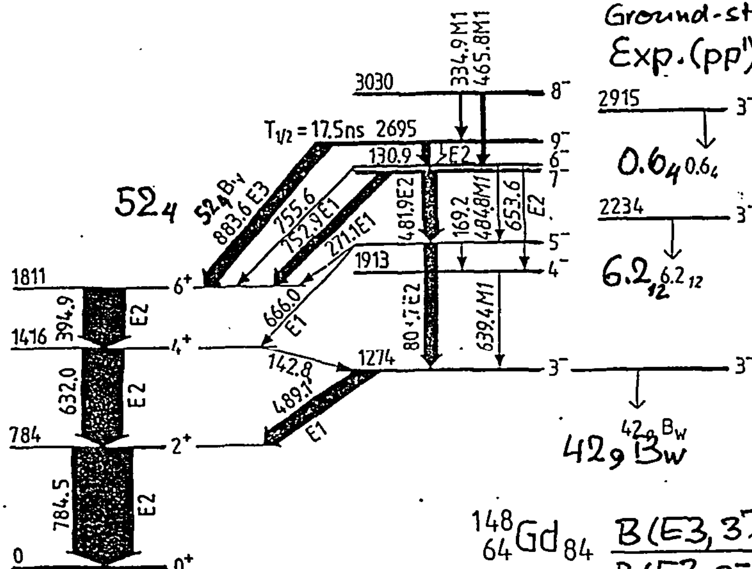

.08₁₈

5.2₅

35.9₆ Bw

$$^{148}_{64}\mathrm{Gd}_{84} \quad \frac{B(E3, 3^-_1 \to 0)}{B(E3, 3^-_2 \to 0)} = 6.8_3 \quad 6.9_7$$

Input Data: $B(E3, 3_{core} \to 0^+) = 37_2$ Bw

$B(E3, \nu i \to \nu f) = 8.1_{25}$ Bw

$(\alpha, 4n)$ $(\tau, 3n)$ γ & e and compositions of initial and final States from diagonalization ^{148}Gd pp'

Piiparinen et al, ZPA 337 (1990) 387 $\quad$ de Angelis et al ZPA 336 (1990) 375

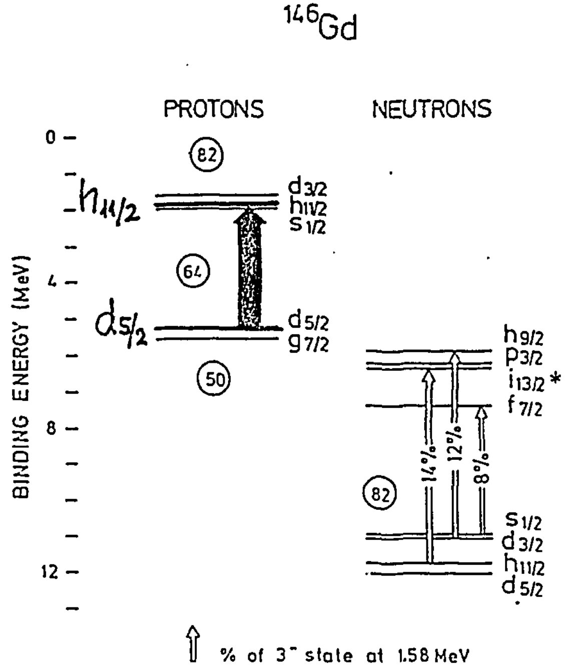

^{146}Gd
PROTONS
NEUTRONS
BINDING ENERGY (MeV)
0
4
8
12
82
64
50
82
$h_{11/2}$
$d_{5/2}$
$d_{3/2}$
$h_{11/2}$
$s_{1/2}$
$d_{5/2}$
$g_{7/2}$
$h_{9/2}$
$p_{3/2}$
$i_{13/2}$ *
$f_{7/2}$
14%
12%
8%
$s_{1/2}$
$d_{3/2}$
$h_{11/2}$
$d_{5/2}$
⇧ % of 3⁻ state at 1.58 MeV

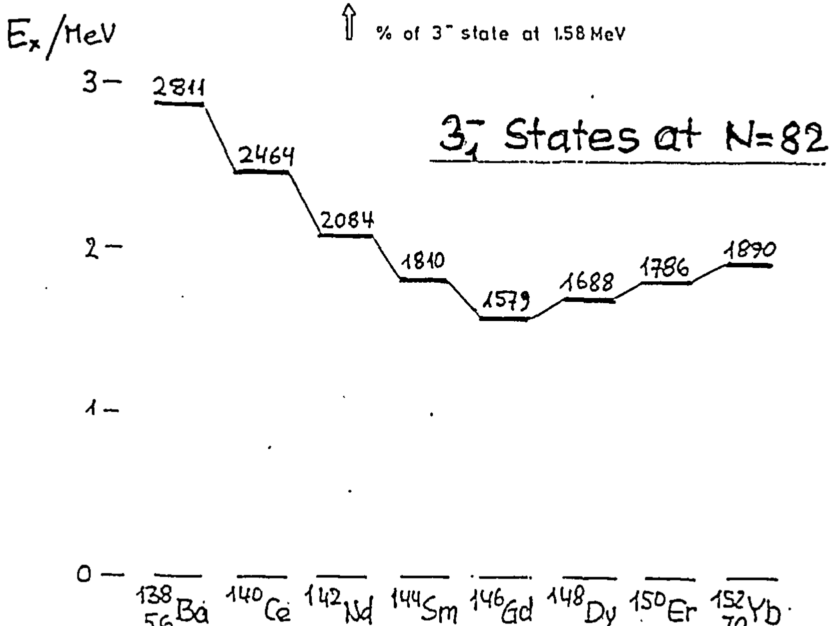

E_x/MeV
3
2
1
0
2811
2464
2084
1810
1579
1688
1786
1890
3_1^- States at N=82
$^{138}_{56}$Ba
^{140}Ce
^{142}Nd
^{144}Sm
^{146}Gd
^{148}Dy
^{150}Er
$^{152}_{70}$Yb

Pauli-Blocking in the aligned $(3^-)^2_{6+}$ State of ^{146}Gd

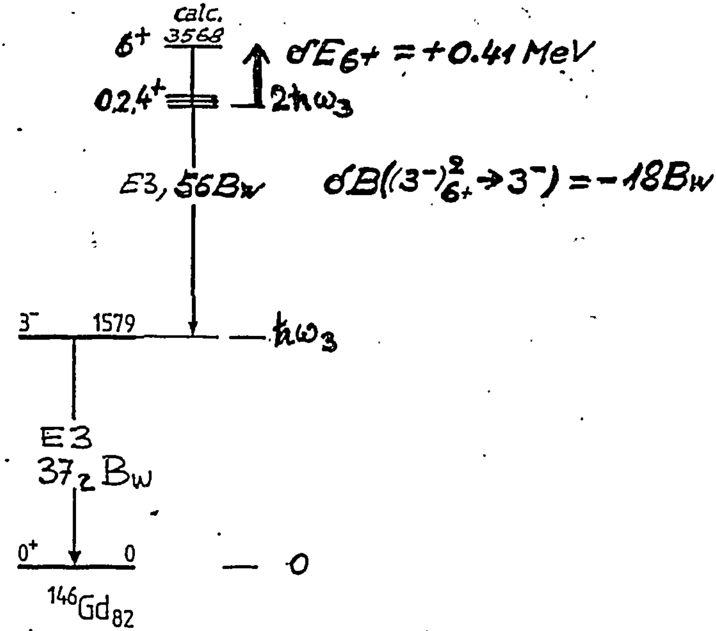

Calculated from butterfly diagram with the

Measured Input data:

- $\boxed{M = 1.1\ \text{MeV from } (^{147}\text{Tb})}$
- $\Delta E = 1.5$ MeV
- $B(E3, \pi h_{11/2} \to \pi d_{5/2}^{-1}) = 5$ Bw
- $B(E3, 3^- \to 0^+) = 37_2$ Bw (^{146}Gd)

Phys. Rev. Lett 48(82) 1457 (J. Blomqvist)

Two-Phonon Anharmonicities from Pauli-blocking

$I = 0, 2, 4, 6^+$

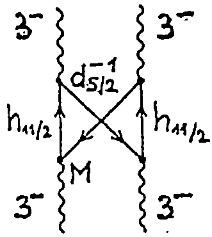

$M = 1.1\,\text{MeV}$
from ^{147}Tb

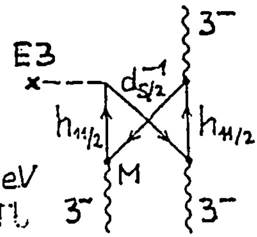

$$\delta E_I = 98\, X\left(\tfrac{11}{2}\tfrac{5}{2}3, \tfrac{5}{2}\tfrac{11}{2}3, 33I\right)\frac{M^4}{(\Delta E)^3}$$

with $M \simeq 1.1_5$ MeV
and $\Delta E \simeq 1.5$ MeV } from ^{147}Tb

$\boxed{\delta E_{6^+} = +.41\ \text{MeV}}$ $\quad \delta E_{0^+,2^+,4^+}$ small

$$\delta B(E3, I\to 3) = -392\, X\left(\tfrac{11}{2}\tfrac{5}{2}3, \tfrac{5}{2}\tfrac{11}{2}3, 33I\right)\frac{M^3}{(\Delta E)^3} \times$$
$$\times \sqrt{B(E3, 3\to 0)\times B(E3, h_{11/2}d_{5/2}^{-1}\to 0)}$$

with $B(E3, 3\to 0) = 37_2\, B_W$ from ^{146}Gd
$B(E3, h_{11/2}d_{5/2}^{-1}\to 0) \simeq 5\, B_W \quad (e_{eff} = 1.56e)$

$\delta B(E3, 6\to 3) = -18\ B_W$

$\boxed{B^{calc}(E3, 6\to 3) = (2\times 37 - 18)B_W \approx 56 B_W}$

Phys. Rev Lett. 48(82)1457

Pauli-Blocking in the $\pi h_{11/2} \times 3^-$ Septet of $^{147}_{65}Tb$

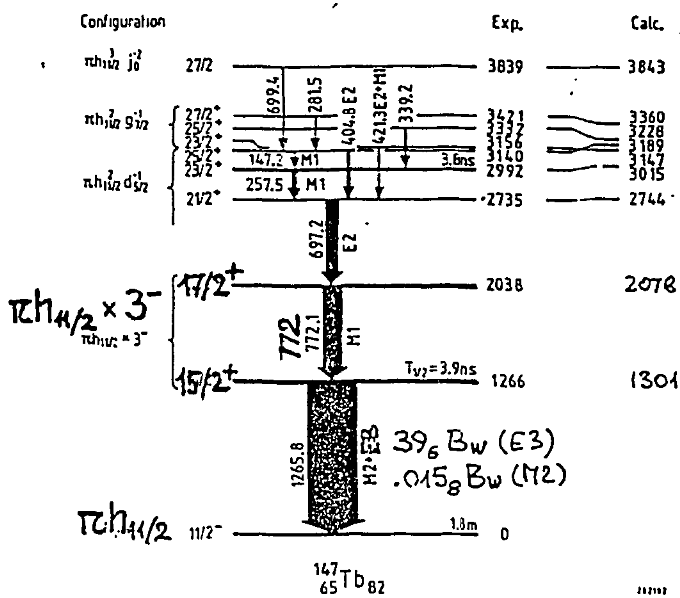

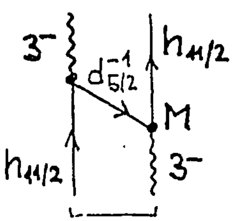

$I = \frac{5}{2}, .. \frac{17}{2}$

$$\delta E_I = 7W(3\tfrac{11}{2}\tfrac{11}{2}3;\tfrac{5}{2}I)\frac{M^2}{\Delta E}$$

$$\Delta E = E_{h_{11/2}} - E_{d_{5/2}} - \hbar\omega_3 \simeq 1.5\,\mathrm{MeV}$$

$\rightsquigarrow$ **$M = 1.1$ MeV**

for $\delta E_{17/2} - \delta E_{15/2} = .772$ MeV

$^{144}Sm\,(^6Li, 3n)\,\gamma\,\&\,e^-$

Styczen et al., ZPA 312 (1983) 149

Broda et al, ZPA 293 (79) 135

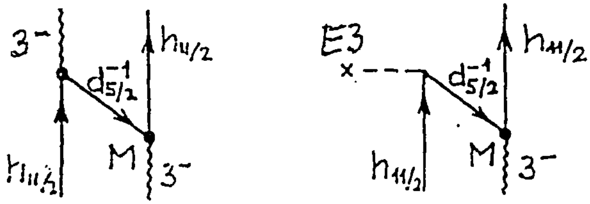

$$\delta B(E3, \tfrac{15}{2} \to \tfrac{11}{2}) = -14 W(3 \tfrac{11}{2} \tfrac{11}{2} 3; \tfrac{5}{2} \tfrac{15}{2}) \times \frac{M}{\Delta E} \times$$

$$\times \sqrt{B(E3, 3 \to 0) \times B(E3, h_{11/2} d_{5/2}^{-1} \to 0)}$$

with $M = 1.1$ MeV from $17/2$ to $15/2$ splitting and
$\Delta E \simeq 1.5$ MeV ,
$B(E3, 3 \to 0) = 37.\ B_W$
$B(E3, h_{11/2} d_{5/2}^{-1} \to 0) \approx 5 B_W \quad (e_{eff}(\pi) = 1.56e)$

$$\boxed{\begin{aligned} \delta B(E3, \tfrac{15}{2} \to \tfrac{11}{2}) &= +6 B_W \\ B^{calc}(E3, \tfrac{15}{2} \to \tfrac{11}{2}) &\simeq \underline{43_2 B_W} \end{aligned}} \quad B^{exp}(E3, \tfrac{15}{2} \to \tfrac{11}{2}) = \underline{39_6 B_W}$$

J. Styczen, M. Piiparinen, [illegible], [illegible] P. Kleinheinz, [illegible], J. Blomqvist, Z. Physik A 312 (83) 149

The $[\nu f^2_6 \times 3^- \times 3^-]_{12^+}$ Two-Phonon State

Within the configuration four 12^+ state will contribute to the 2-phonon excitation

The interaction matrix is completely specified by experimental input data (and angular momentum recoupling:

$$\begin{pmatrix} 5493 & -1403 & 0 & 0 \\ -1403 & 5358 & 56 & -947 \\ 0 & 56 & 5407 & 0 \\ 0 & -947 & 0 & 6011 \end{pmatrix} \begin{pmatrix} f^2_6 \times (3^-)^2 \\ f\,i_{10} \times 3^- \\ f\,i_9 \times 3^- \\ i^2_{12} \end{pmatrix}$$

E3 transitions :

$B(E3, \nu i \to \nu f) = 8.1_{25}$ Bw

$B(E3, 3^- \to 0^+) = 37_2$ Bw

$B(E3, (3^-)^2_6 \to 3^-) = 56_3$ Bw

Diagonalization ↳

E_x	Amplitudes $f^2_6 \times 3^2$	$f\,i_9 \times 3$	$f\,i_{10} \times 3$	i^2_{12}	$B(12^+ \to 9^-)$	Experiment E_x	$B(E3)$
3758	−0.58	−0.72	0.15	−0.35	**78_6**	3981	**77_{11}**
5080	−0.35	−0.10	−0.82	0.44	2.9		
6154	0.54	−0.25	−0.53	−0.61	0.002		
7277	0.50	−0.64	0.17	0.56	0.03		

$^{th}B(E3, 12^+ \to 9^-, {}^{148}Gd) = 78_6$ Bw

$^{exp}B(E3, 12^+ \to 9^-, {}^{148}Gd) = 77_{11}$ Bw

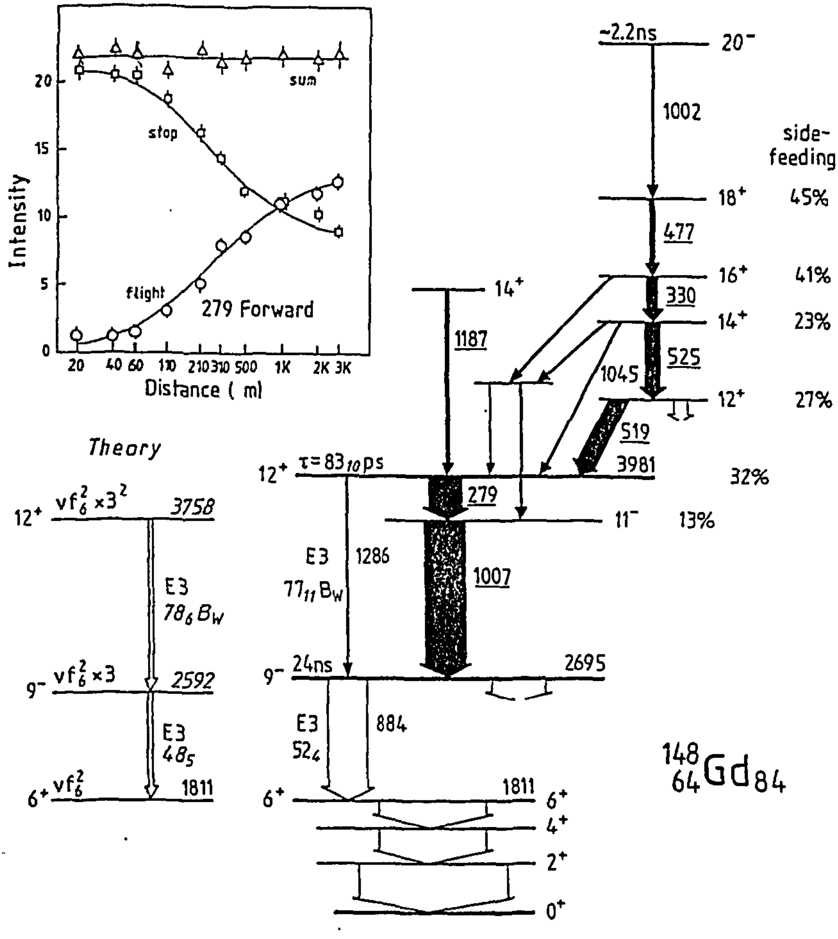

Fig. 1: Schematic partial level scheme of ^{148}Gd as observed in the present experiments. The filled γ–transitions were included in the decay time fit, individual timing data were obtained for the underlined γ's. Transitions without energies are symbolic & represent the inclusion in the fit of komplex known weak branches. Theoretical results are from ref. [2]. Insert: Fit to the data points for the 279 keV 12^+ to 11^- transition measured in the 5 forward detectors at 37^0 to the beam direction.

Two- to One-Phonon E3 strength in ^{148}Gd

$$\psi^{(1)}_{12+} = +.35\,(i^2_{12}) + 0.72\,(f i_9 \times 3) - .15\,(f i_{10} \times 3) + .58\,(f^2_6 \times$$

$i \to f$ 8.1 B_w $\quad$ $3 \to 0$ 37 B_w $\quad$ $i \to f$ 8.1 B_w $\quad$ $6 \to 3$ 56 B_w

$$\psi_{9-} = +.65\,(f i_9) + .76\,(f^2_6 \times 3)$$

With $B(E3, \nu_i \to \nu_f) = 8.1\ B_w$

$B(E3, 3^- \to 0^+) = 37\ B_w$

$B(E3, (3^- \times 3^-)_6 \to 3^-) = (2 \times 37 - 18)\, B_w = 56\, B_w$

(Pauli blocking in 6^+

$$\underline{B(E3, 12^+ \to 9^-)} = \left\{ .65 \cdot 0.35 \sqrt{\tfrac{7}{5} 8.1} + 0.65 \cdot 0.72 \sqrt{37} + 0.76 \cdot 0.72 \sqrt{\tfrac{20}{13} 8.1} + 0.76 \cdot 0.58 \sqrt{56} \right\}^2 B_w =$$

$$= \underline{78\ B_w},$$

Significantly above the pure two- to one-phonon $6^+ \to 3^-$ transition of the ^{146}Gd c

SUMMARY:

$B(E3, 12^+ \rightarrow 9^-, {}^{148}Gd) = 77_{11}$ Bw from Plunger experiment at Nordball with ^{19}F beam at the Coulomb barrier

The Two-Phonon Octupole nature for the ^{148}Gd 12^+ state is established through

- Observation of the double-E3 deexcitation-cascade to the νf_6^2 level, and through
- The measured E3 transition strengths of $B(E3, 12^+ \rightarrow 9^-) = 77_{11}\, B_W$ and $B(E3, 9^- \rightarrow 6^+) = 52_4$ B

The deviations from harmonic vibration are quantitatively determined through the anharmonicities measured in the $\nu f_{7/2} \times 3^-$ and $\pi h_{11/2} \times 3^-$ septets in the one-valence-particle nuclei ^{147}Gd and ^{148}Tb

These parameterfree calculations exploit exclusively angular momentum symmetries since all dynamic quantities – the nucleon-nucleon- and nucleon-Phonon twobody-interactions, as well as the elementary B(E3) valu. are taken from Experiment.

IDEA

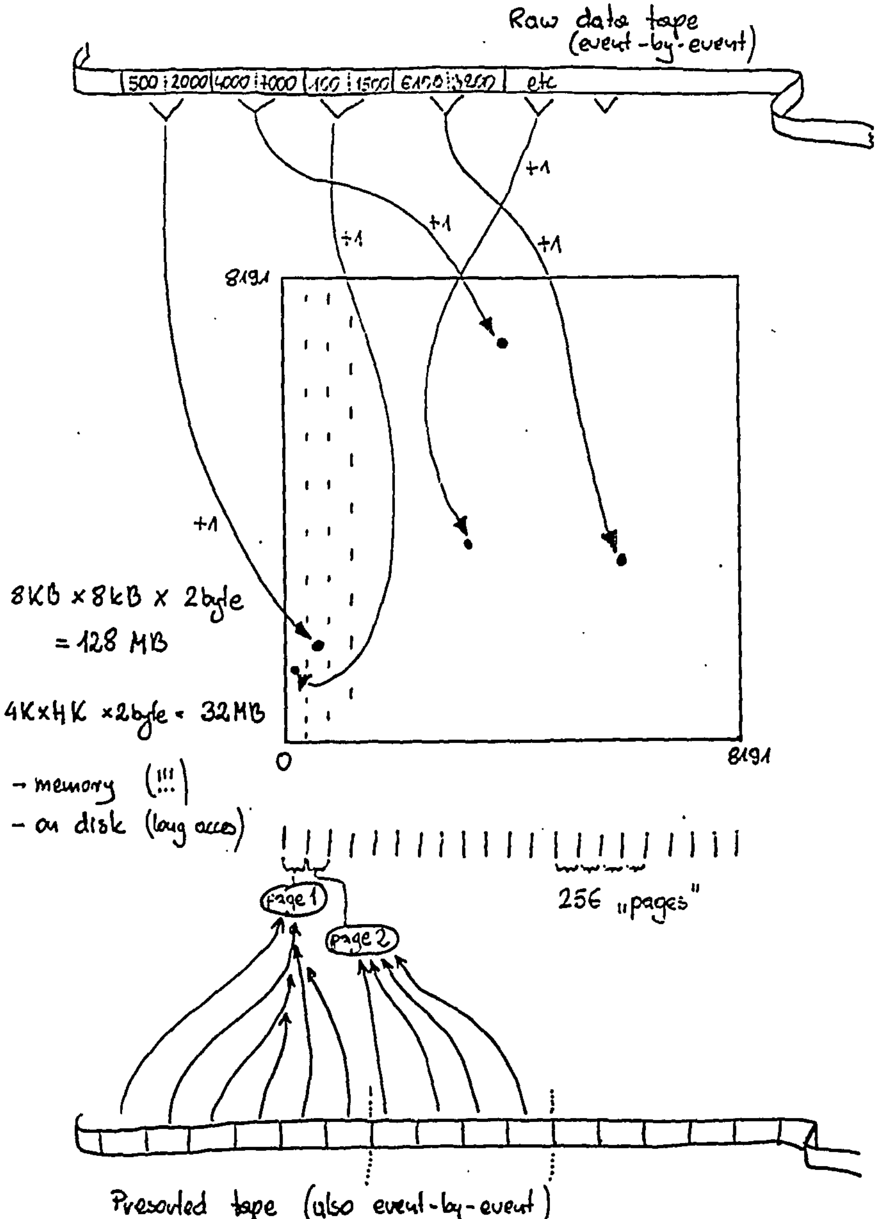
Raw data tape
(event-by-event)
500 | 2000 | 4000 | 7000 | 100 | 1500 | 6100 | 3200 | etc
+1
+1
+1
+1
+1
8191
0
8191
8KB × 8kB × 2byte
= 128 MB
4K×4K ×2byte = 32MB
→ memory (!!!)
→ on disk (long acces)
page 1
page 2
256 „pages"
Presorted tape (also event-by-event)

IMPLEMENTATION

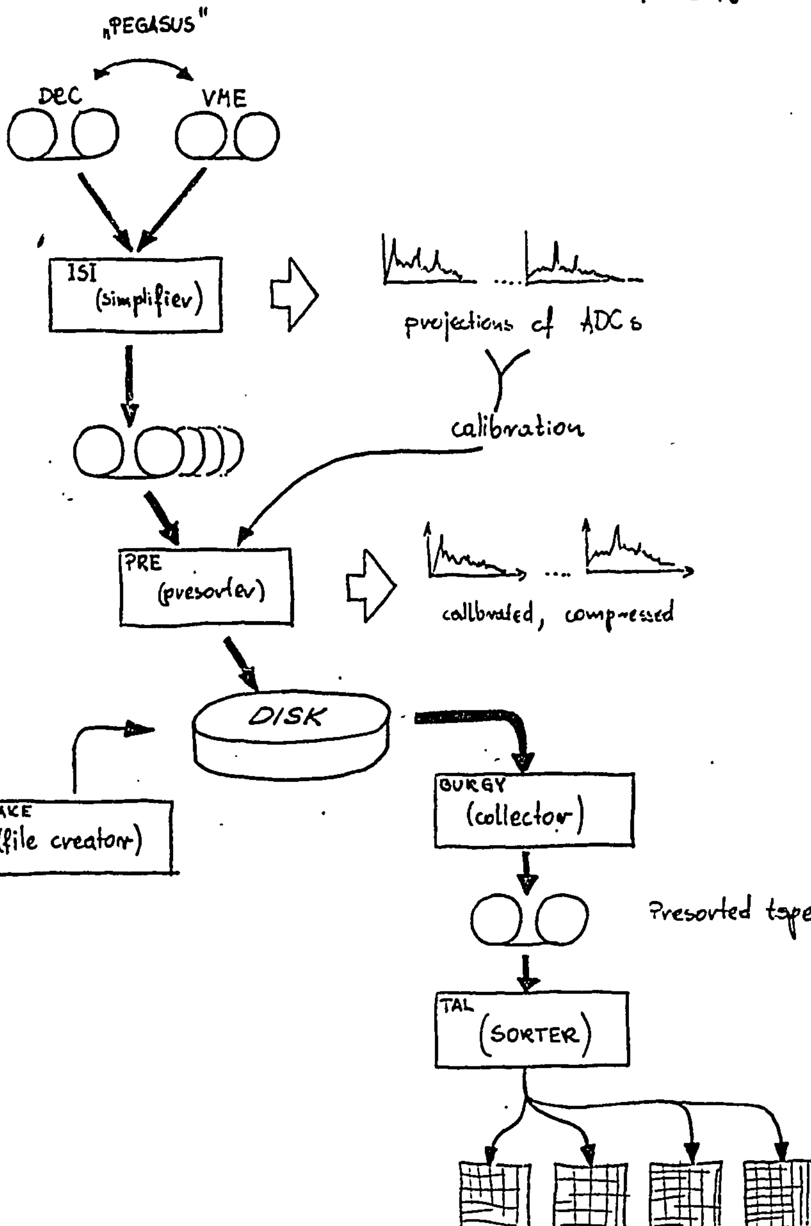

PEGASUS

Program for converting raw data EXABYTE tapes — Version 1.9

Author : Jerzy Grebosz — 15 October 1990

MAIN MENU

Show events from Strasbourg tape

Transform Strasbourg tape to FASTSORT tape

Create artificial FASTSORT tape for testing

RECORD tape operations

General help

Exit

PEGASUS

Program for converting raw data EXABYTE tapes — Version 1.9

Author : Jerzy Grebosz — 15 October 1990

MAIN MENU

Show events from Strasbourg tape

Transform S

Create arti

RECORD tape

General hel

Exit

RECORD tape operations menu

Directory of INPUT tape EXA0:

Directory of OUTPUT tape EXA1:

Swap RECORD Tape from DEC format to VME format

Chopper long files to shorter ones (and swap)

Return to main menu (= 2 times Esc)

Swap RECORD Tape from one format to opposite

STRUCTURE OF TAPES

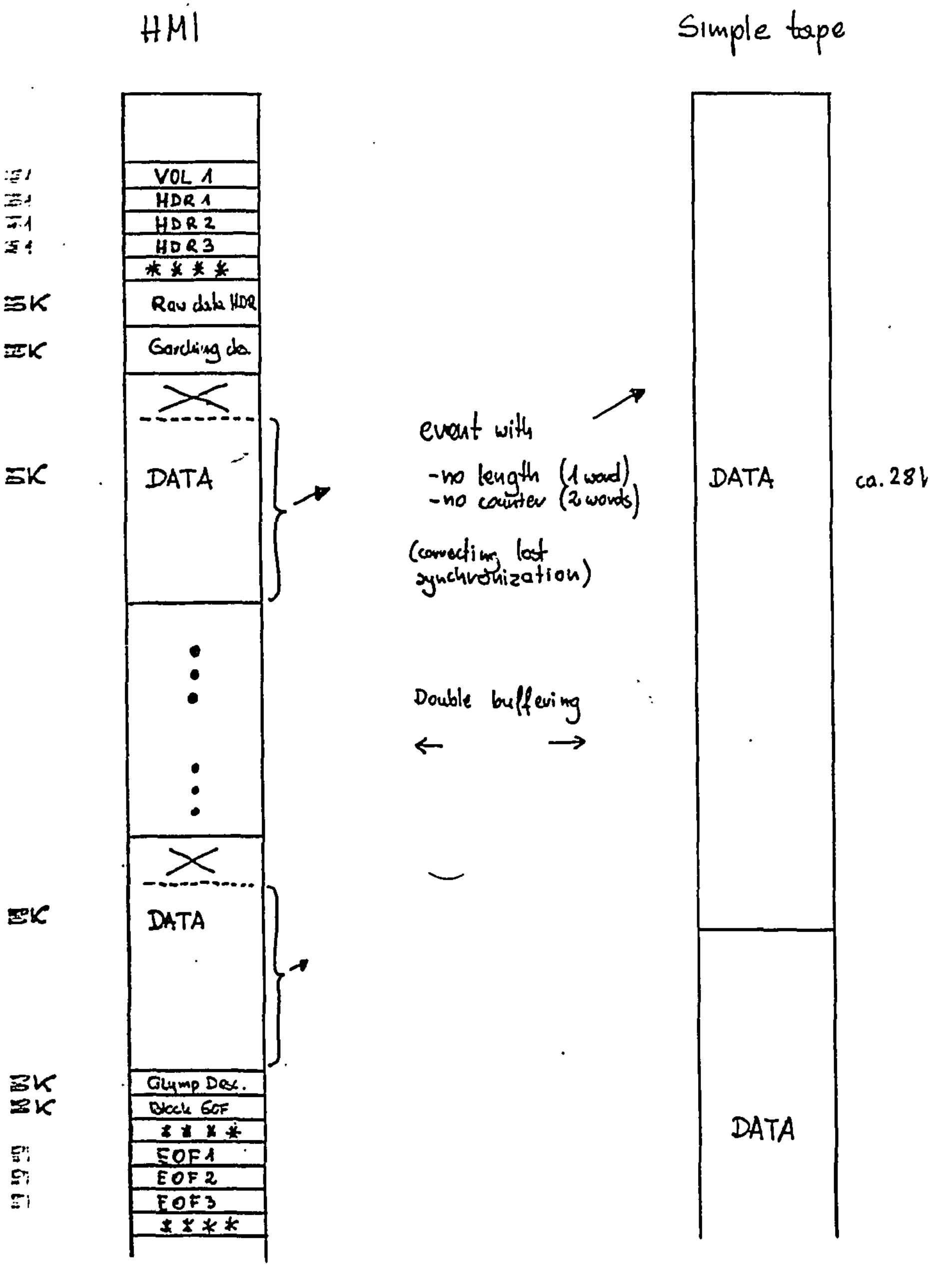

Event Data Block

<table>
<tr><td colspan="4">GAT #</td><td colspan="4">SGR #</td><td colspan="8">length of event</td></tr>
<tr><td colspan="16">Tagword</td></tr>
<tr><td colspan="16">Tagword</td></tr>
<tr><td colspan="3">WIN #</td><td colspan="13">ADC data</td></tr>
<tr><td colspan="3">WIN #</td><td colspan="13">ADC data</td></tr>
<tr><td colspan="3">...</td><td colspan="13">...</td></tr>
<tr><td colspan="3">...</td><td colspan="13">...</td></tr>
<tr><td colspan="16">event count (low)</td></tr>
<tr><td colspan="16">event count (high)</td></tr>
<tr><td>15
bit</td><td>14</td><td>13</td><td>12</td><td>11</td><td>10</td><td>9</td><td>8</td><td>7</td><td>6</td><td>5</td><td>4</td><td>3</td><td>2</td><td>1</td><td>0</td></tr>
</table>

_1DUA12:[FFM.SOR]ISIS.LOG;5

Simplifier log book

Accumulated event statistic
made for root >>temp<< after pack : A
Analysis of event multiplicity:

statistics made every ca. 300 000 events

fold	actual	accumulated
0)	51	
1)	202	
2)	285631	351654
3)	13627	19722
4)	1034	1439
5)	50	85
6)	5	5
7)	0	0
......		
12)	0	0

Total counts of each ADC:

En.	1)	44629	2)	60121	3)	47010	4)	40606
	5)	48339	6)	55871	7)	45462	8)	65347
	9)	54736	10)	63588	11)	44108	12)	46944
Tim.	13)	44786	14)	60348	15)	47271	16)	40699
	17)	48454	18)	56073	19)	45672	20)	65708
	21)	55023	22)	63969	23)	44318	24)	47078
Flight	25)	16121	26)	[illegible]	27)	208374	28)	16630
	29)	66147	30)	67108	31)	69980	32)	73002

Particles

Events with no corresponding energy and time:

Detector	E_solo	T_solo
1)	44629	44786
2)	60121	60348
3)	47010	47271
4)	40606	40699
......		
10)	63588	63969
11)	44108	44318
12)	46944	47078

also makes projections:

tempA.a001
tempA.a002
tempA.a003
⋮

Analyzed events total : 300600 (or 3 min)
Analyzed events run : 300600
Defective events total : 0
Events with neutron : 0
Last Hopsy block number : 857
Number of blocks on tape : 171 !
Max. bytes per tape block: 27636
Number of bytes total : 4681904

Accumulated event statistic
made for root >>temp<< after pack : B
Analysis of event multiplicity:

fold	actual	accumulated
0)	110	
1)	398	

„PRE" Presorter

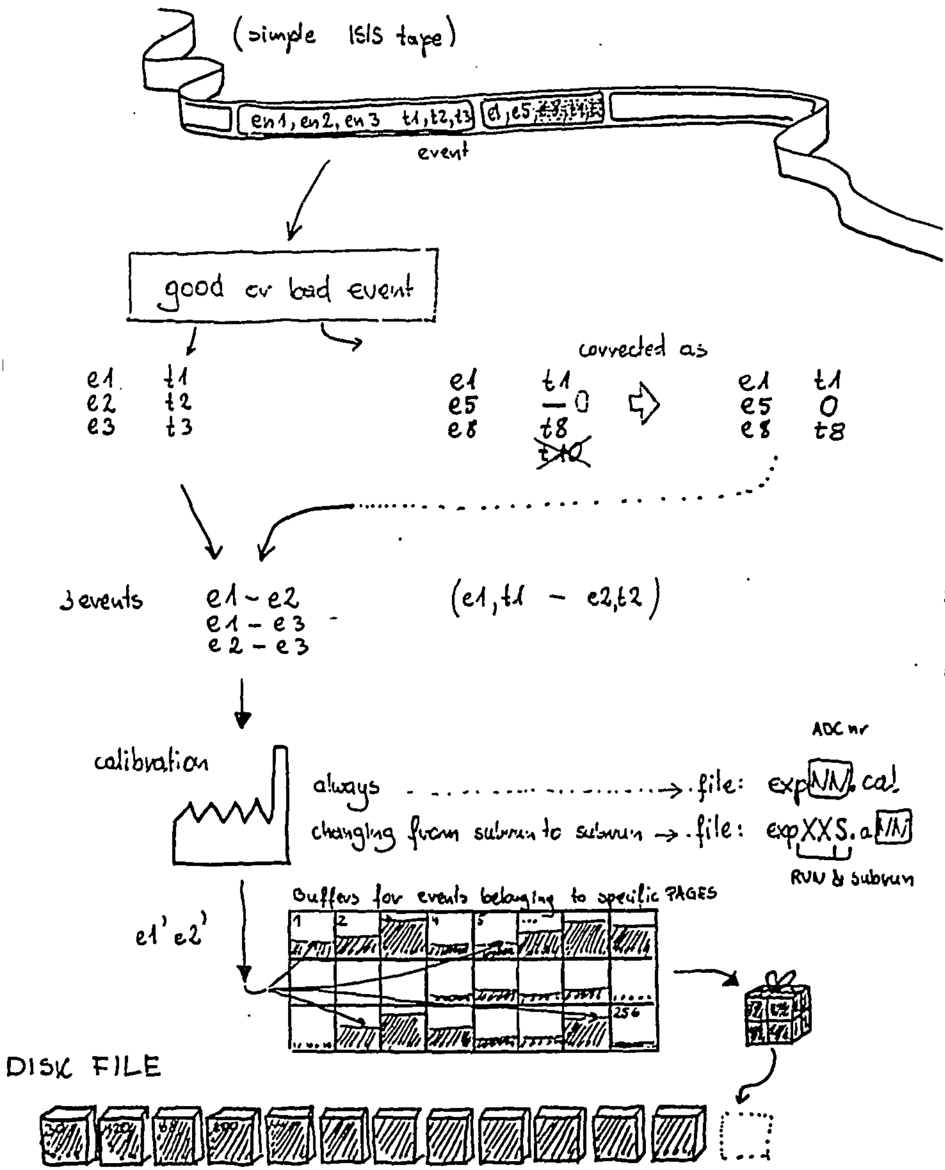

Structure of an Event Block

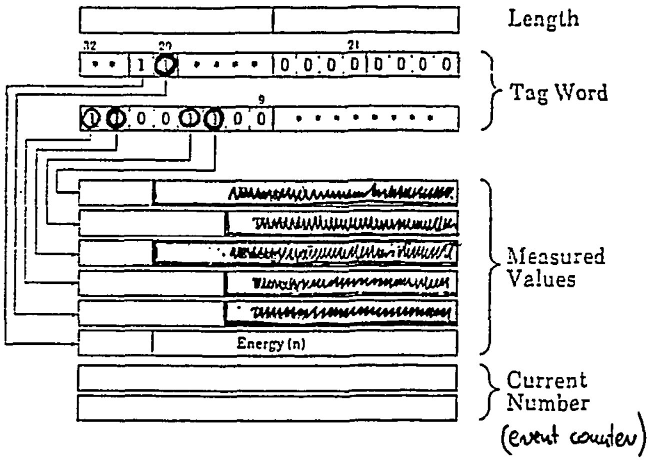

During Rüdiger's experiment :

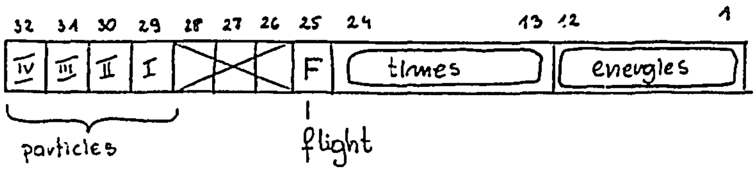

PRESORTED EVENT

Energy X
Energy Y
Detect_nr X   (ei - ti
Detect_nr Y   ej - tj)
Time X
Time Y

- - - - - - - - - - - - - - -

flight
particle1
particle2
particle3
particle4

13 bytes

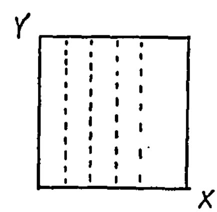


```
struct   presorted_event   {
        int  ( Ex,                  (:4)
               Ey,                  (:12)
             ( Dx,                  (:5)
               Dy,                  (:5)
             ( Tx,                  (:8)
               Ty,                  (:8)
            - - - - - - - -
               flight,              (:13)
               p1, p2, p3, p4 ;     (:10)
} event ;
```

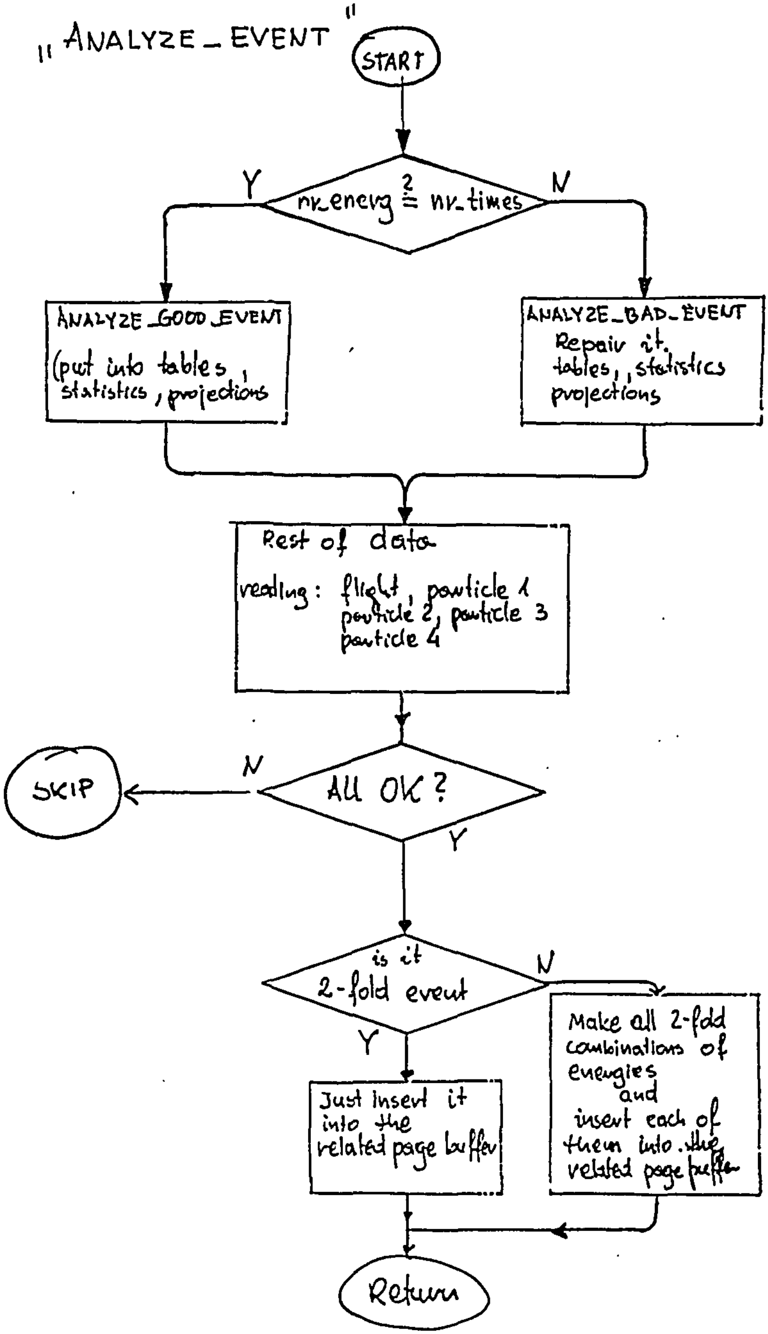
"ANALYZE_EVENT"
START
nr_energ $\stackrel{?}{=}$ nr_times
Y
N
ANALYZE_GOOD_EVENT
(put into tables, statistics, projections
ANALYZE_BAD_EVENT
Repair it.
tables, , statistics
projections
Rest of data
reading: flight, particle 1
particle 2, particle 3
particle 4
N
SKIP
All OK?
Y
is it
2-fold event
N
Y
Just insert it
into the
related page buffer
Make all 2-fold
combinations of
energies
and
insert each of
them into the
related page buffer
Return

CALIBRATION SECRETS

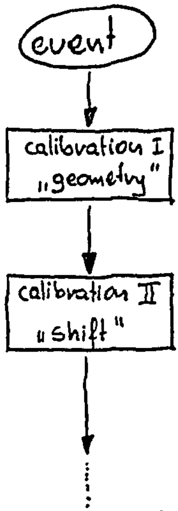

run_name.cal

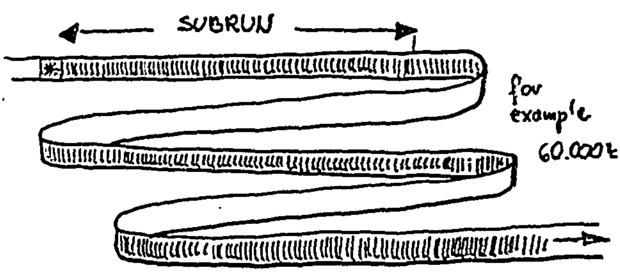

calibr. II changed every subrun

filename run_nameX.shk

↳ A, B, C.... subrun ide.

↳ any chars run (tape) ide.

Entry table for det nr... 1.

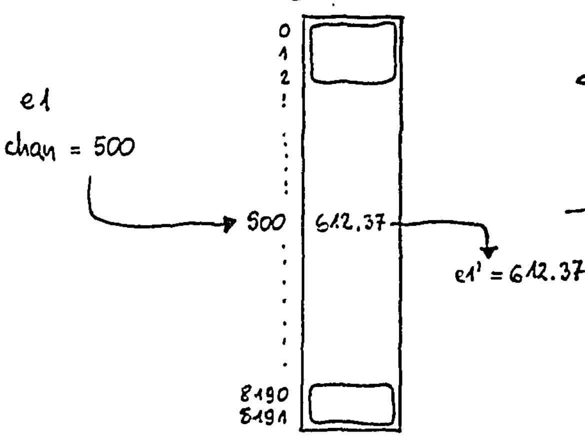

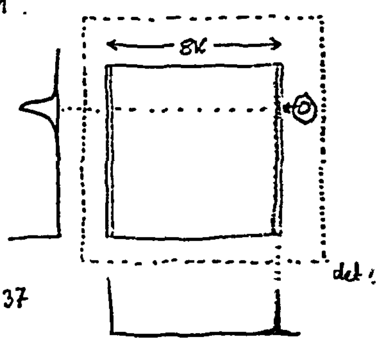

_1DUA12:[PFM.SOR]JAN01.PSL;99

```
  1800 tape blocks analyzed
3090137         events analyzed
3427099         2-fold events presorted

693294             0-fold events
722236             1-fold events
3689814            2-fold events
140344             3-fold events
10747              4-fold events
523        5-fold events
28         6-fold events
```

	1 ~~0)~~ ADC: 460460 events	
	1) ADC: 616726 events	
	2) ADC: 484008 events	
	3) ADC: 417497 events	
	4) ADC: 496559 events	
Energies .	5) ADC: 571512 events	
	6) ADC: 468001 events	
	7) ADC: 671888 events	
	8) ADC: 563959 events	
	9) ADC: 655741 events	
	10) ADC: 453236 events	
	11) ADC: 482898 events	and produces projections .
	12) ADC: 460446 events	
	13) ADC: 616706 events	
	14) ADC: 483993 events	proj : expXXS.eNN
	15) ADC: 417421 events	
times	16) ADC: 496479 events	
	17) ADC: 571411 events	
	18) ADC: 467926 events	JAN01A.e01
	19) ADC: 671651 events	2
	20) ADC: 563583 events	3
	21) ADC: 655250 events	⋮
	22) ADC: 452897 events	
	23) ADC: 482280 events	
	24) ADC: 164180 events	.tNN
	25) ADC: 0 events	.esm
	26) ADC: 0 events	

Events with no corresponding energy and time signals:

Detector	energy	time
1)	560	2251
2)	548	2869
3)	339	2889
4)	980	1954
5)	703	1839
6)	536	2640
7)	311	2506
8)	606	4135
9)	771	3534
10)	740	4484
11)	409	2751
12)	617	2083

„BURGY"

COLLECTOR

SC: PRESORT_FILE.

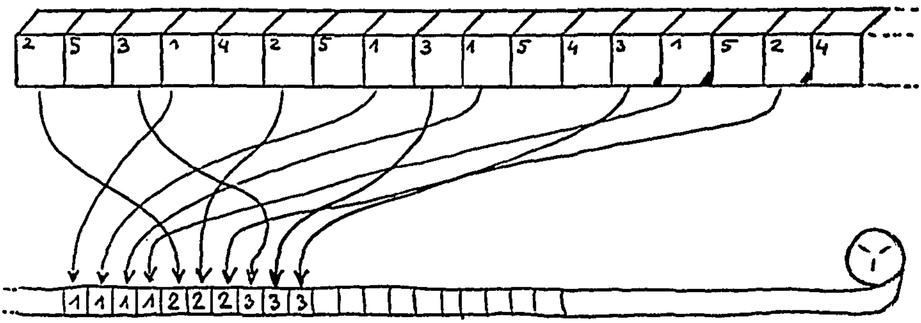

presorted tape

Resets Presort pointer

SORTER

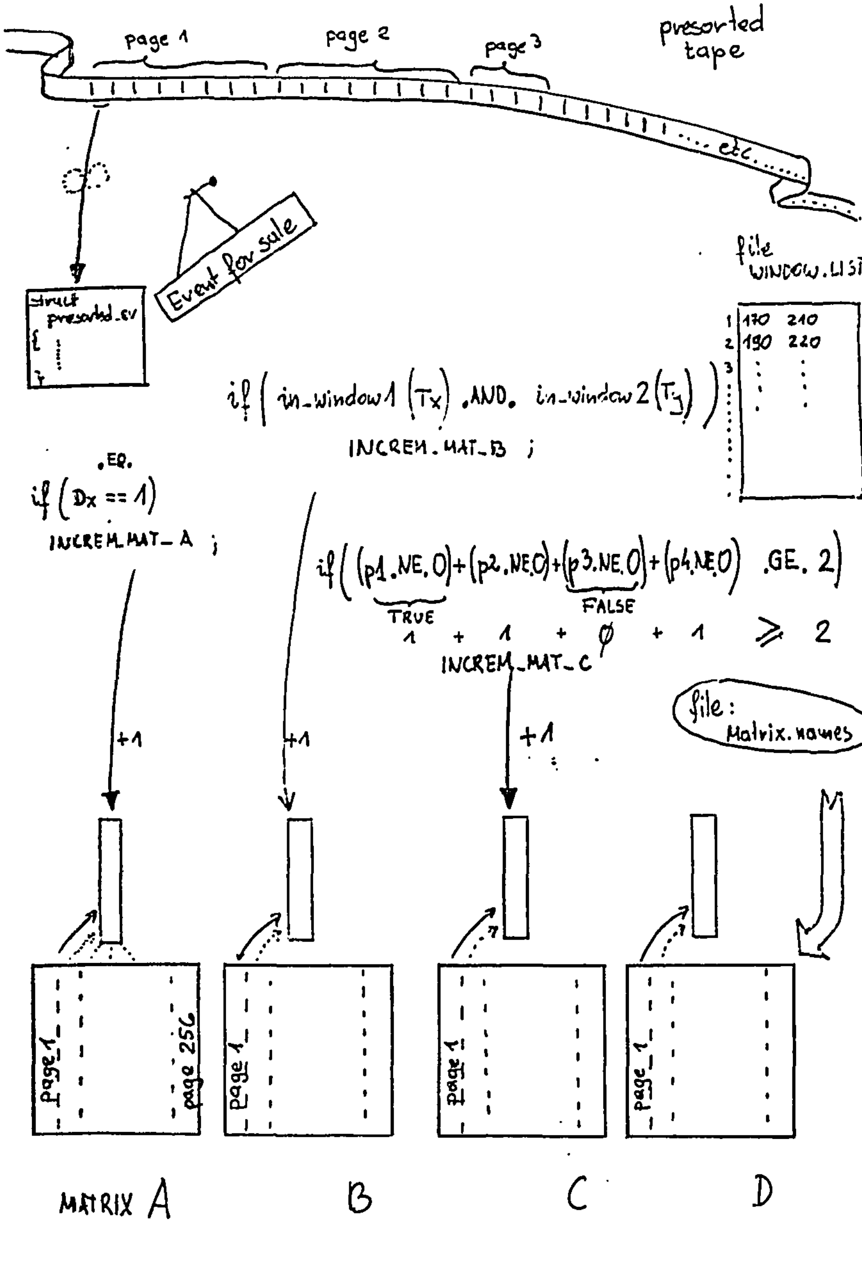
page 1
page 2
page 3
presorted tape
etc.
struct presorted_ev
{
}
Event for sale
file WINDOW.LIST
1 170 210
2 190 220
3
if (in_window1 (Tx) .AND. in_window2 (Ty))
INCREM_MAT_B ;
.EQ.
if (Dx == 1)
INCREM_MAT_A ;
if ((p1.NE.0)+(p2.NE.0)+(p3.NE.0)+(p4.NE.0) .GE. 2)
TRUE
FALSE
1 + 1 + ∅ + 1 ≥ 2
INCREM_MAT_C
file: Matrix.names
+1
+1
+1
page 1
page 256
page 1
page 1
page 1
MATRIX A
B
C
D

The spectrum integral is : 1,303,050

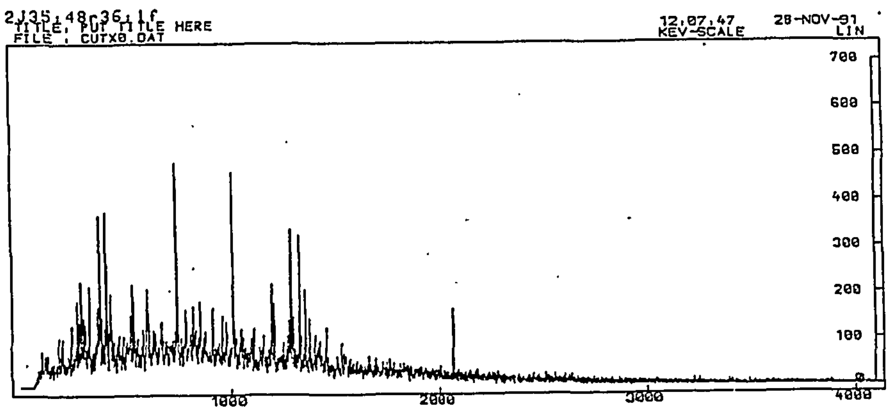

The spectrum integral is : 1,410,820

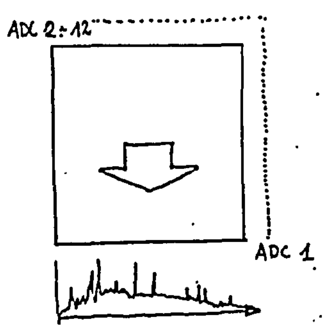

Giant Dipole Resonances. Can a recoil detector help?

Adam Maj (Kraków)

in collaboration with

J.J. Gaardhøje, A. Atac, B. Herskind (Copenhagen)

F. Camera, B. Million, A. Bracco, M. Pignanelli (Milano)

ABSTRACT

The basic relations between the shape of the Giant Dipole Resonance (GDR) and angular distributions of γ-rays depopulating GDR, and the shape and type of rotation of atomic nuclei, are presented. The evolution of nuclear shape when the angular momentum and temperature of nucleus are increasing, and the effect of thermal shape fluctuations on the measured observables, are overviewed. The multidetector array HECTOR for high energy γ-rays detection (installed in Niels Bohr Institute) is described and the techniques used in GDR experiments are discussed. The experimental data for two nuclei: ^{110}Sn and ^{162}Yb, are presented and compared to the theoretical calculations. Problems associated to non-fusion reaction channels are pointed-out, and the use of the recoil detector, as a possible solution of these problems, is considered. Plans for the nearest future are given.

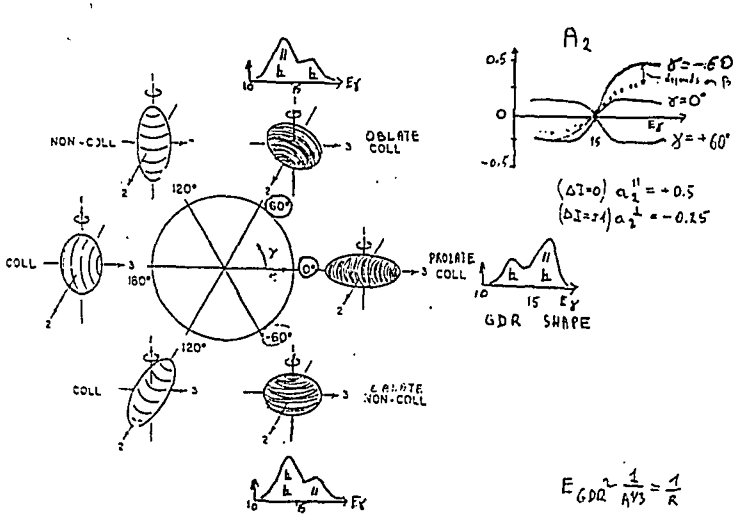

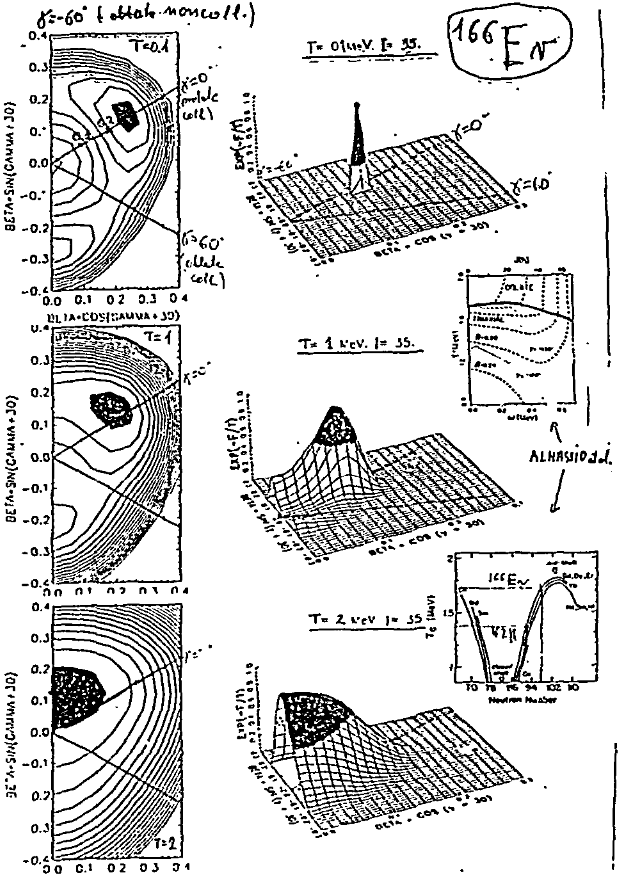

γ=-60° (oblate noncoll.)
166Er
T= 0.1MeV. I= 35.
T= 1 MeV. I= 35.
T= 2 MeV I= 35
T=0.1
T=1
T=2
γ=0° prolate coll.
γ=60° oblate coll.
BETA•SIN(GAMMA+30)
BETA•COS(GAMMA+30)
ALHASSID et al.
166Er
Neutron Number

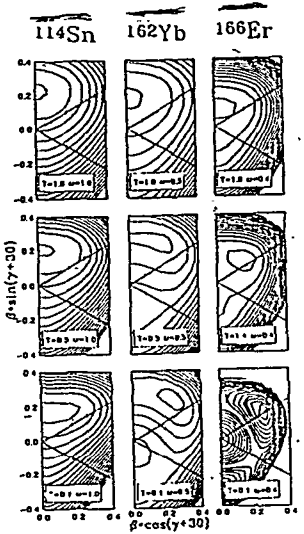

114Sn
162Yb
166Er
β•sin(γ+30)
β•cos(γ+30)

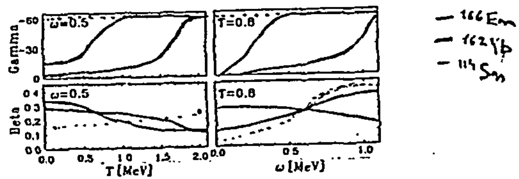

ω=0.5
T=0.8
Gamma
Beta
T [MeV]
ω [MeV]
— 166Er
— 162Yb
— 114Sn

A.Maj et al. . Sept. 20, 1991 3:00:05 PM

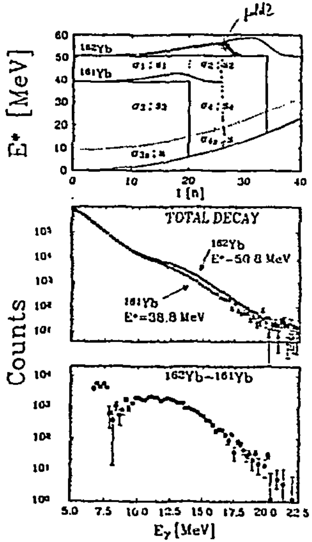

gate on fold 2

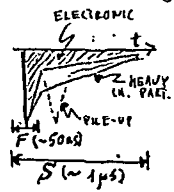

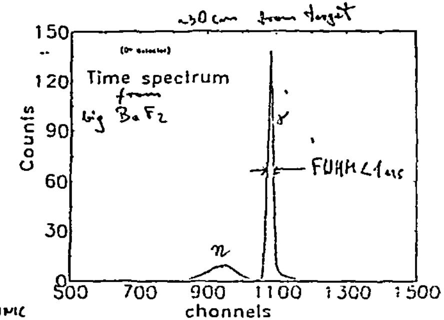

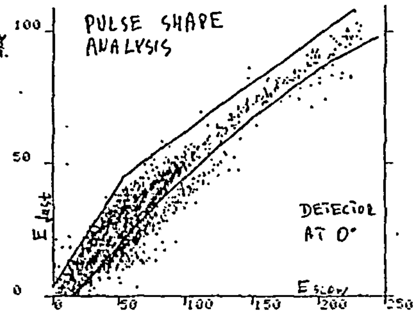

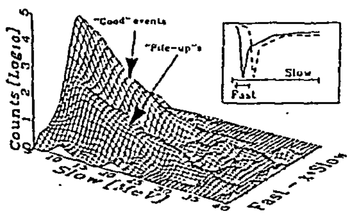

GDR-SHAPE SIMULATIONS

(PC-program)

from Alhassid. parameters

$$f_{GDR}(T,\omega;E_\gamma,\theta) = \int \underline{f_{GDR}(\beta,\gamma;E_\gamma,\theta)} \cdot \exp(-F(T,\omega,\beta,\gamma))\ \beta d\beta d\gamma$$

θ: ∢ beam–γ-ray

another metric: $\beta^4 |\sin 3\gamma|\, d\beta d\gamma$ (Yale group)

$$\underline{E_i} = E_0 \exp\left[-\sqrt{\frac{5}{4\pi}}\ \beta\ \cos\left(\gamma - \frac{2\pi}{3} i\right)\right] \qquad (i=1,2,3)$$

$$E_0 = 79\ A^{-1/3} \quad [\mathrm{MeV}]$$

$$\underline{f_{GDR}}(\beta,\gamma;E_\gamma,\theta) = \mathrm{const} \sum_{i=1}^{3} \frac{\Gamma_i^2 E_\gamma^2}{(E_\gamma^2 - \underline{E_i}^2)^2 + \underline{\Gamma_i}^2 E_\gamma^2}\, \underline{W_i}(\theta)$$

$$\underline{\Gamma_i} = \Gamma_0 \left|\frac{E_i}{E_0}\right|^{\delta} \qquad (\delta = 1.9)$$

$$\underline{W_i}(\theta) = 1 + a_2 P_2(\cos\theta)$$

$$a_2^i = \begin{cases} -0.25 & (i = \perp) \\ +0.5 & (i = \parallel) \end{cases}$$

Orientation fluctuations

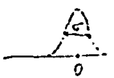

$\vec{\sigma}$ $\quad \sigma \sim \frac{T}{I^2}$ $\quad$ Not included!

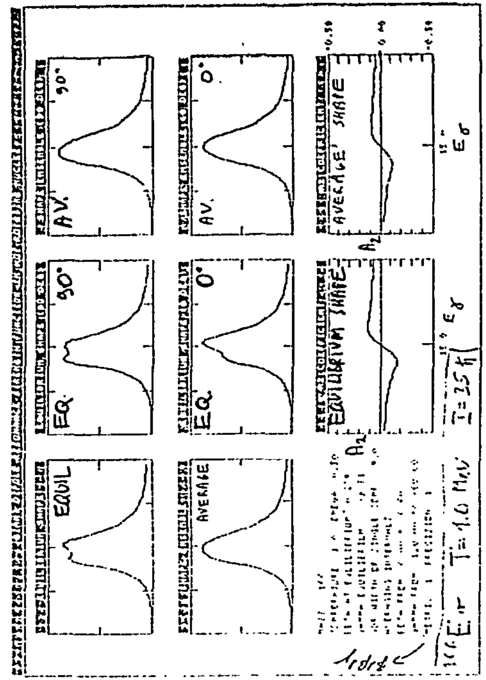

$$f_{GDR}(T,\omega;E_\gamma) = \int f_{GDR}(\beta,\gamma,E_\gamma) \cdot \exp\left[-F(T,\omega,\beta,\gamma)/T\right] \cdot \beta d\beta d\gamma$$

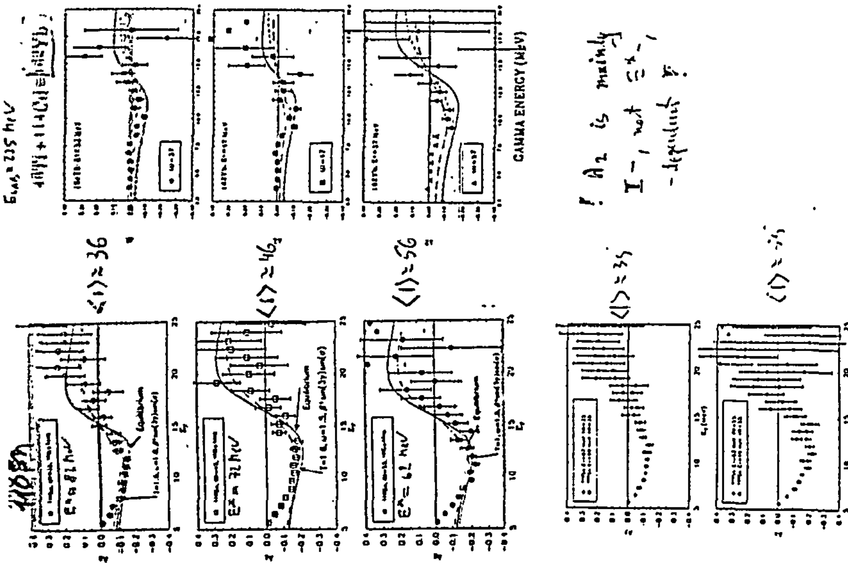

$$S = S(\Delta I \overset{\perp}{=} \pm 1) + S(\Delta I \overset{\parallel}{=} 0)$$

$$\boxed{\begin{aligned} S(\Theta) = {} & S^{\Delta I=\pm1}\left(1+\alpha\, a_2^{\Delta I=\pm1} P_2(\cos\theta)\right) + \\ & + S^{\Delta I=0}\left(1+\alpha\, a_2^{\Delta I=0} P_2(\cos\theta)\right) \end{aligned}}$$

$\Delta I = \pm 1$ vibr. $\perp$ $\vec{I}$

$\Delta I = 0$ vibr. $\parallel$ $\vec{I}$

$a_2^{\Delta I=\pm1} = -0.25$

$a_2^{\Delta I=0} = +0.5$

α - attenuation coeff. ($\simeq 0.4$)

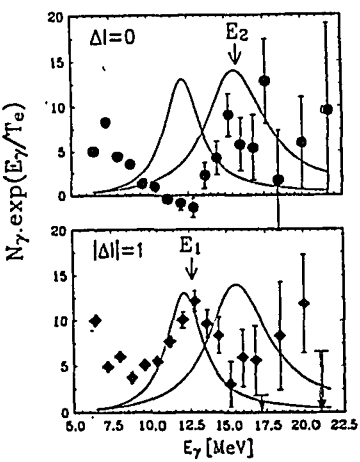

$$\beta \simeq \frac{\Delta R}{R} = \frac{\frac{1}{E_1} - \frac{1}{E_2}}{e_0} \simeq \frac{\Delta E}{E_0} \simeq 0.22$$

$$\Gamma(\Delta I = 0) \approx 3.5 \div 4.0 \text{ MeV}$$

Giant Dipole Resonance built on excited states of ^{55}Mn studied in compound nucleus reactions

W. Królas, P. Bednarczyk, B. Fornal, A. Maj, W. Męczyński, J. Styczeń

High energy γ rays emitted in the decay of the Giant Dipole Resonance (GDR) built on excited states can be observed in compound nucleus reactions. In experiments described in this thesis we measured γ rays depopulating the GDR in ^{55}Mn compound nucleus that was formed at an excitation energy of 31 MeV.

The measurements were performed on U-120 cyclotron of the Institute of Nuclear Physics in Kraków. For each event two parameters were registered: the γ energy deposited in a BGO detector and the time between the beam burst and the detection of the γ. In some of the measurements coincidence between BGO and one of two NaI counters was required.

In this work we calibrated our BGO detector using slow neutrons capture lines of 10.2 MeV and 7.4 MeV. For low energy calibration we used a ^{60}Co source giving sum peak energy of 2.5 MeV. However, during the experiment we did not need a neutron source. It was discovered that slow neutrons are an important part of the background existing during cyclotron operation. Capture of this neutrons provided an on-line calibration.

Reaction used: $^{51}V + \alpha\ (26.5\ MeV) \rightarrow {}^{55}Mn^{*}$

$E_{exc} = 31\ MeV$

Experimental setup:

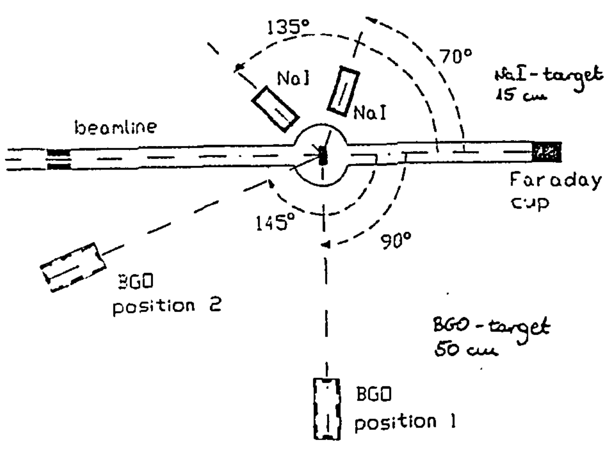

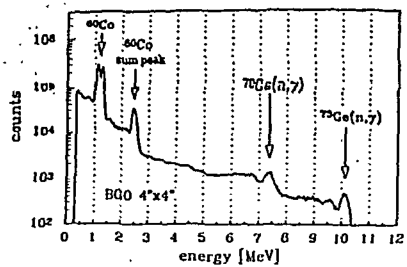

Figure . : The BGO response to neutrons.

Table . : The isotopes in the BGO compound and their abundances, thermal neutron capture cross sections and the capture energies.

isotope	abundance %	σ (b)	capture energy [MeV]
^{16}O	99.762	0.000178	4.14
^{17}O	0.038	0.235	8.04
^{18}O	0.200	0.00016	3.96
^{70}Ge	20.5	3.2	7.42
^{72}Ge	27.4	0.98	6.78
^{73}Ge	7.8	15	10.20
^{74}Ge	36.5	0.143	6.51
^{76}Ge	7.8	0.09	6.07
^{209}Bi	100	0.014	4.60

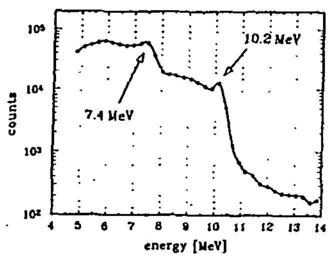

Figure : A background in-beam spectrum measured using the BGO detector.

Final GDR-spectra :

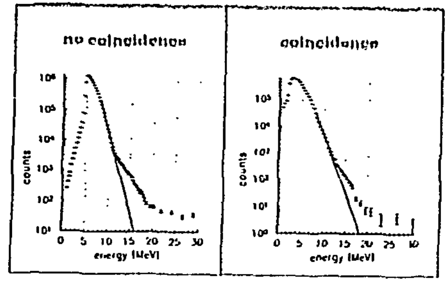

GDR parameters obtained from CASCADE code calculations fitted to the experimental spectra :

$$E_{GDR} = 18.6 \pm 0.5 \text{ MeV}$$
$$\Gamma_{GDR} = 10.5 \pm 1.0 \text{ MeV}$$

for ^{55}Mn* nucleus at $T \simeq 1.4$ MeV

COMPETITION BETWEEN PN and D EMISSION IN α + ^{51}V, ^{54}Fe and ^{59}Co REACTIONS at 26.5 MeV.

Z. Bednarczyk, E. Bożek, B. FORNAL, M. Lach
A. Maj, W. Męczyński, T. Pawłat, J. Styczeń.

COMPETITION BETWEEN TWO PROCESSES: PN, NP and D- EVAPORATION HAS BEEN OBSERVED IN ORDER TO EXTRACT AN INFORMATION ABOUT THE INTERMEDIATE NUCLEI.

THREE REACTIONS WERE CHOSEN:

$\alpha + {}^{51}V \rightarrow {}^{55}Mn$ (CN)
$\alpha + {}^{54}Fe \rightarrow {}^{58}Ni$ (CN)
$\alpha + {}^{59}Co \rightarrow {}^{63}Cu$ (CN)

EXPERIMENTAL SETUP:

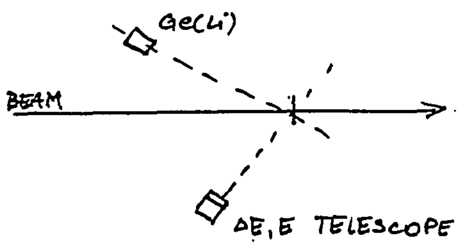

METALIC TARGETS: ^{51}V, ^{54}Fe, ^{59}Co WERE BOMBARDED BY 26.5 MeV α- BEAM FROM KRAKÓW CYCLOTRON.
COINCIDENCES BETWEEN γ-RAYS AND CHARGED PARTICLES WERE REGISTERED.
PROTON, DEUTERON AND GAMMA SPECTRA WERE GENERATED OFF LINE.
THE σ_{pn}/σ_d RATIOS WERE DETERMINED AS A RATIOS OF INTENSITIES OF PROPER LINES IN GAMA-p AND GAMA-d SPECTRA.

THE CALCULATIONS USING STATISTICAL CODE CASCADE WERE PERFORMED FOR DIFFERENT VALUES OF LEVEL DENSITY PARAMETER "a_{LDM}"
COMPARISON BETWEEN EXPERIMENTAL RESULTS. AND CALCULATIONS SHOWED STRONG DEPENDENCE OF THE σ_{pn}/σ_d RATIO ON LEVEL DENSITY FUNCTION. CALCULATED FOR INTERMEDIATE NUCLEUS.

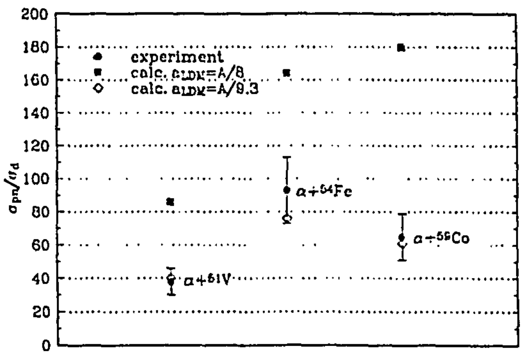

THE σ_{pn}/σ_d RATION OBTAINED FROM EXPERIMENT AND FROM CALCULATIONS

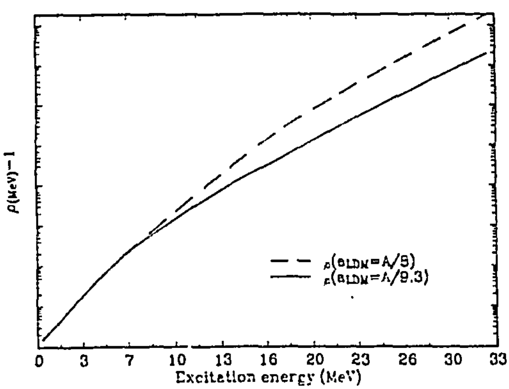

LEVEL DENSITY CURVES FOR ^{54}Cr CALCULATED USING DIFFERENT VALUES OF a_{LDM}.